DEVELOPING IMPROVED CATALYST FOR METHANE ACTIVATION ON OXIDES USING FIRST PRINCIPLE CALCULATION

Thesis Submitted for the Award of the Degree of

DOCTOR OF PHILOSOPHY

In

Chemistry

By

QURAT UL AIEN

(41900173)

Supervised By

Name of Supervisor (UID)

Dr. Tanmoy Kumar Roy (23715)

Assistant Professor

Department of Chemistry

Lovely Professional University

Phagwara Punjab.

Co-Supervised by

Name of Co-supervisor

Dr. Mudit Dixit

Senior Scientist CSIR- Central Leather Research Institute (CLRI) Chennai

LOVELY PROFESSIONAL UNIVERSITY, PUNJAB

2024

LOVELY PROFESSIONAL UNIVERSITY, PUNJAB

September 2024

DECLARATION

I, hereby declared that the presented work in the thesis entitled "Developing Improved Catalyst for Methane Activation on Oxides Using First Principle Calculation" submitted in fulfilment of degree of **Doctor of Philosophy (Ph. D.)** is outcome of research work carried out by me under the supervision of Dr. Tanmoy Kumar working as Assistant Professor in Department of Chemistry of Lovely Professional University, Punjab, India. In keeping with general practice of reporting scientific observations, due acknowledgements have been made whenever work described here has been based on findings of another investigator. This work has not been submitted in part or full to any other University or Institute for the award of any degree.

(Signature of Scholar)

Name of the scholar: Qurat Ul Aien

Registration No.: 41900173

Department/school: Chemistry

Lovely Professional University,

Punjab, India

CERTIFICATE

This is to certify that the work reported in the Ph. D. thesis entitled "Developing Improved Catalyst for Methane Activation on Oxides Using First Principle Calculation" submitted in fulfillment of the requirement for the reward of degree of **Doctor of Philosophy (Ph.D.)** in Department of Chemistry is a research work carried out by Ms. Qurat Ul Aien (Registration No.) 41900173 , is bonafide record of her original work carried out under my supervision and that no part of thesis has been submitted for any other degree, diploma or equivalent course.

Signature of Supervisor
Dr. Tanmoy Kumar Roy (23715)
Assistant Professor Chemistry
Lovely Professional University
Phagwara Punjab

Signature of Co-Supervisor
Dr. Mudit Dixit
Senior Scientist CSIR - CLRI
Chennai

Abstract

Since recent past, the accessibility to large stocks of methane in the shale gas reserves and the development of hydraulic fracking technology has raised significant interest in conversion of methane to high-value chemicals and fuels. But owing to the kinetic restrictions hindering the conversion, this process is still not commercially viable. To overcome this challenge, there is a dire need of some effective and selective catalysts. The transition Metal oxides due to their surface heterogeneity and Lewis acidic (metal) and basic (oxygen) site-pairs prove ideal for the activation of C-H bonds of methane. Here density function theory (DFT) was applied to analyse the activation of C-H bond on pristine and doped γ-Al_2O_3 clusters. The C-H activation was studied under two potential pathways namely the radical and polar and it was concluded that amongst the two, the activation barriers are lower for polar pathways on γ-Al_2O_3. Boron and Gallium doping in addition of altering catalytic activity of dopant sites, also have significant effect on the adjacent sites. Gallium is seen to greatly enhance the catalytic activity on most the site pairs of pristine γ-Al_2O_3. We could find a correlation between dissociated H_2 binding energies and C-H activation free energies for the preferred polar pathway. The same can be utilized in discovering a better catalyst for methane and shale gas. In this work we describe the role of dopants on C-H activation of methane on (γ-Al_2O_3).

Preface/ Acknowledgement

My ultimate thanks to my Lord, my Creator, Cherisher and Sustainer!

Words cannot express my gratitude to my guide/mentor Dr. Mudit Dixit for his valuable time, encouragement, guidance, meticulous scrutiny, scholarly advice and scientific approach that has helped me in completing my work.

Special thanks are due to my supervisor Dr. Tanmoy Kumar Roy for his timely support, encouragement and love that surely helped me to complete my work.

I am profusely thankful to my loving mother, the only unique and unparalleled support who has always been there to push me forward and ready to sacrifice her each and every comfort for my success and happiness who has stood by me through every thick and thin.

I owe a deep sense of gratitude to my husband for his moral and emotional support to complete my academic journey. For a nursing mother like me this would not have been possible to carry on my journey without his profound sense of collective responsibility.

My privilege to thank my father and my younger brother for their consistent encouragement.

Sincere gratitude and warm appreciation is due to my younger sister an amazing girl, reason of my smile, my techno support, who sacrificed her valuable time and comfort till completion of my thesis.

I am sincerely grateful to my lab mates for their inspiration and encouragement. Vote of thanks would not be complete without mentioning Ms. Priti Singh for always providing invaluable support and encouragement during compilation of this research work.

Finally, I am in debt to my friends and my well-wishers for their support and good wishes.

Contents

List of figures

List of tables

Chapter 1: Introduction

Alkanes or saturated hydrocarbons are the substantial ingredients of natural gas and petroleum but practically there exist very few methods of converting them into some valuable product[1]. The reason behind this limitation is the chemical inertness of alkanes, also known as Paraffins meaning "Not enough affinity"[1]. This inertness of alkanes is attributed to strong and localized C-C and C-H bonds. As a consequence, alkanes lack the required orbitals that could actively take part in a chemical reaction[1]. Also, the easy accessibility of alkanes such as methane due to recent development of hydraulic fracking technology makes it a potent source for its conversion to value added chemicals and fuel[2-4]. Direct combustion of methane in chemical industry does not prove to be an energy efficient process[5].Moreover, most of the world's natural gas reserves are located in remote areas like north slope of Alaska where there is no demand for such gases[1]. Also the transportation of methane from rural areas turns out quite expensive and challenging, owing to its low the low-volumetric density hence paving the need for its conversion value added products. Presently, the conversion is achieved via steam distillation[6] and syngas(H_2 and CO_2) formation[7] which however require energy intensive reaction conditions (temperatures >970K) making the process commercially inviable[8-10].

There is a growing interest in discovering a commercially viable process to selectively and efficiently facilitate the conversion of methane. With the right strategies in place, methane can be effectively transformed into methanol[1]. Although the conversion of methane to methanol presents an intriguing prospect, it encounters kinetic constraints due to the high energy associated with the Carbon-Hydrogen bonds (438.8 kJ/mol) [2, 11]. Consequently, extensive research has been conducted over the last decade to address C-H activation and, by extension, methane conversion[1, 12-35]. Among the myriad catalysts available, metal oxides stand out for their ability to activate C-H bonds in methane. This ability arises from the presence of both Lewis acidic and basic sites on their surfaces [36-40]. The dual nature of these oxides plays a crucial role in facilitating C-H activation in methane molecules. Given the diverse Lewis acidity and basicity of oxide surfaces, the substantial heterogeneity necessitates the identification of structure-

activity correlations. These correlations serve as an invaluable tool for comprehending catalytic activity and are instrumental in designing catalysts with enhanced performance. In recent years, substantial advancements have been made in this field. However, over the past few decades, our understanding of nonoxidative C-H activation of methane on oxide surfaces (specifically, acid-base pair sites) has lagged behind oxidative C-H activation, which primarily involves a single oxygen site. Furthermore, there remains a lack of a systematic approach for screening oxide catalysts for various catalytic reactions. A significant challenge in uncovering structure-activity relationships for nonoxidative C-H activation lies in the numerous non-equivalent sites on oxide materials, each with varying Lewis acidity and basicity. In this study, we delve into the catalytic capabilities of γ-Al_2O_3 in the context of methane C-H activation. Specifically, we investigate how the catalytic activity of γ-Al_2O_3 is altered when doped with trivalent dopants such as Barium and Gallium.[41]. We apply Density Function theory calculations to explore the surface heterogeneity of the catalyst and get to know the most active site pairs for C-H bond activation[36, 42]. Moreover, among the two proposed mechanisms (radical and polar pathway) we discover the energetically least demanding pathway for C-H activation. Additionally, we noticed that the catalytic action of γ-Al_2O_3 was site-dependent and that the C-H activation activity and H_2 binding energy (BE) at the various site pairs exhibited a volcanic relationship. Due to the high level of surface heterogeneity and high catalytic activity of γ-Al_2O_3 we concentrate on its ability of methane activation. Because of these characteristics, utilizing γ-Al_2O_3 is an excellent decision for exploring structure-activity relationships in the realm of nonoxidative C-H activation. In our study, we employed First-Principle Calculations, taking into consideration surface hydration, to identify the most effective mechanism for C-H activation on various low-index surface facets of γ-Al_2O_3.[41] We identified structure-activity correlations for C-H activation of methane, which can be applied to the rapid screening of metal oxides for catalysts[41].

1.1: Review of literature

Several research attempts have been performed for the conversion of methane over the past ten years by various groups[1, 12-20, 22-35]. There is ample evidence of highly selective C–H bond activation at transition-metal centres, under noticeably mild conditions[1]. A lot of research has been done to look at both theoretical and practical aspects of the activation of methane by transition metals, oxides, sulphides, carbides, and zeolites[9, 43-45]. Among the other catalysts, metal oxides are known to activate the C-H bonds in methane[46-47] because of their surface Lewis acidic (metals) and basic (oxygen) sites[35-40]. The Lewis acidic and basic properties of the metal oxide surfaces, which are inherent to them, are essential for catalysing the methane activation process. The C-H bond activation has previously been examined using a variety of experimental and computational methods.

Yoshizawa, K., et al. reported C-H bond methane activation at the interfacial oxygen sites of a Ni_4-CeO_2 catalyst. They used the DFT + U method to explain the optimal route (non-radical pathway) for C-H bond activation, as well as the best site (bridging site) for methane activation[48]. They tried to comprehend how the introduction of Nickle alters the microstructural, structural, and redox features that change the CPO activity of CeO_2 supported Ni catalysts. The preparation techniques utilised were selected to produce tiny support crystallite sizes and small NiO particles with varying levels of metal support interaction. They performed XRD, XPS, TPR, and TGA tests to monitor the physical and chemical characteristics of the catalysts and their changes throughout the catalytic reaction. They confirmed the Nickle catalysts supported over Ceria to be well suited for the reaction. The activity and stability of the reaction are dependent on the size of the crystallites and their interaction with CeO_2, which are controlled by various catalyst production techniques.[49-50] They observed that the development of tiny NiO crystallites that do not necessarily interact with the support and prove extremely advantageous for catalytic activity[51].

By examining a variety of metal oxides and doped metal oxide catalyst surfaces, Janik et al. discovered a correlation between methane activation energy and catalyst reducibility[18]. They observed that the surface reducibility correlates with the C-H

activation energetics on both reducible and irreducible oxides. They also observed that the subsequent adsorption of the methyl radical formed during the C-H activation exhibits an identical correlation, resulting in a deeper oxidation and a trade-off between OCM (Oxidative Coupling of Methane) activity and selectivity. They determined the oxygen vacancy formation energy and reduced surface work function of various "reducible" and "non-reducible" metal-oxide surfaces as a measure of surface reducibility. Doping the metal oxide with various transition metals effects the surface reducibility and hence the methane activation energy by changing the Hubbard U corrections in DFT+U formula.[18]

Cholewinski et al studied methane activation activity of γ-Al_2O_3 based on its high level of surface heterogeneity and strong catalytic activity [52-54]. They used first-principles calculations, to determine the optimal mechanism of C-H activation on several low-index surface facets of γ-Al_2O_3. The researchers identified structure–activity relationships for C–H activation of methane, which may be used to the rapid screening of metal oxides for better and efficient catalysis[36]. Their calculations showed that the C-H activation barriers for polar pathway on γ-Al_2O_3 are considerably lower than those of the radical pathways. They defined the C-H activation energy descriptors for the preferred polar route as the dissociated H_2 binding and final state energy. Also they developed structure-activity correlations for the C-H activation of methane on γ-Al_2O_3 that take into consideration surface Lewis acid-base characteristics and may be used to search the catalysts for conversion of methane to value added products[36].

Dixit et al. investigated the dehydrogenation of propane on hydroxylated and non-hydroxylated surfaces of γ-Al_2O_3 [48, 55-56]. They explored both concerted and stepwise mechanisms. Through the use of density functional theory calculations and first-principles molecular dynamics simulations, they provided fundamental insights into the processes involved in propane dehydrogenation on different facets of γ-Al_2O_3 and established corresponding structure-activity relationships. Their findings revealed site-specific catalytic behaviours on γ-Al_2O_3, and notably, they discovered a volcano relationship between catalytic activity and the dissociative H_2 binding energy for propane dehydrogenation. The results indicated a clear preference for a concerted surface mechanism over a sequential one, particularly on the most active site,

underscoring the site-dependent catalytic behaviour of γ-Al_2O_3. Furthermore, they conducted ab initio metadynamics simulations on the most active sites of γ-Al_2O_3 to investigate surface dynamics and hydrogen production during the dehydrogenation process. Their simulations suggested that the poisoning of active sites by hydrogen adsorption was improbable under experimental conditions. The established structure-activity relationships (SARs) were envisioned as valuable tools for screening metal oxide surfaces and expediting the search for efficient catalysts for the conversion of alkanes to olefins[57].

Asthagiri and their team delved into the pathways of C-H bond activation for methane and ethane σ-complexes adsorbed on the PdO (101) surface, employing both conventional density functional theory (DFT) and dispersion-corrected DFT (DFT-D3) calculations. They made a significant observation of the formation of a sigma complex on the Pd (101) surface during the activation of C-H bonds. Their calculations revealed that the coordination with the Pd centre substantially weakens the alkane C-H bonds, consequently lowering the energy barriers for C-H bond cleavage. The weakening of C-H bonds is a direct result of Pd complex formation.[18, 58] The dissociation of C-H bonds occurs through the activation of hydrogen radicals on the surface oxygen atom and is subsequently reduced on the metal oxide[59-62] Furthermore, they focused on microkinetic models for the precursor-mediated dissociation of methane and ethane on PdO(101). Remarkably, their findings indicated that the 3N - 2 model accurately predicts kinetic pre-factors and dissociation probabilities, aligning with previous research in the field[58].

Valla et al. demonstrated the activation of tri-coordinated Al site of γ-Al_2O_3 via high-temperature treatment for olefin metathesis[63]. This group inferred that the formation of metathesis-active Re sites in CH_3ReO_3/Al_2O_3 depends critically on Al^{III} defect sites. This research also demonstrates the necessity of high-temperature pre-treatments of the alumina support to produce Al^{III} "defect" sites upon dihydroxylation that help obtain efficient propylene metathesis catalyst.[63]

Jordan Meyet et al studied the conversion of methane to methanol on mononuclear Cu^{II} sites supported on Al_2O_3.Methane was partially oxidized to methanol sequentially utilizing well-dispersed Cu^{II} sites that were produced on transition alumina via a

molecular approach. The distinct EPR signature of the reactive Cu^{II} centers allowed for their spectroscopic identification. Working in pairs, a structure for these unique Cu^{II} monomers was postulated based on DFT modelling, reactivity studies, and advanced spectroscopic characterisation.[64] They observed that the transition aluminas expose various low-index planes and facets, hence offering distinct anchoring sites on the support[64].Unlikely to α-Al_2O_3 , the γ- and η-Al_2O_3 phases are of considerable interest due to their comparable reactivity and strong Lewis acidity which is absent in α-Al_2O_3 because of no Lewis acidic under-coordinated sites present on the surface[64]. The group described the use of surface organometallic chemistry to create well-dispersed monomeric Cu^{II} species supported on alumina, as well as their reactivity towards the selective and stepwise conversion of methane to methanol. [64] They concluded that the selective conversion of methane to methanol occurs via a two-electron process, incorporating two Cu^{II} sites[64].

Sautet and co-workers computationally explained C-H bond activation on γ-Al_2O_3.C-H bond activation on γ-Al_2O_3 was computationally analysed by Sautet and co-workers. They observed that the C-H activation of methane occurs via polar routes at several Al_2O_3(110) catalytic sites (Al^{III}-O^{II} and Al^{III} O^{III}) [65-68]. The scientists also probed into the effect of surface hydration on methane activation, and they concluded that C-H activation occurs as the consequence of heterolytic C-H bond dissociation, resulting in the formation of hydroxyl (OH) and methyl-aluminium species. On the other hand, one of the hydrogen atoms in methane interacts with surface oxygen in the radical mechanism of the C-H activation of methane on oxides, which may result in the synthesis of the methyl radical [57]. Additionally, methyl radicals can interact with other

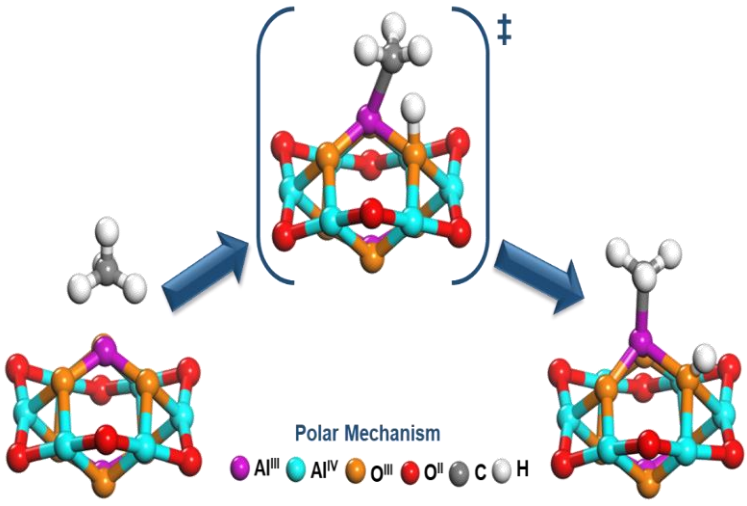

Figure 1: Polar mechanism for C-H bond activation of methane on the Al^{III}-OI^{II} site-pair of γ-Al_2O_3. The transition state is denoted with double daggers (‡).

substances or one another to create high-value byproducts[69-70]. The representative mechanistic pathway for the C-H bond activation of methane following the polar mechanism is shown in Figure1. The detailed explanation of mechanistic pathway of C-H activation via polar mechanism is given in chapter 2, section 2.1 of this thesis report.

In recent years, it has been shown that dopants can significantly improve the activity of pristine metal oxides. For instance,, Abdelgaid et al. investigated the effect of dopant on the catalytic activity of γ-Al_2O_3[71]. They observed that doping γ-Al_2O_3 with Ga^{IV} improves the non-oxidative dehydrogenation of ethane, propane, and isobutane as the activation barrier decreases with an increase in the content of dopant through the concerted mechanism. The intensity of the Lewis acidity and basicity of the active sites were taken into account while identifying the dissociated H_2 binding energy as an activity descriptor for alkane dehydrogenation. In both the concerted and stepwise processes, they noted a direct relationship between the binding energy of dissociated H_2 and the activation barriers of the rate-determining steps. The authors also established that the stability of carbenium ions serves as a quantifiable descriptor of the reactant type, showing a correlation with the activation barriers for C-H activation in various alkanes. They developed a model for alkane dehydrogenation that incorporates the influence of reactant substitution and catalyst acid-base surface characteristics, with dissociated H_2 binding energy and carbenium ion stability as key parameters. By utilizing the frequencies of dissociated H_2 binding energy, the complete dehydrogenation turnover can be predicted[71]. This has valuable applications in the screening and discovery of catalysts for alkane dehydrogenation and suggests the potential benefits of catalyst doping to enhance the catalytic process.[71].

Vlachos and co-workers used DFT calculation and microkinetic method to investigate the dehydrogenation of ethane on Ga doped and Ga grafted γ-Al_2O_3 (110) surface[72]. Depending on the Ga loading, grafted and doped surfaces were created and the outcome of microkinetic models were compared with those of kinetic results. Different loadings of Ga on Al_2O_3 were synthesized to investigate the associated reaction rates, apparent activation energies, and reaction orders, and to compare them with those observed on

pristine γ-Al_2O_3. In contrast to pristine γ-Al_2O_3, the dehydrogenation rates were notably higher, and the apparent activation energies were significantly lower when Ga-doped Al_2O_3 catalysts were employed. Furthermore, it was established that the Ga sites that were grafted onto the catalyst were not active for catalysis, while only the doped sites were capable of enhancing the activity of γ-Al_2O_3 (110)[72].

Due to the pronounced surface heterogeneity and catalytic activity, our attention is directed towards understanding the role of γ-Al_2O_3 in methane C-H activation. These attributes position γ-Al_2O_3 as a promising contender for elucidating the structure-activity relationship in non-oxidative C-H activation. Furthermore, it's worth noting that pre-heated γ-Al_2O_3 (subjected to high temperatures exceeding 400 °C) has previously been recognized as one of the most efficient catalysts for methane C-H activation.[73-75] The obtained structure activity relationships aid in screening various metal oxides and hence accelerate the discovery of selective and efficient catalyst. Although there is ample evidence for pristine and doped metal oxides in enhancing the C-H activation of methane**,** there are fewer reports pointing towards the role of dopant in enhancing the activity of pristine metal oxide catalysts.

In this work we explore the catalytic role of γ-Al_2O_3 in C-H activation of methane. We study the change in catalytic activity of γ-Al_2O_3 on doping with trivalent dopants Barium and Gallium[41]. Here in we apply Density Function theory calculations to explore the surface heterogeneity of the catalyst and get to know the most active site pairs for C-H activation[36, 42]. Moreover, among the two proposed mechanisms (radical and polar pathway) we discover the energetically least demanding pathway for C-H activation[41].

1.2: Objectives

Natural gas has become an attractive resource for the synthesis of high-value compounds, thanks to the advancements in hydraulic fracking technologies and the increasing shale gas reserves. However, methane, the primary component of natural gas, cannot be fully utilized within the chemical industry. The challenges of transporting methane from remote shale formations, mainly due to its low volumetric

density, add to the complexity. Therefore, there is a pressing need to convert methane into high-density, high-value compounds. Currently, the industrial transformation of methane follows an indirect process involving its conversion to syn-gas ($CO + H_2$) at high temperatures (>970 K). Regrettably, this approach is both energetically and economically inefficient. The quest for a commercially viable method for the efficient and selective conversion of methane into more valuable compounds remains unfulfilled, primarily due to the formidable strength of the C-H bonds in methane. It is intriguing to note that, while the conversion of methane presents kinetic challenges, it remains thermodynamically feasible. To overcome these kinetic barriers, the development of efficient and selective catalysts is imperative. Metal oxides, recognized for their surface Lewis acid (metal) and base (oxygen) sites, are well-known for catalysing processes involving C-H activation. Extensive experimental and computational investigations have explored various metal oxides' abilities to activate the C-H bond of methane. Remarkably, one of the most effective catalysts for methane C-H activation is preheated γ-Al_2O_3 (heated to temperatures exceeding 400 °C). Notably, the exceptional activity of preheated γ-Al_2O_3, especially at 500 °C, in alkane C-H activation and dehydrogenation has been recently demonstrated. In this work we explore the catalytic role of γ-Al_2O_3 in C-H activation of methane. We study the change in catalytic activity of γ-Al_2O_3 on doping with trivalent dopants Barium and Gallium. Here in we apply Density Function theory calculations to explore the surface heterogeneity of the catalyst and get to know the most active site pairs for C-H activation. Moreover, among the two proposed mechanisms (radical and polar pathway) we discover the energetically least demanding pathway for C-H activation. Herein, we focussed to

- Unravel the exact mechanism of C-H activation over metal oxide surface
- Identify the most active site of for C-H bond activation
- Demonstrate the effect of dopant on kinetics and thermodynamics of reaction
- Identify the effect of dopant on γ-Al_2O_3 at neighbouring site pair for C-H activation

1.3 Summary

Alkanes, the primary components of natural gas and petroleum, are chemically inert due to strong C-C and C-H bonds, limiting their conversion to valuable products[1]. Methane, a major alkane, is abundant due to hydraulic fracking technology but is challenging to transport and inefficient to combust directly for energy[2-4]. Current industrial conversion processes like steam distillation and syngas formation are energy-intensive and commercially unviable[8-10].

The study focuses on the catalytic conversion of methane to methanol using γ-Al_2O_3 doped with trivalent elements like Barium and Gallium[41]. Metal oxides, including γ-Al_2O_3, can activate methane's C-H bonds due to their Lewis acidic (metal) and basic (oxygen) sites[35-37]. However, understanding and enhancing this process requires identifying the most active catalytic sites and pathways for C-H activation[41].

Previous research has shown that transition metals and metal oxides can activate methane C-H bonds under mild conditions[41]. It has been reported that surface Lewis acidity and basicity are critical for the catalytic activity of metal oxides. Also, doping the metal oxides can enhance their catalytic properties by altering surface characteristics and reducibility. It has been studied that γ-Al_2O_3 is highly effective for C-H activation due to its surface heterogeneity and strong catalytic activity.

Therefore, this study aims to:

- Elucidate the mechanism of C-H activation on γ-Al_2O_3 surfaces.
- Identify the most active site pairs for C-H bond activation.
- Investigate the impact of doping γ-Al_2O_3 with Barium and Gallium on the kinetics and thermodynamics of the reaction.
- Determine how dopants influence neighbouring site pairs for C-H activation.

Density Functional Theory (DFT) calculations were employed to explore the surface heterogeneity of γ-Al_2O_3 and to identify the most active sites for C-H activation. This study also aimed to determine the energetically preferred pathway for C-H activation, whether radical or polar. The study discovered structure-activity correlations for C-H

activation of methane on γ-Al_2O_3, useful for rapid screening of metal oxide catalysts. Doping γ-Al_2O_3 with trivalent elements like Barium and Gallium significantly enhances catalytic activity by modifying surface acidity and basicity, reducing activation barriers, and improving the overall reaction efficiency. The polar pathway for C-H activation was found to be energetically more favourable compared to the radical pathway, indicating a lower energy barrier for the polar mechanism [41].

The study underscores the potential of γ-Al_2O_3, particularly when doped with Barium and Gallium, as an efficient catalyst for methane C-H activation. These findings provide valuable insights for designing improved catalysts, thereby enhancing the commercial viability of methane conversion processes. This comprehensive understanding can accelerate the development of effective catalysts for methane transformation, ultimately contributing to more efficient and sustainable utilization of natural gas resources.

Chapter 2: Unravelling the exact mechanism of C-H activation over metal oxide surface

To assess the bi-functional activity (acidity and basicity) of metal oxides for C-H activation of methane, we investigated methane activation over γ-Al_2O_3 as a catalyst. In molecular calculations, as it is computationally challenging to study the full γ-Al_2O_3 surface, we utilized the previously reported 20-atom molecular cluster[76-77] of γ-Al_2O_3 to study the dissociation of the C-H bond of methane. To assess the feasibility of methane activation on the catalyst surface, we calculated the activation free energy barrier for various symmetrically inequivalent site pairs of γ-Al_2O_3. Specifically, we selected aluminum metal with different coordination numbers such as tri coordinated (Al^{III}) and tetracoordinated (Al^{IV}) sites. Similarly, two symmetrically different oxygen sites are di-coordinated (O^{II}) and tri-coordinated (O^{III}) (Figure 2a). In addition to pristine systems, we also investigated boron-, gallium-doped γ-Al_2O_3 on different site-pairs, such as Al^{IV}-O^{II}, Al^{IV}-O^{III}, Al^{III}-O^{III}, Al^{III}-O^{II}, B^{IV}-O^{II}, B^{IV}-O^{III}, B^{III}-O^{III}, B^{III}-O^{II}, Ga^{IV}-O^{II}, Ga^{IV}-O^{III}, Ga^{III}-O^{III}, Ga^{III}-O^{II} (Figure 2). We further extended our investigation by varying the content of the dopant (Figure 2d and 2e).

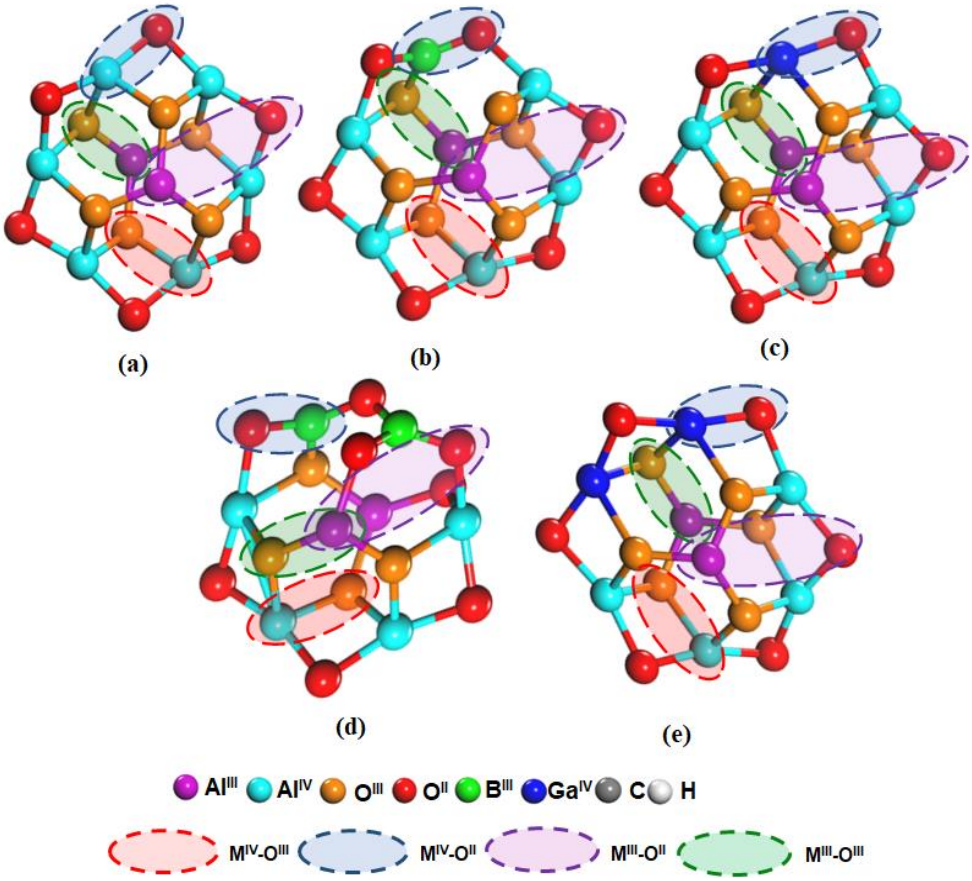

Figure 2: Graphical representation for structures of (a) pristine γ-Al_2O_3, (b) boron-dopedγ-Al_2O_3(c) gallium doped γ-Al_2O_3, catalyst surface. Metal oxide catalyst surface with different site pairs, M^{IV}-O^{II} (Blue oval), M^{IV}-O^{III} (Red oval), MI^{II}-O^{III} (Green oval), M^{III}-O^{II} (Purple oval) (M= Al, B, Ga). Structures d and e represents the double doped boron, and gallium systems respectively. {Obtained using Pople 6-311G(d)/MO6-2x}

2.1 The polar C-H Activation Mechanism

As reported, the C-H bond dissociation over γ-Al_2O_3 surface could occur through two possible pathways, (a polar or radical mechanism), therefore we initially focused on the polar mechanism of C-H activation. This mechanism initiates from the cleavage of C-H bond in heterolytic fashion to generate CH_3^- and H^+ species on the surface of the catalyst. Through the course of C-H bond activation, the CH_3^- gets adsorbed on the metal center and H^+ gets stabilized by a surface oxygen site. On the other hand, the radical mechanism proceeds via dissociation of C-H bond to generate hydrogen radical which gets adsorbed over an oxygen site on the surface, and methyl radical remains in the gas phase (Figure 3).

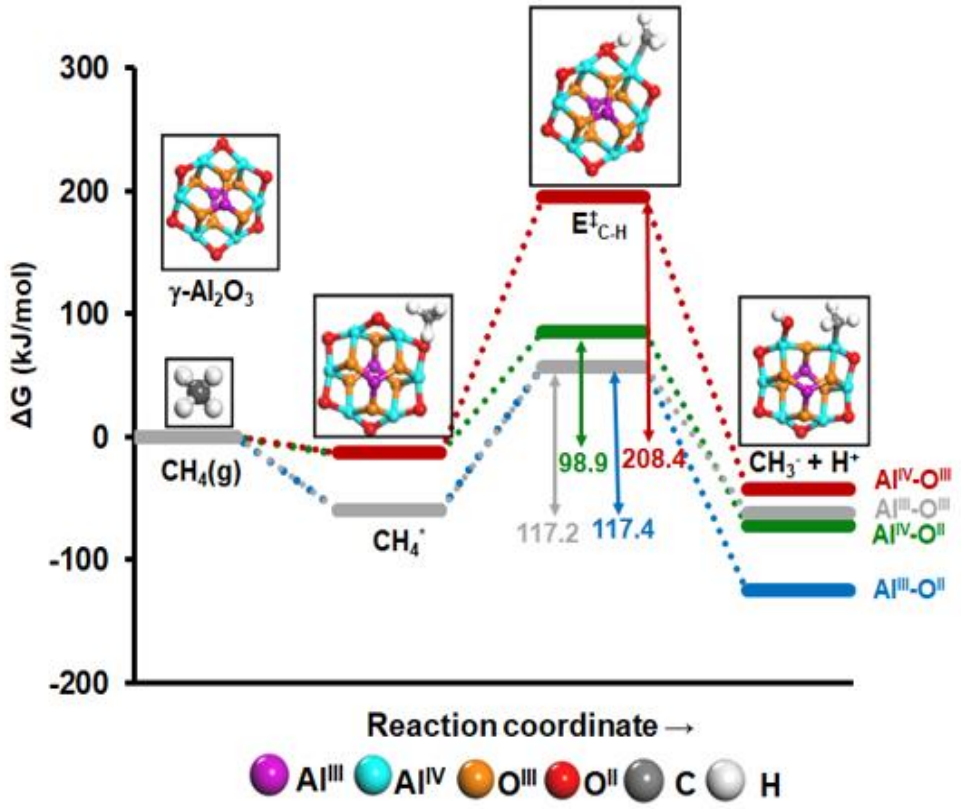

Figure 3: Free-energy barrier profile for C-H bond activation of methane through the polar mechanism on site pairs, Al^{IV}-O^{II}, Al^{IV}-O^{III}, Al^{III}-O^{III} and Al^{III}-O^{II} of pristine γ-Al_2O_3, catalyst surface. Transition state denoted with a dagger (‡). The adsorption over the lowest free-energy barrier site pair (Al^{IV}-O^{II}) is shown with the corresponding structure of adsorbent and catalyst {Obtained using Pople 6-311G(d)/MO6-2x}

2.1.1 Identifying the most active site pair for C-H activation

We investigated C-H activation of methane over four different site pairs of pristine γ-Al_2O_3 i.e., Al^{IV}-O^{II}, Al^{IV}-O^{III}, Al^{III}-$O^{III,}$ and Al^{III}-O^{II} through the polar mechanism (Figure 4).

We observed that the site pairs Al^{IV}-O^{II}, Al^{III}-O^{II} and Al^{III}-O^{III} exhibit relatively lower activation free-energy barriers (98.9 kJ/mol, 117.4 kJ/mol and 117.2 kJ/mol, Figure 3) than the other site pair (Al^{IV}-O^{III}, 208.4 kJ/mol). We conclude that the Al^{IV}-O^{II} is the most active site pair for C-H activation. The site pairs with low activation energy possess strong acidic and basic properties due to the low surface coordination number of these site pairs. Generally, as the surface coordination of the metal center increases the Lewis acidity decreases[42, 67-68]

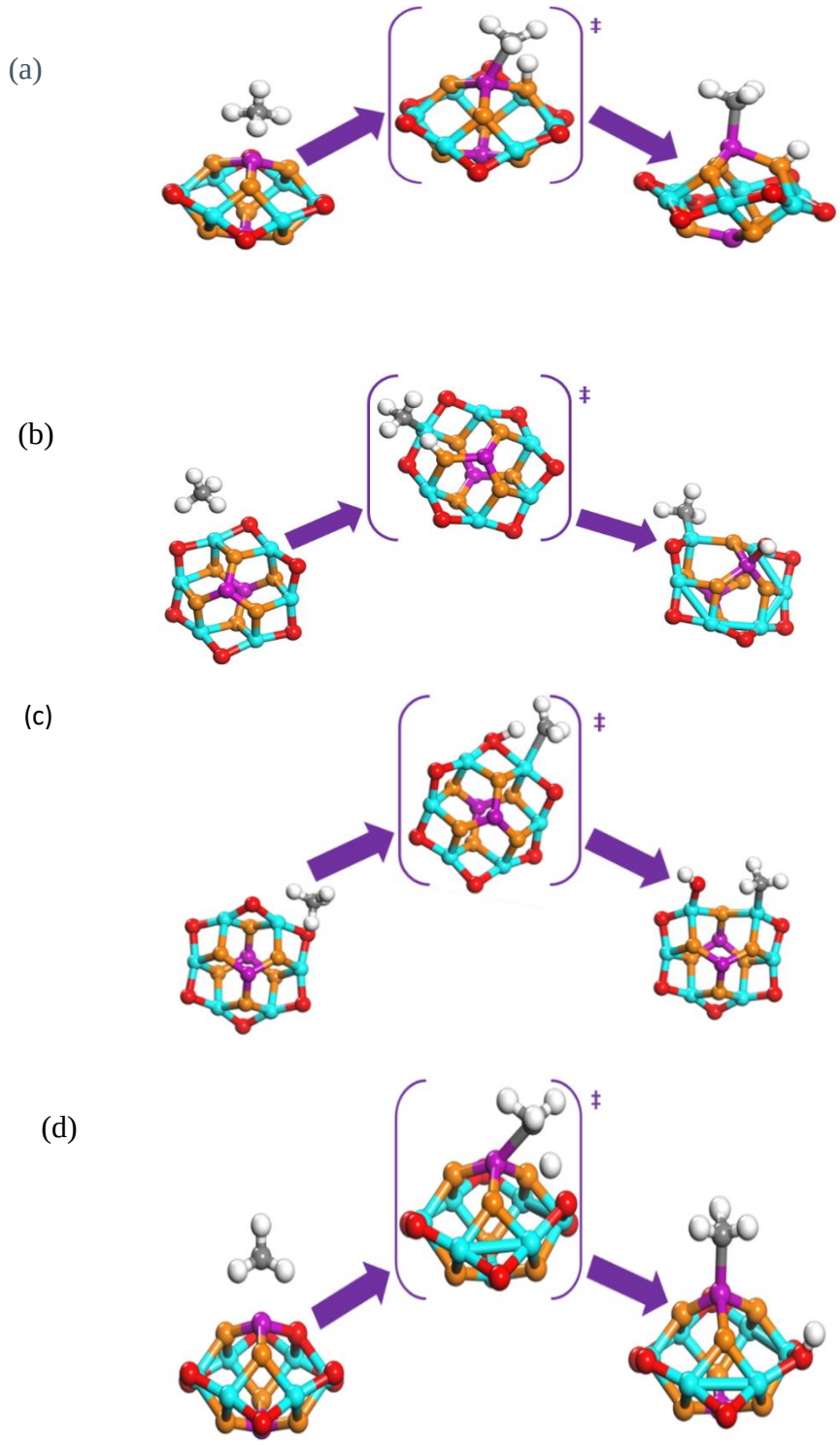

Figure 4**:** Mechanism of C-H bond dissociation of methane over site pair(a) Al^{III}-O^{III} (b) Al^{IV}-O^{III}(c) Al^{IV}-$O^{I\,I}$(d) Al^{III}-O^{II} site pair of γ-Al_2O_3, catalyst surface {Obtained using Pople 6-311G(d)/MO6-2x}

2.2 The radical C-H mechanism

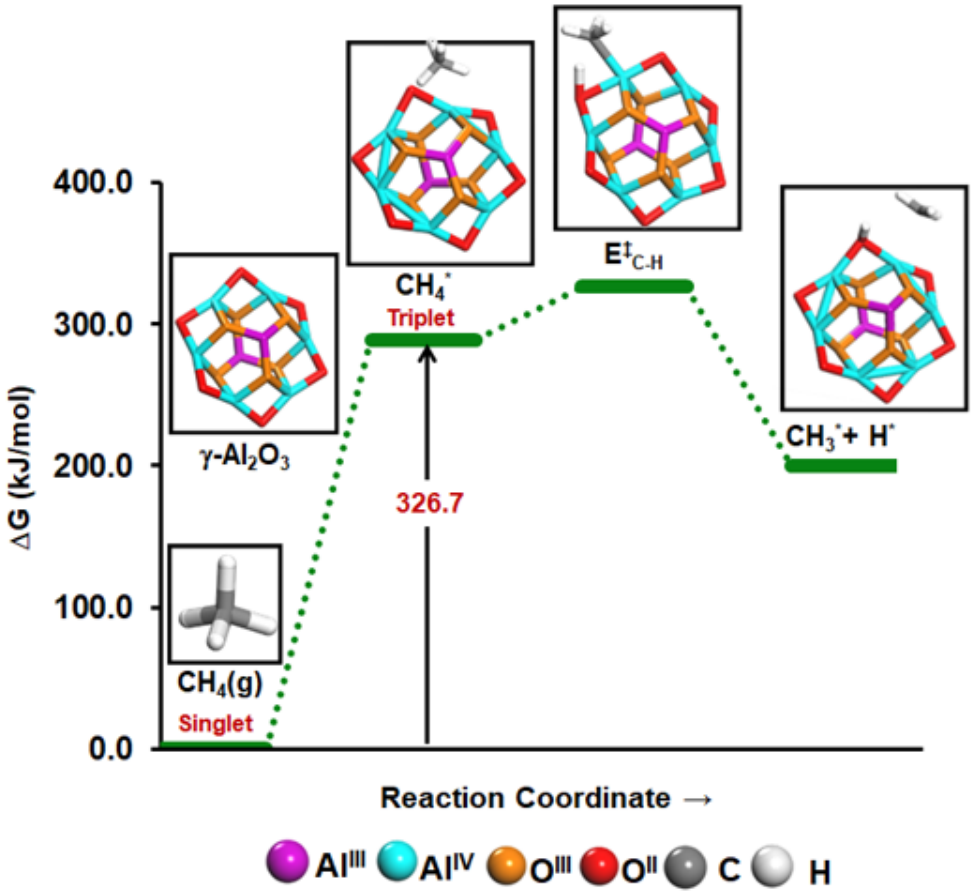

Figure 5: Free-energy barrier profile for C-H bond activation of methane through the radical mechanism on-site pair, Al^{IV}-O^{II} of pristine γ-Al_2O_3 catalyst surface. Transition state denoted with a dagger (‡) {Obtained using Pople 6-311G(d)/MO6-2x}

We investigated the methane activation on the catalyst surface through the radical mechanism on the most active site pair (Al^{IV}-O^{II}) of pristine γ-Al_2O_3 (Figure 5). The radical mechanism is characterized by homolytic dissociation of the C–H bond of methane. In this mechanism, a surface oxygen atom abstracts a hydrogen radical, breaking the C–H bond and leaving a methyl radical in the gas phase.

We studied the radical mechanism in both the singlet as well as triplet state and observed that the radical pathway requires the triplet state for C-H bond activation. The ground state of methane adsorbed on pristine γ-Al_2O_3 is a singlet state and the conversion required remarkably high energy (326.7 kJ/mol, Figure 5) through the radical mechanism. Additionally, all the attempts of finding a singlet transition state were failed and even all the starting points with the singlet product state barrier easily converged to the corresponding reactant state, ruling out the possibility of the singlet-only pathway for the radical mechanism (Figure 6).

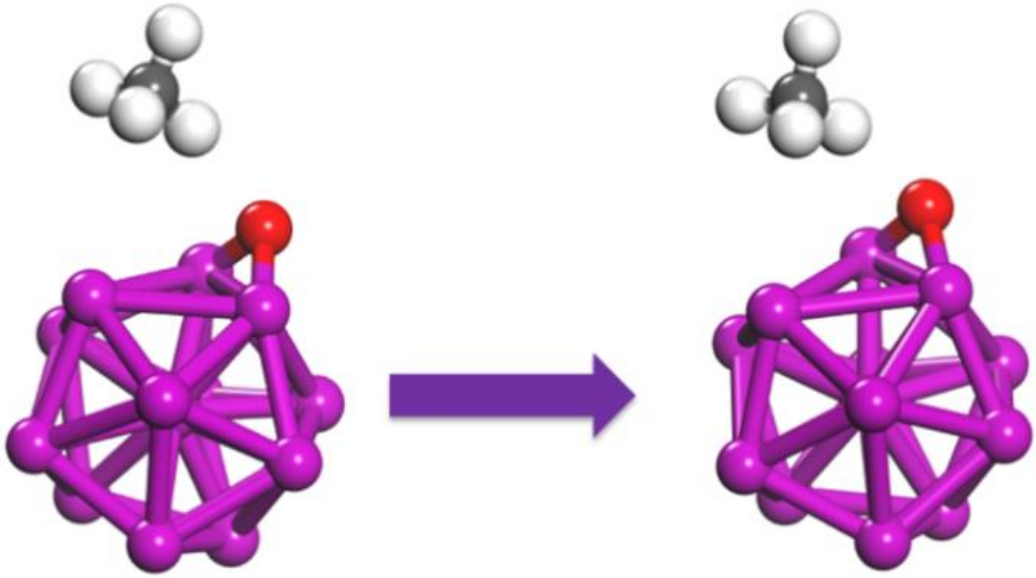

Figure 6: Structural representation of reactant state and product state of aluminum cluster of 13 atoms doped with single oxygen atom in singlet state through radical mechanism {Obtained using Pople 6-311G(d)/MO6-2x}

2.3 Summary

In order to unravel the exact mechanism of C-H activation over metal oxide surface, we investigated methane activation over γ-Al_2O_3 as a catalyst, utilizing the previously reported 20-atom molecular of γ-Al_2O_3[75-76]. we calculated the activation free energy barrier for various symmetrically inequivalent site pairs of γ-Al_2O_3. We focused our study on two probable pathways i.e. the polar and the radical mechanism for C-H activation of methane over γ-Al_2O_3.

The polar mechanism initiates from the cleavage of C-H bond in heterolytic fashion to generate CH_3^- and H^+ species on the surface of the catalyst. Through the course of C-H bond activation, the CH_3^- gets adsorbed on the metal center and H^+ gets stabilized by a surface oxygen site. We conclude that the Al^{IV}-O^{II} possessing the lowest activation energy is the most active site pair for C-H activation, resulting in strong acidic and basic properties due to the low surface coordination number of this site pair. On the other hand, the radical mechanism proceeds via dissociation of C-H bond to generate hydrogen radical which gets adsorbed over an oxygen site on the surface, and methyl radical remains in the gas phase. The methane activation on the catalyst surface through the radical mechanism was studied on the most active site pair (Al^{IV}-O^{II}) of pristine γ-Al_2O_3 in both singlet and triplet state and it was observed that the singlet state did not yield a transition state, indicating that the radical pathway is not viable in singlet state. Also we observed a significantly high activation energy (326.7kj/mol) for the radical mechanism. It can be inferred that the radical mechanism proceeds via energy intensive triplet state. It is therefore concluded that the polar mechanism on γ-Al_2O_3, specifically at the Al^{IV}-O^{II} site pair, is more feasible for methane C-H activation compared to the radical mechanism. Also, doping with elements like boron and gallium further influences the catalytic activity by potentially lowering activation barriers and enhancing the overall efficiency of the process. These results confirm the preference of the polar mechanism over the radical mechanism for methane activation on γ-Al_2O_3. This finding is in line with a previous study on γ-Al_2O_3 periodic surfaces.[36]

Allegra A. Latimer in their study addressed the challenge of finding efficient catalysts for converting methane into valuable chemicals and fuels, a problem that has persisted

for over a century without a viable industrial solution. The authors proposed a unifying framework using hydrogen affinity (E_H) as a universal descriptor to predict methane C–H activation barriers across a diverse range of catalysts[78]. Their study aimed to simplify the computationally expensive process of transition state (TS) barrier calculations, thereby accelerating the discovery of new materials for methane activation. They explored various categories of catalysts for C-H activation, including non-noble metals, specific oxides, cation-exchanged zeolites, metal-organic frameworks (MOFs), and decorated graphene nanosheets. These Catalysts generally exhibited one of two TS geometries. Some were able to stabilize the methyl group via unsaturated surface atoms, while others, when stabilization was not feasible, proceeded via a radical-like TS[79]. Certain oxides and non-noble metals, possessing unsaturated surface atoms that stabilized the methyl group in the transition state. On the other hand, a radical-like transition state was seen when the CH_3surface interaction was energetically unfavourable or geometrically inaccessible[80-81].

Previous research has demonstrated that methane activation can happen through one of two routes,[18] the polar and the radical: In the first, the catalyst stabilizes the methyl group, whereas in the second, a radical-like intermediate is generated and the OH bond, not the surface, stabilizes the methyl group[82]. There are clear differences in the energy scaling behaviour of transition states (TS) between these two paths. The linear dependency of TS energies on more compute-friendly descriptors, like the energy of the final state or a crucial adsorbate, is typically described using TS scaling relationships. These connections make it easier to do first-pass catalyst screening since they let estimate the total surface area (TS energy) before completing a costly barrier calculation[83].Systems that follow a radical-like pathway's methane activation TS energies scale with the active site's hydrogen abstraction energy[20, 34] whereas metals and transition metal compounds that follow a surface-stabilized pathway's TS energies scale with the energy of the final state [84-85].In order to estimate the TS energy using the appropriate scaling relation, it is crucial to know which catalyst features favour one pathway over another. It is obvious that the radical pathway will be supported in catalysts with isolated active sites, such as zeolites and other porous materials, because of the great distance between active sites[83].Similarly, it has long been believed that

catalysts with a large density of active sites, like metals, will activate methane through methyl-surface stabilization since a surface-stabilized pathway looks more energetically beneficial than the creation of a methyl radical[80, 86].

Chapter 3: Effect of Dopants on C-H Activation

To design improved C-H activation catalysts, we extended our investigations to identify dopants that can improve the activity of γ-Al_2O_3. Specifically, we doped γ-Al_2O_3 with trivalent dopants (boron and gallium). We investigated the activation of methane over different metal dopant site pairs such as Ga^{IV}-O^{II}, Ga^{IV}-O^{III}, Ga^{III}-O^{III}, and Ga^{III}-O^{II}, B^{IV}-O^{II}, B^{IV}-O^{III}, B^{III}-O^{III}, B^{III}-O^{II} by initially doping with only one metal site of the catalyst surface[41].

3.1 Doping with Gallium

We studied the mechanism of doping the catalyst with Gallium over different metal dopant site pairs such as Ga^{IV}-O^{II}, Ga^{IV}-O^{III}, Ga^{III}-O^{III}, and Ga^{III}-O^{II}. (Figure 7) In Ga-doped systems, we noticed low activation barriers on local site pairs, where the dopant was added, Ga^{IV}-O^{II} (101.6kJ/mol, Figure 8b) and Ga^{III}-O^{III} (106.9kJ/mol, Figure 8b.) whereas site pair Ga^{IV}-O^{III} (170.8 kJ/mol) shows relatively higher activation free-energy barrier than Ga^{IV}-O^{II}, Ga^{III}-O^{II} and Ga^{III}-O^{III} site pairs

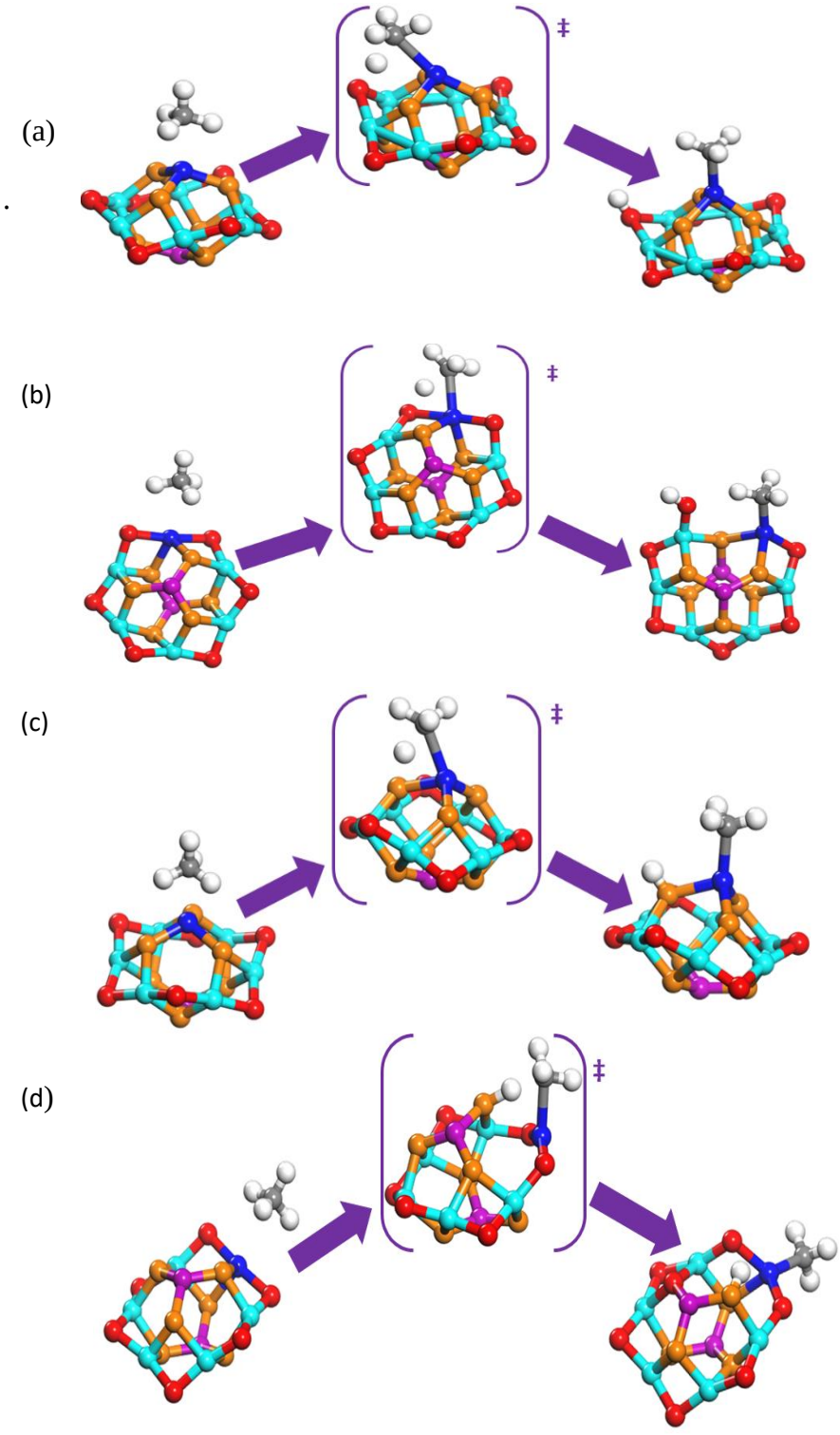

Figure7: Mechanism of C-H bond dissociation of methane over site pair (a) Ga^{III}-$O^{II,}$ (b) *Ga^{IV}-O^{II} (c)Ga^{III}-O^{III} (d) Ga^{IV}-O^{III} of doped* γ-Al_2O_3 catalyst surface.

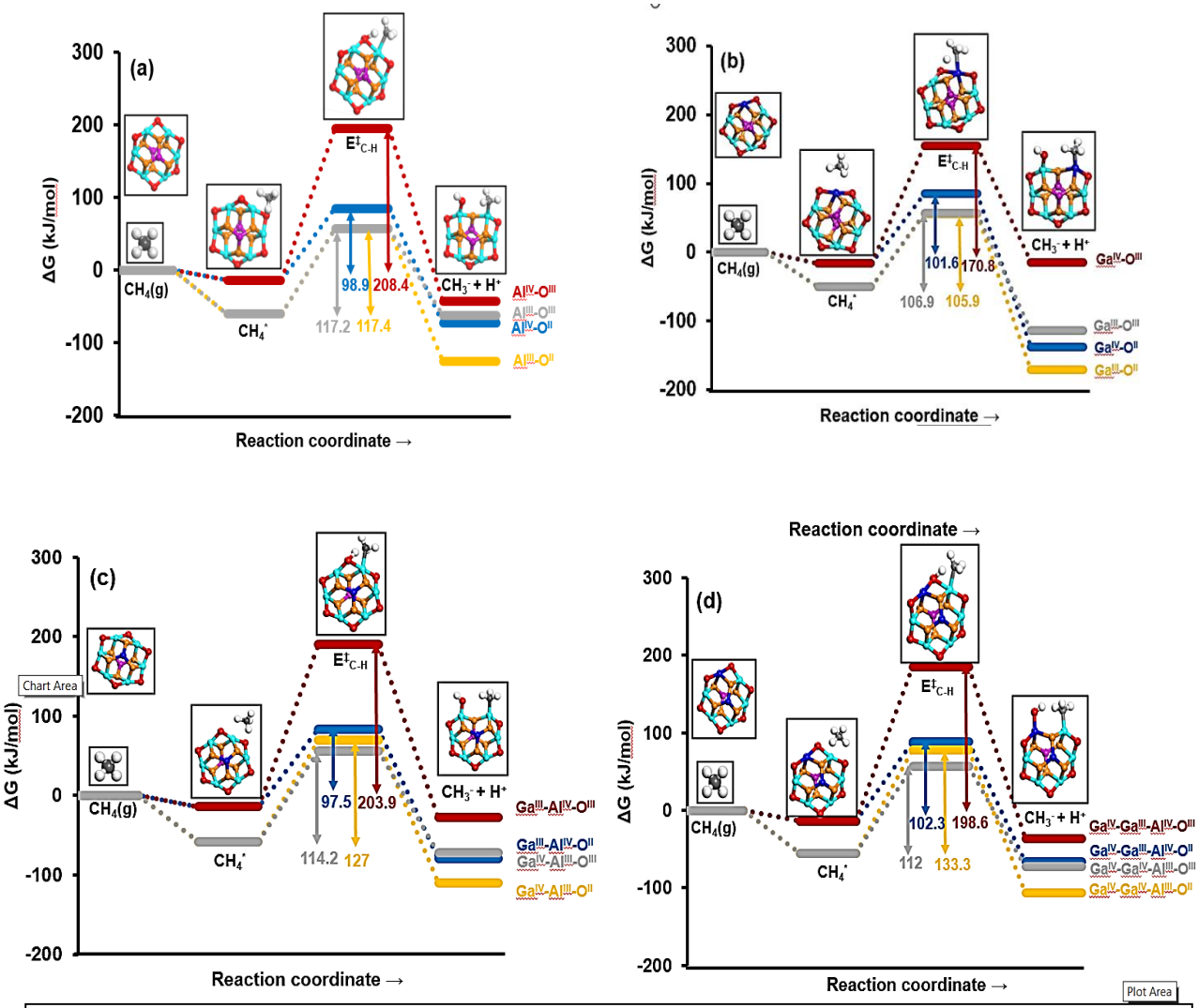

Figure 8: C-H bond activation free-energy profiles of methane on a) tricoordinated and tetracoordinated Al^{IV}-O^{II}, Al^{IV}-O^{III}, Al^{III}-O^{II}, Al^{III}-O^{III} site - pairs of pristine γ-Al_2O_3 (b), Ga^{IV}-O^{II}, Ga^{IV}-O^{III}, Ga^{III}-O^{II}, Ga^{III}-O^{III} site-pairs of Ga-doped γ-Al_2O_3 (c) adjacent tricoordinated and tetracoordinated (Al^{III} , Al^{IV}) single gallium atom doped γ-Al_2O_3 ,(d) neighboring tricoordinated and tetracoordinated (Al^{III} , Al^{IV}) double gallium atom doped γ-Al_2O_3 catalyst surface respectively via the polar pathway {Obtained using Pople 6-311G(d)/MO6-2x}

3.1.1Effect of gallium doping at non local sites (single doping)

As seen from Figure 8a and 8b, doping significantly reduces the activation free-energy barrier for most of the site-pairs (significantly reduces for tetracoordinated site, Ga^{IV}-O^{III}, 208.4 → 170.8 kJ/mol) but slightly increases the activation free-energy barrier on the site pair Al^{IV}-O^{II} (98.9 kJ/mol, pristine γ-Al_2O_3) Therefore, we further extended our analysis to study the effect of dopant on non-local (neighboring) sites of dopant, and

interestingly, we noticed the effect of dopant (gallium) is not only limited to the local dopant sites, indeed, it is also more pronounced on the site-pairs adjacent to the dopant (neighboring sites) (Figure 8c and 8d). Initially, we started to study the non-local effect of dopant (Ga) with a single gallium atom doped γ-Al_2O_3 catalyst surface. We observed the effect of Ga^{IV} (doping on tetracoordinated site) over neighboring Al^{III}-O^{II} and Al^{III}-O^{III} site-pairs and Ga^{III} (doping on tri-coordinated site) on neighboring Al^{IV}-O^{II} and Al^{IV}-O^{III} site-pairs. We found that Ga^{III} effectively influence the C-H bond activation on Al^{IV}-O^{II} site-pair with an activation free-energy barrier (97.5 kJ/mol) (Figure 8a and 8c The other non-local site pairs of doped structures also show lower barrier (Al^{III}-O^{III}, 114.2 kJ/mol, Al^{IV}-O^{III}, 203.9 kJ/mol, Figure 8c) than the pristine γ-Al_2O_3 site-pairs.[41].

3.1.2 Effect of gallium doping at non local sites (Double doping)

As we found the positive effect of doping on accelerating the C-H bond activation, we further increase the content of dopant (gallium). Next, we studied the double-doped γ-Al_2O_3 catalyst (Ga^{IV}-Ga^{IV}_γ-Al_2O_3, Ga^{IV}-Ga^{III}_ γ--Al_2O_3) (Figure 9)

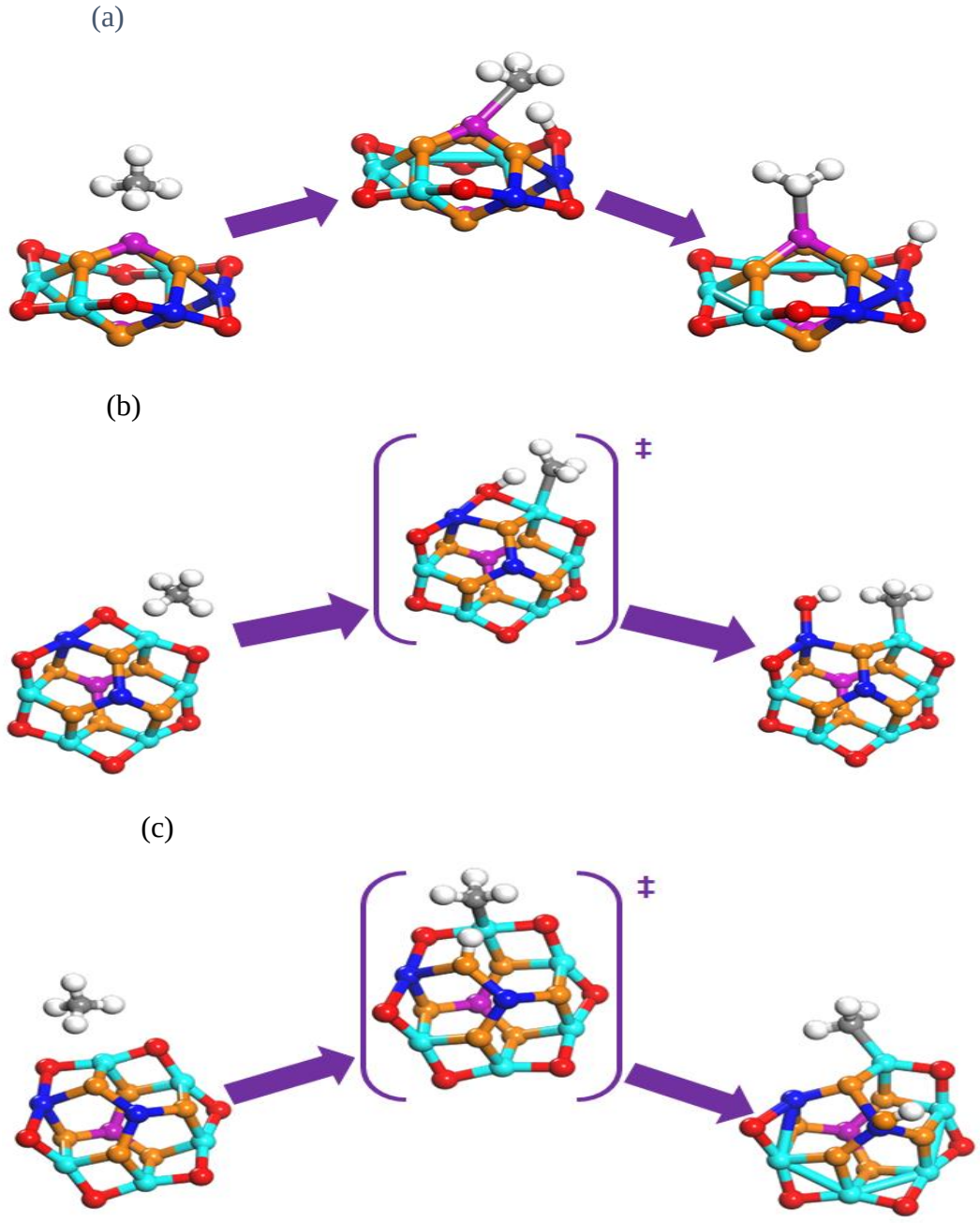

Figure 9: Mechanism of C-H bond dissociation of methane over site pair(a) Al^{III}-O^{II} of(b) Al^{III}-O^{II} (c) Al^{III}-O^{III} of two gallium (Ga^{III} and Ga^{IV}) doped γ-Al_2O_3catalyst surface {Obtained using Pople 6-311G(d)/MO6-2x}

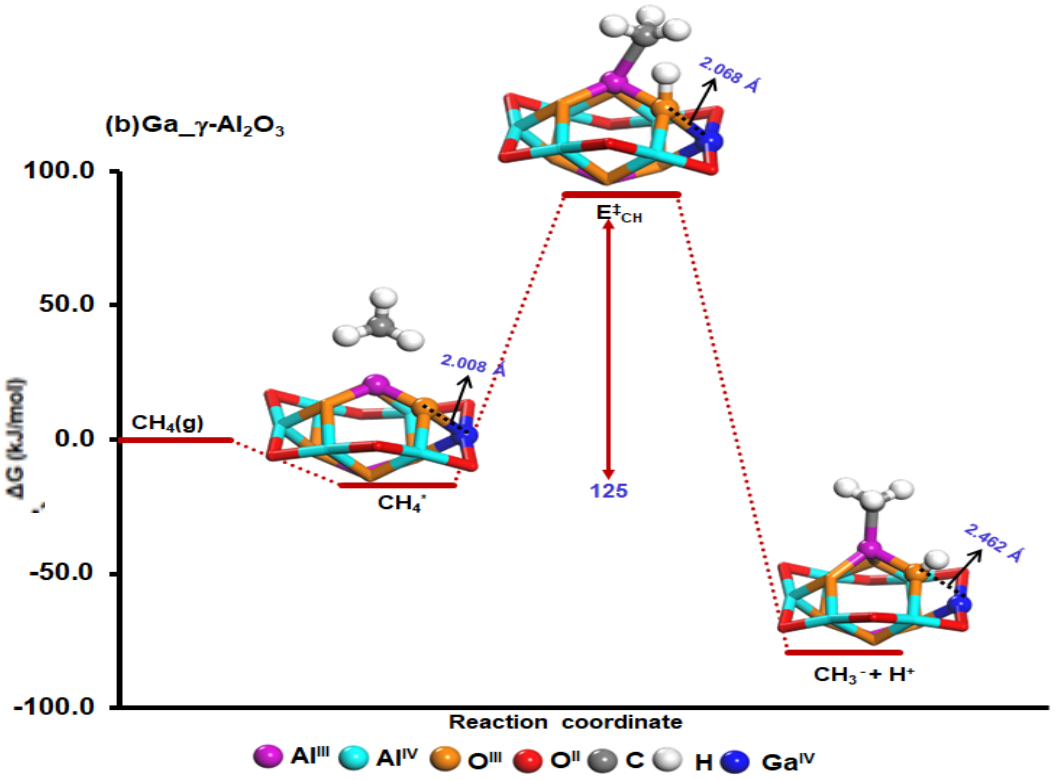

Figure10: The C-H bond activation free energy profile of methane on the site pair Al^{III}-O^{III} of gallium doped γ-Al2O3 catalyst surface. The bond distances between Ga^{IV} and O^{III} are shown with dotted lines. {Obtained using Pople 6-311G(d)/MO6-2x}

We noticed that even in a double doped system, the effect of doping on the non-local Al^{IV}-O^{II} site-pair (102.3 kJ/mol) is consistent with the activation free-energy barrier for Al^{IV}-O^{II} site-pair (98.9 kJ/mol) of pristine γ-Al_2O_3 (Figure 8 c, d). Although no significant reconstruction takes place after doping (the pristine γ-Al_2O_3 and Ga-doped γ-Al_2O_3 systems are structurally similar), the activation free-energy barrier for the site-pair Al^{III}-O^{II} (117.4 kJ/mol) of pristine γ-Al_2O_3 is reduced to 105.9 kJ/mol for single gallium doping (Ga^{IV} Al^{III}-O^{II}). (Figure 8a-d). On further increasing the content of Ga, the activation free-energy barrier reduced by 5-9 kJ/mol for some of the site-pairs (Al^{III}-O^{III}, Al^{IV}-O^{III}) and for the rest of the site-pairs, the activation free-energy barriers

remain consistent with pristine γ-Al_2O_3 site-pairs. This is due to the increasing heterogeneity in the single Ga doped-γ-Al_2O_3 catalyst. The heterogeneous metal environment in the Ga doped -γ-Al_2O_3 catalyst lowers the coordination of Al^{III}-O^{III} to Al^{III}-O^{II} with increasing adjacent Ga^{IV}-O^{III} bond distance (reactant, 2.008 Ǻ → 2.462 Ǻ, product) (Figure 10). This indicates that the small structural change can improve the catalytic efficiency (structural rearrangement reduces the activation free- energy barrier for C-H bond activation). On the other hand, Al^{IV}-O^{III} site-pair exhibits high activation free energy barrier in pristine and Ga-doped γ-Al_2O_3 catalyst (Figure 8a-d). From the above discussion we inferred that

(1) the non-local (neighboring) effect of Ga doping was not observed on Al^{IV}-O^{III} site-pair,

(2) Al^{IV} and O^{III} sites (high activation free energy barrier site-pair) remain in high coordination state, hence the Al^{IV}-O^{III} site-pair was considered to be least preferred site-pair for methane activation.

(3) Apart from doped site-pair, the non-local site-pairs can also participate in C-H bond activation with proper concentration of dopant required to activate the catalytic activity of non-local site-pairs.

3.2 Doping with Boron

Unlike to that of Gallium doping, we observed that in the case of the boron-doped γ-Al_2O_3 catalyst system, severe reconstructions take place in the structure as a result of doping (Figure 11 a-d)

This reconstruction respectively can be attributed to the preference of boron to the trigonal planar geometry due to the absence of empty d-orbitals We noticed that the

$B^{III'}$-O^{II}, $B^{III'}$-O^{III} and B^{III}-$O^{II'}$ site pairs show relatively lower activation free-energy barriers (207.1 kJ/mol, 136 kJ/mol, and 206 kJ/mol, Figure 12a) than B^{III}-O^{II}

(267.3kJ/mol) site pairs (since the tetracoordinated boron sites get transformed to new tricoordinated ($B^{III'}$-O^{II}, $B^{III'}$-$O^{II'}$) state during optimization whereas original

tricoordinated B^{III}-O^{III}, B^{III}-O^{II} site pairs remain in their tricoordinated state)

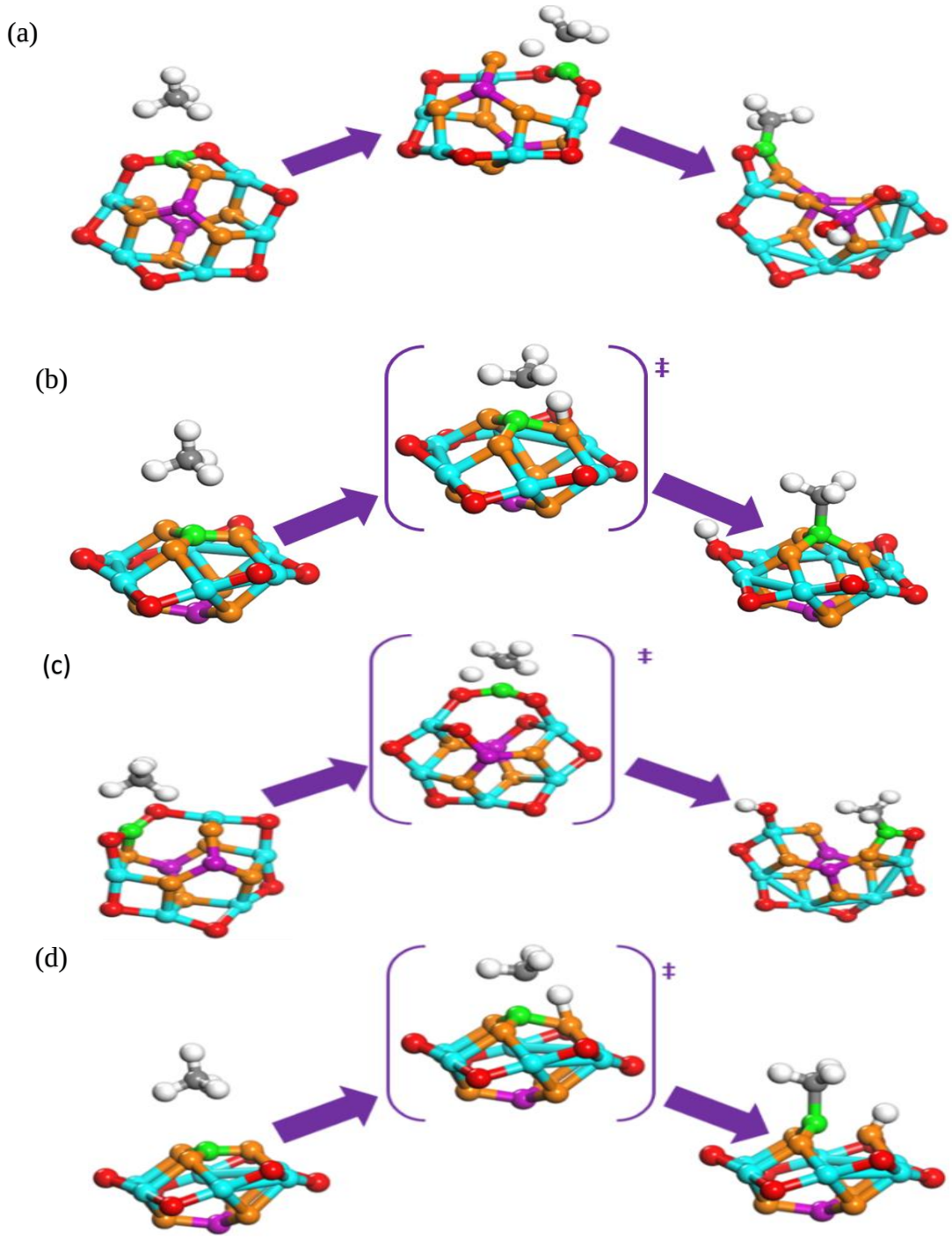

Figure 11: Structural representation of C-H bond dissociation over(a)B^{IV}-O^{III} (b) B^{III}-O^{II} (c B^{IV}-O^{II} (d) B^{III}-O^{III} site pair of doped γ-Al_2O_3 catalyst surface {Obtained using Pople 6-311G(d)/MO6-2x

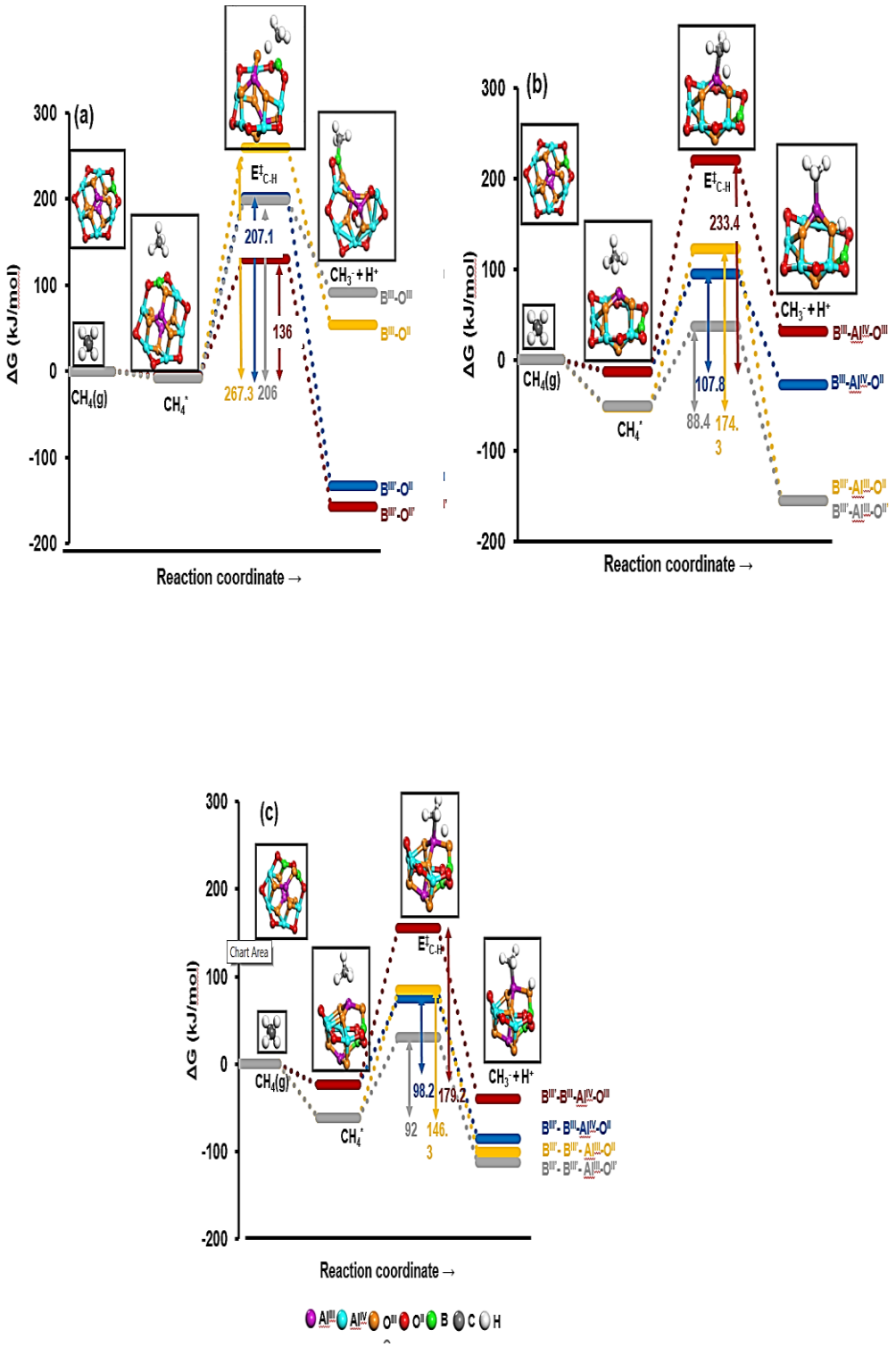

Figure 12: C-H bond activation free-energy profiles of methane on (a) tricoordinated and tetracoordinated B^{IV}-O^{II}, B^{IV}-O^{III}, B^{III}-O^{II}, B^{III}-O^{III} site - pairs of boron doped γ-Al_2O_3 (b) neighboring tricoordinated and tetracoordinated (Al^{III}, Al^{IV}) single boron atom doped γ-Al_2O_3 (c) neighboring tricoordinated and tetracoordinated (Al^{III} , Al^{IV}) double boron atom doped γ-Al_2O_3 catalyst surface respectively via the polar pathway. {Obtained using Pople 6-311G(d)/MO6-2x}

The apparent lower coordination number (three) of ($B^{III'}$) favors the adsorption and activation of the methane, as evident by more exothermic reaction energies for methane activation on the site pairs involving ($B^{III'}$) sites. However, on the site pairs involving tricoordinated (originally present Boron sites (B^{III}), the adsorption and activation of methane was relatively less preferred due to the inherent preference of boron to attain Tri coordination.

3.2.1 Effect of Boron doping at non local site (single doping)

We started with examining the effect of Boron doping the neighboring sites of single boron doped γ-Al_2O_3 catalyst. In this case, we noticed that the modified tricoordinated boron ($B^{III'}$) site influences the catalytic activity of neighboring Al^{III}-O^{III} and Al^{III}-O^{II}

site pairs, and similarly, the effect of tricoordinated (B^{III}) over Al^{IV}-O^{II} and Al^{IV}-O^{III} site pairs were seen. (Figure 13)

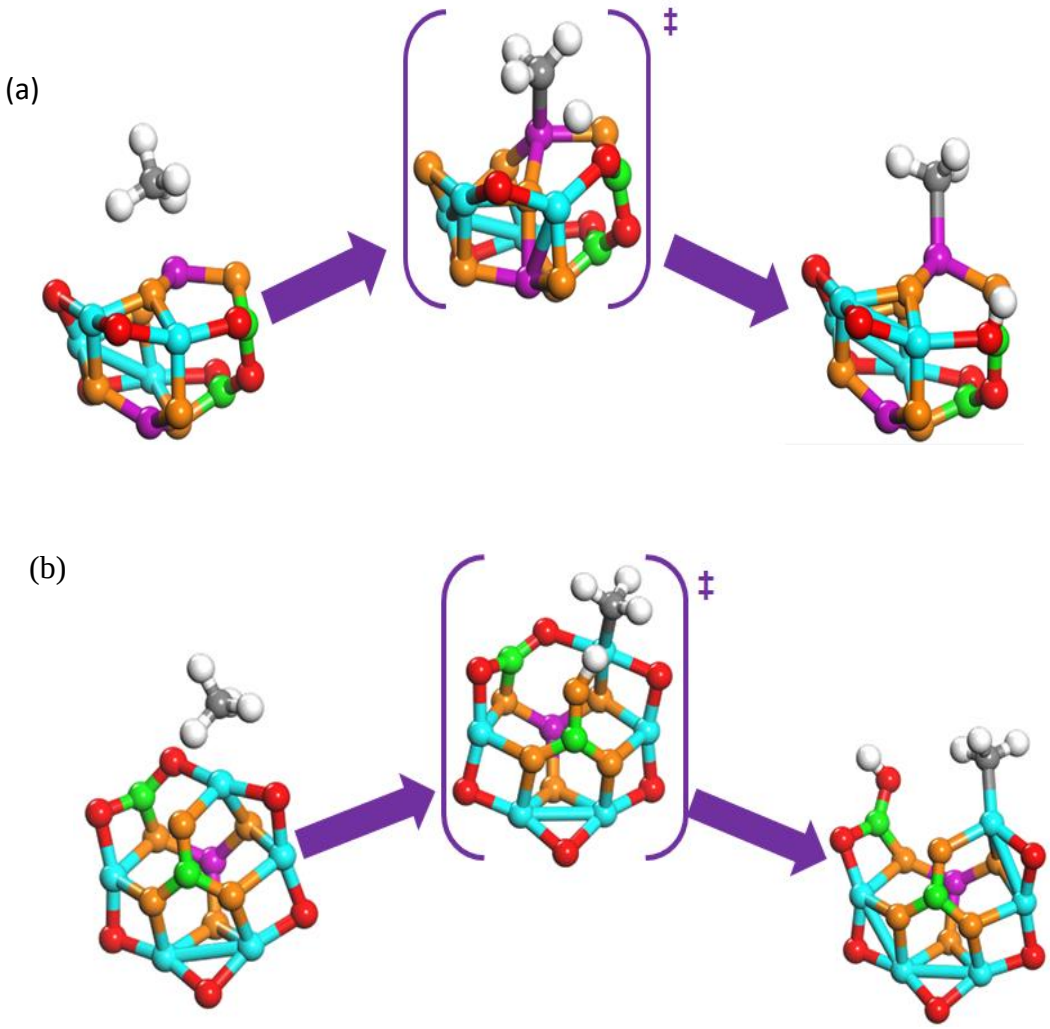

Figure 13: Mechanism of C-H bond dissociation of methane over site pair (a)Al^{III}-O^{II} (b) Al^{III}-O^{III} of two boron atoms (B^{IV} and B^{III}) doped γ-Al_2O_3 catalyst surface. {Obtained using Pople 6-311G(d)/MO6-2x}

We observed a comparatively lower activation free-energy barrier on Al^{III}-O^{III} site-pair (88.4 kJ/mol) of the boron doped catalyst than the Al^{III}-O^{III} site-pair (117.2 kJ/mol) of pristine γ-Al_2O_3. (Figure 12b, 8a). This unexpected behavior of boron-doped system was attributed to the structural rearrangement (reconstruction) of the B-doped γ-Al_2O_3 catalyst. The boron doping makes $B^{III'}$-O^{III} coordination weak, as evident by large B-O bond distance (2.942 Å) (Figure 14), making O^{III} further under-coordinated ($O^{II'}$). Although boron doping influences the catalytic activity of non-local site-pairs of γ-Al_2O_3 catalyst but the activation free energy barrier for these site-pairs were found to

be higher (Al^{III}-O^{II}, 174 kJ/mol, Al^{IV}-O^{II}, 107.8 kJ/mol, Al^{III}-O^{III}, 233.4 kJ/mol) than the site-pairs of pristine and Ga doped γ-Al_2O_3 (Fig 8 a to d)

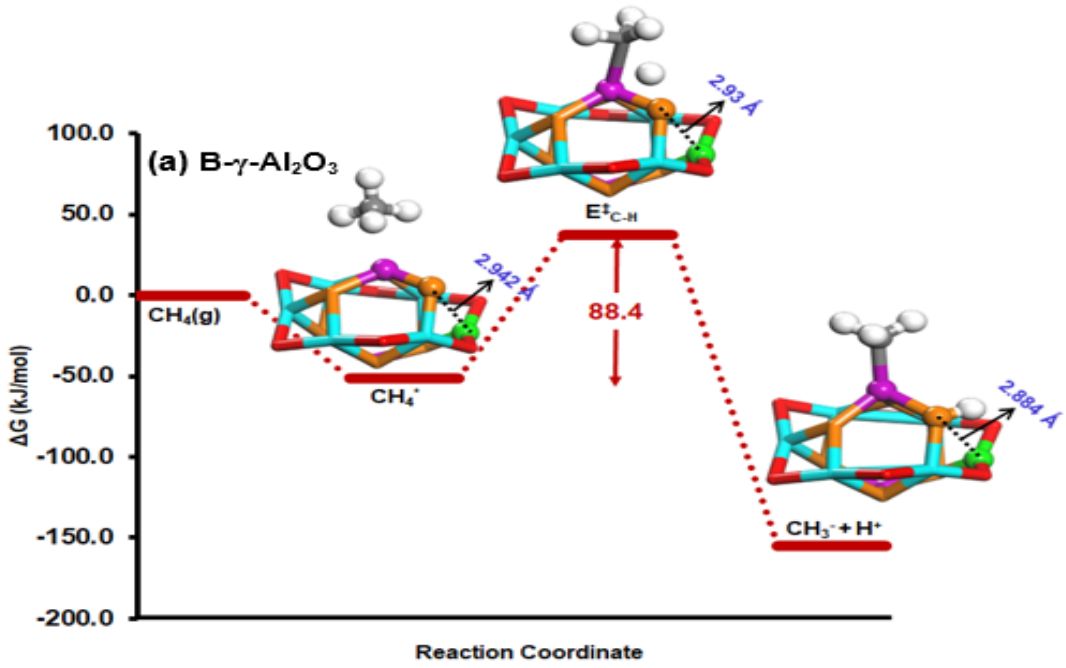

Figure 14: The C-H bond activation free energy profile of methane on the site pair Al^{III}-O^{III} of boron-doped γ-Al_2O_3 catalyst surface. The bond distances between B^{IV} and O^{III} are shown with dotted lines {Obtained using Pople 6-311G(d)/MO6-2x}

3.2.2 Effect of Boron doping at non local site (Double doping)

Next, we doped the pristine γ-Al_2O_3 with two boron atoms on tri- and tetracoordinated sites ($B^{III'}$-$B^{III'}$- γ-Al_2O_3, $B^{III'}$-B^{III}- γ-Al_2O_3 (Figure 12c). The single boron atom doped and double boron doped γ-Al_2O_3 catalyst systems show similar trend of activation free-

energy barriers (Al^{III}-$O^{II'}$, 179.2 kJ/mol > Al^{IV}-O^{II}, 146.3 kJ/mol > Al^{IV}-O^{III}, 98.2 kJ/mol >Al^{IV}-O^{III}, 92 kJ/mol) (Figure 12 b-c). Thus, we conclude that

(1) gallium and boron doping improve the catalytic activity of non-local (Al-O) site-pairs of Ga- / B-doped γ-Al_2O_3 catalyst,

(2) Ga-doped γ-Al_2O_3 catalyst system is more active than B-doped -γ–Al_2O_3, as evident by lower activation barriers for different local and non-local site-pairs in Ga-doped system.

(3) In addition to Lewis acidity and basicity of pristine γ-Al_2O_3 or doped γ-Al_2O_3, the other properties like structural orientation (varies from atom to atom) is also responsible to alter the catalytic activity of γ-Al_2O_3.

3.3 Summary

In order to study the effect of doping on the catalytic activity of γ-Al_2O_3 for methane C-H bond activation, we doped the catalyst with trivalent elements like boron and gallium at various metal dopant site pairs (e.g., Ga^{IV}-O^{II}, Ga^{III}-O^{III}, B^{III}-O^{II}). We observed significantly lower activation barriers for Ga^{IV}-O^{II} and Ga^{III}-O^{III} site pairs (101.6 kJ/mol and 106.9 kJ/mol respectively). Among all the sites, the highest activation barrier was seen for Ga^{IV}-O^{III} site, (170.8 kJ/mol). Doping not only influences the local site but has an impact on the neighboring site pairs as well. Ga^{III} doping reduces the activation barrier for Al^{IV}-O^{II} to 97.5 kJ/mol. Non-local site pairs like Al^{III}-O^{III} (114.2 kJ/mol) and Al^{IV}-O^{III} (203.9 kJ/mol) show reduced barriers compared to pristine γ-Al_2O_3. As we dope the catalyst with two Gallium atoms, we see that the double-doped systems (e.g., Ga^{IV}-Ga^{IV}) show consistent effects with reduced barriers for non-local site pairs. We could also observe that the activation barriers for Al^{III}-O^{II} and Al^{IV}-O^{III} are reduced by 5-9 kJ/mol with increased gallium content. The Al^{IV}-O^{III} site pair remains the least preferred due to high activation energy and high coordination state. However, we observed significant structural reconstruction in the catalyst structure upon doping with Boron due to its preference to stay in trigonal planer geometry. During optimization, new tricoordinated boron sites($B^{III'}$) are formed that show lower activation barriers than tetracoordinated sites. We observed that $B^{III'}$-O^{II}

and $B^{III'}$-O^{III} site pairs exhibit lower activation barriers (207.1 kJ/mol and 136 kJ/mol) compared to B^{III}-O^{II} (267.3 kJ/mol). Doping with boron influences the catalytic activity at neighbouring sites Al^{III}-O^{III} and Al^{IV}-O^{II} as well. We see that for Al^{III}-O^{III} site pair, the activation barrier reduces to 88.4kJ/mol. A similar trend was observed even after increasing the content of dopant. We observed lower activation barriers for Al^{III}-$O^{II'}$(179.2kJ/mol) and Al^{IV}-O^{III}(92kJ/mol) compared to single boron doped system. Hence, it can be concluded that both gallium and boron doping enhance the catalytic activity of γ-Al_2O_3 by reducing activation energy barriers for methane C-H activation. Generally, we can say that Gallium-doped γ-Al_2O_3 is more effective than boron-dopedγ-Al_2O_3. Also we can observe that in addition to Lewis acidity and basicity, structural orientation and coordination states play significant roles in determining the catalytic efficiency.

Chapter 4: Natural Bond Order (NBO) Charge and Molecular Orbital Analysis

We further performed NBO charge analysis to understand the charge localization for different metal centers (Al, B, and Ga) of pristine γ-Al_2O_3, boron and gallium doped γ-Al_2O_3. We noticed comparatively higher charge localization over all the site-pairs (Al^{IV}-O^{II}, Al^{IV}-O^{III}, Al^{III}-O^{II}, Al^{III}-O^{III}) of pristine γ-Al_2O_3 than B- and Ga- doped γ-Al_2O_3 site pairs (Table 1). Specifically, aluminum tricoordinated (Al^{III}) (Al^{III}-O^{III}, Al^{III}-2.058) (Al^{III}-O^{II}, Al^{III}- 2.069) sites show more electron-deficient character, followed by gallium (Ga^{III}) doped site-pairs[41]. Boron doped site pairs show the lowest charge localization. To understand the effect of B and Ga doping, we further computed NBO charges over neighboring aluminum site-pairs (Al^{III}-O^{II}, Al^{III}-O^{III}, Al^{IV}-O^{II}, Al^{IV}-O^{III}) of B and Ga-doped γ-Al_2O_3 (Table 1). The adjacent aluminum site pairs (Al^{III}-O^{II}, Al^{III}-O^{III}) of B and Ga-doped systems exhibit similar charge distribution (marginal variation) as tri- and tetracoordinated aluminum sites of pristine γ-Al_2O_3 (Table 1). Since the NBO charge analysis does not show significantly large difference of charge localization on various tri- and tetracoordinated site-pairs, we used proton affinity (PA) as a descriptor to explain the basicity of O^{II} and O^{III} sites (Table 1). We noticed that the non-local sites (O^{II} and O^{III}) of Ga and B doped systems show appreciably large proton affinity than pristine γ-Al_2O_3. This indicates the active participation of dopant to improve the catalytic activity of γ-Al_2O_3.

On inspecting the highest occupied molecular orbital (HOMO) and lowest unoccupied molecular orbital (LUMO) (Figure 15), we notice that for pristine γ-Al_2O_3 the lowest energy orbitals were found on Al^{III}- site whereas highest occupied molecular orbitals were observed mostly over O^{II}- and partially on O^{III}- sites. This suggests the relatively higher acidity and basicity of Al^{III}-O^{II} site-pair than other Al-O site-pairs in pristine γ-Al_2O_3.

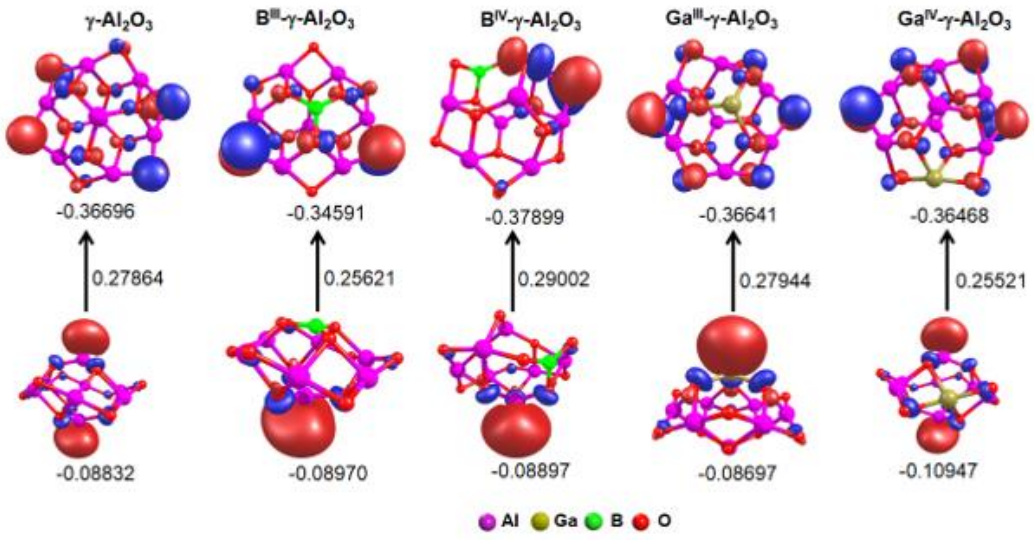

Figure15: Frontier orbitals (±0.05 au) in pristine γ-Al_2O_3, boron and gallium doped γ-Al2O3 catalysts {Obtained using Pople 6-311G(d)/MO6-2x}

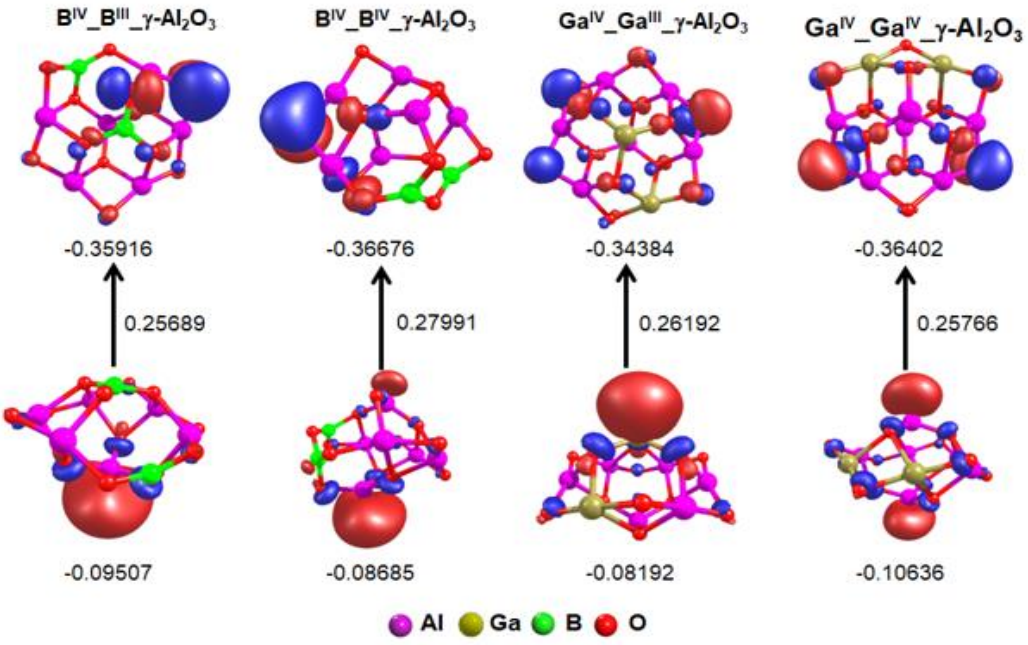

Figure 16: Frontier orbitals (±0.05 au) on the non-local sites in boron and gallium doped γ-Al_2O_3 catalysts {Obtained using Pople 6-311G(d)/MO6-2x}

Next, we analyzed the molecular orbitals of B and Ga-doped γ-Al_2O_3. We notice that

(1) the LUMO energy orbitals were observed over tricoordinated gallium site (Ga^{III}) but not on the tricoordinated B^{III} and tetracoordinated Ga^{IV} (Figure 15)

(2) In the case of tricoordinated (B^{III}-doped γ-Al_2O_3) and tetracoordinated (Ga^{IV}-doped γ-Al_2O_3), lowest unoccupied molecular orbitals (LUMO) were localized more on neighboring Al-O site pairs (Figure 15, 16).

From the molecular orbital analysis for pristine and Ga-doped system we noticed that the lowest unoccupied orbitals were found significantly on tricoordinated metal sites and HOMO on dicoordinated oxygen, OII. This indicate that Al and Ga both possess similar acidity but they differ in terms of atomic size. Therefore, the tricoordinated metal (Al/Ga) and dicoordinated oxygen involving sites of pristine and Ga-doped γ-al_2O_3 show lower activation free-energy barriers M^{IV}-O^{III} (M=Al/Ga) site-pair. This was found to be in good agreement with proton affinity of tri-and tetracoordinated sites (Table 1).

This suggests the fact that as the coordination number decreases Lewis acidity and basicity increases.[57] On the other hand, B-doped system shows a contrasting behavior. Here we observed that the lowest unoccupied orbitals were not found on tricoordinated boron site but it was more localized on neighboring site-pairs (Figure 15). Additionally, the NBO charges do not show large difference for Al and Ga sites whereas significant difference was noticed for B-doped sites (Table 1*). This suggests that the acidity of B is appreciably lower than Al and Ga (due to absence of empty d orbital). The similar effect we noticed with high activation free-energy barriers for most of the site-pairs of B-doped γ-Al_2O_3 (Figure 12a).

Table 1* The Natural Bond Orbital (NBO) analysis and Proton Affinity for different site pairs of pristine γ-Al_2O_3, boron and gallium single doped and double doped system. QM (charges on the metal, Al, B, Ga) (electron acceptor) and QO (charges on the oxygen) (electron donor atom) have been presented in the table 1

		NBO Charges			Proton affinity
Systems	Acceptor	Q_M	Donor	Q_O	PA(kj/mol)
Al^{IV}-O^{II}	AI(IV)	2.034	O(II)	-1.359	-880.624
Al^{IV}-O^{III}	AI(IV)	2.034	O(III)	-1.413	-778.400
Al^{III}-O^{III}	AI(III)	2.068	O(III)	-1.42	-778.400
Al^{III}-O^{II}	AI(III)	2.059	O(II)	-1.348	-880.624
Ga^{IV}-O^{II}	Ga(IV)	1.908	O(II)	-1.30-2	-870.051
Ga^{IV}-O^{III}	Ga(IV)	1.909	O(III)	-1.397	-791.068
Ga^{III}-O^{III}	Ga(III)	1.984	O(III)	-1.388	-791.068
Ga^{III}-O^{II}	Ga(III)	1.984	O(II)	-1.388	-870.051
B^{IV}-O^{II}	B(IV)	1.314	O(II)	-1.075	-811.804
B^{IV}-O^{III}	B(IV)	1.325	O(III)	-1.26	-929.077
B^{III}-O^{III}	B(III)	1.383	O(III)	-1.187	-929.077
B^{III}-O^{II}	B(III)	1.365	O(II)	-1.345	-811.804
Ga^{III}_Al^{IV}_O^{II}	AI(IV)	2.035	O(II)	-1.357	-1528.216
Ga^{III}_Al^{IV}_O^{III}	AI(IV)	2.036	O(III)	-1.369	-1490.002
Ga^{IV}_Al^{III}_O^{III}	AI(III)	2.058	O(III)	-1.409	-1490.002
Ga^{IV}_Al^{III}_O^{II}	AI(III)	2.067	O(II)	-1.288	-1528.216
B^{III}_Al^{IV}_O^{II}	AI(IV)	2.058	O(II)	-1.352	-1441.900
B^{III}_Al^{IV}_O^{III}	AI(IV)	2.046	O(III)	-1.165	-1343.681
B^{IV}_Al^{III}_O^{III}	AI(III)	2.024	O(III)	-1.377	-1343.681
B^{IV}_Al^{III}_O^{II}	AI(III)	2.025	O(II)	-1.072	-1441.900

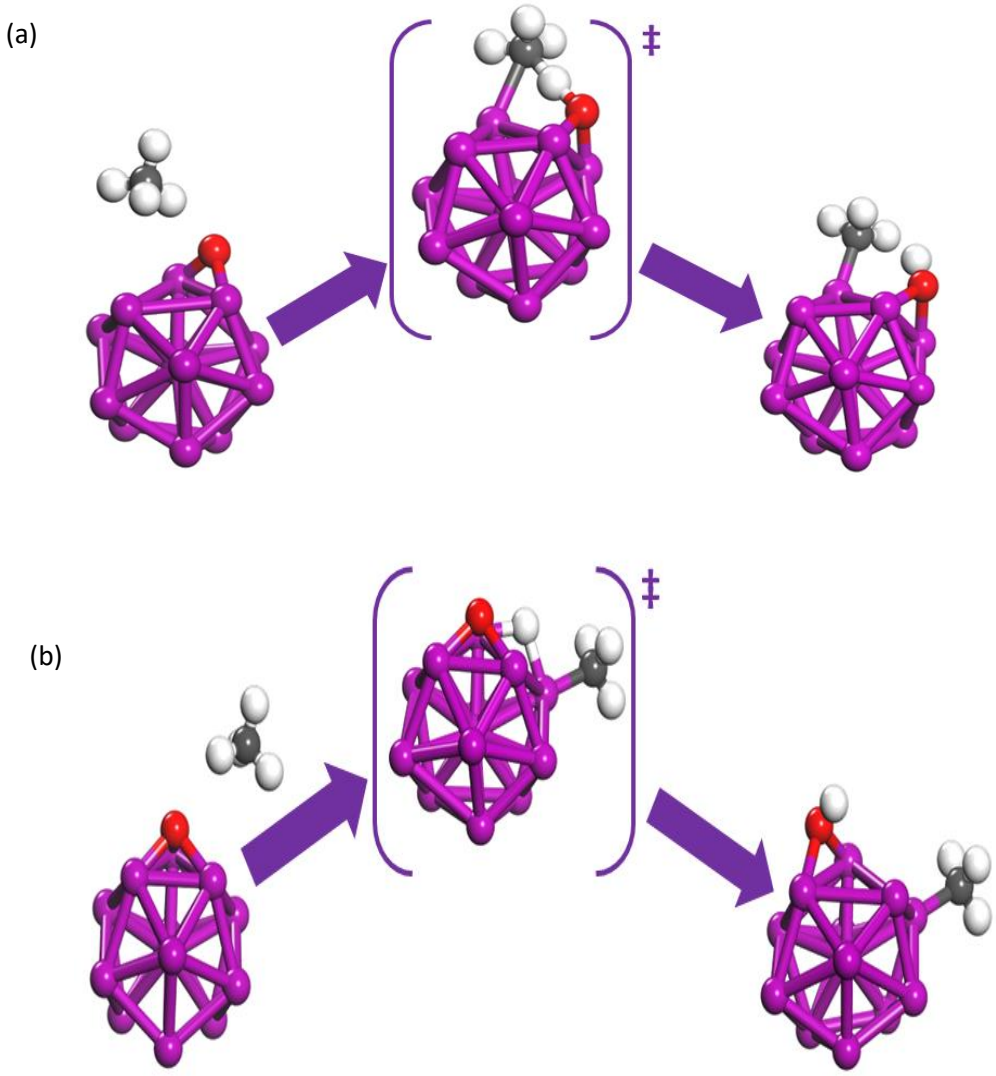

Figure 17: Structural representation of Aluminium cluster of 13 atoms doped with single oxygen atom oriented in(a) parallel (b) opposite direction in singlet state. {Obtained using Pople 6-311G(d)/MO6-2x}

To examine the preference of polar mechanism vs. the radical mechanism on a structurally dissimilar catalyst, we investigated methane activation on 13-atom aluminum cluster with a single pre-adsorbed oxygen atom $[Al_{13}O]^-$.

Two distinct structures with variable oxygen adsorption sites were considered in singlet state (conf A1, oxygen oriented in parallel direction to adsorbed methane, (conf A2, oxygen oriented in opposite direction to adsorbed methane) (Figure 17). Similarly, two conformers of $[Al_{13}O]^-$ cluster were considered for the polar pathway (conf B1, oxygen oriented in parallel direction to adsorbed methane, conf B2, oxygen oriented in opposite direction to adsorbed methane) (Figure 18).

(a)

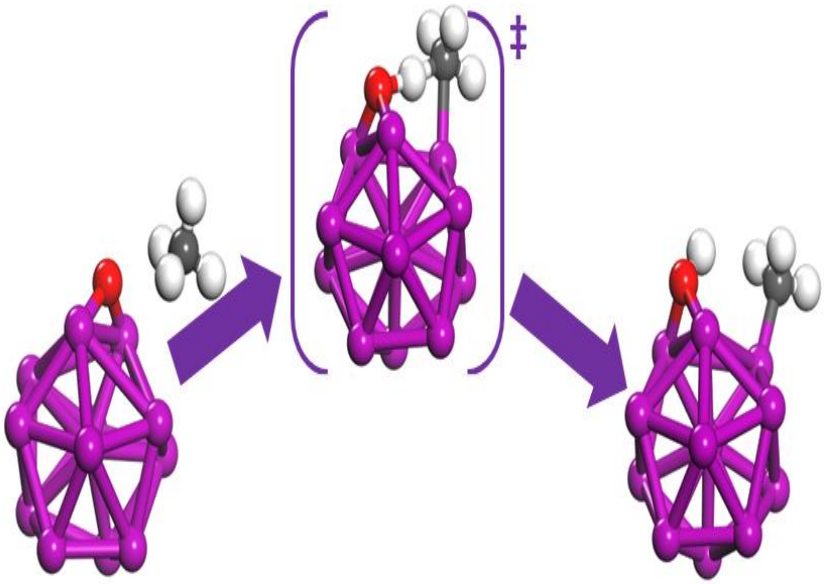

(b)

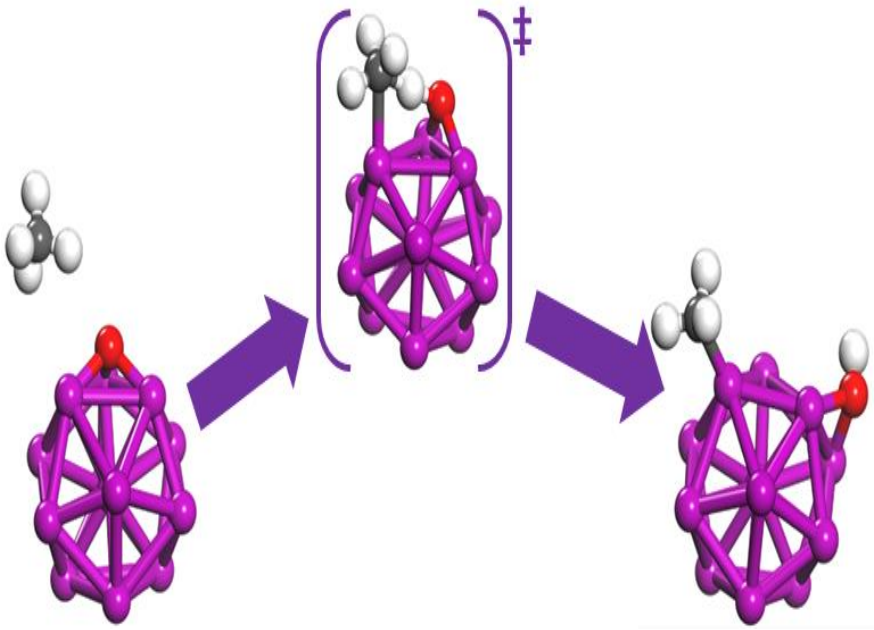

Figure 18: Structural representation of Aluminum cluster of 13 atoms doped with single oxygen atom oriented in(a) parallel (b) opposite direction to methane in triplet state {Obtained using Pople 6-311G(d)/MO6-2x}

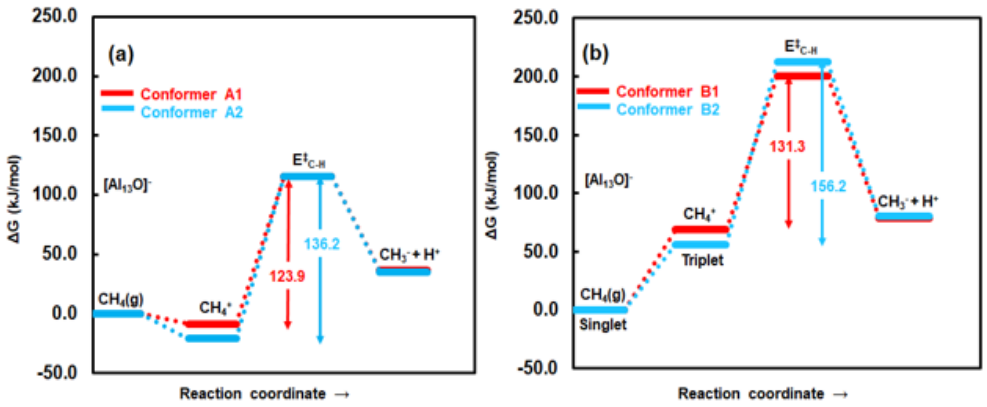

Figure 19: Activation free-energy diagram for (a) site-pairs (conf. A1, orientation of oxygen is in parallel direction to adsorbed methane and conf. A2, oxygen oriented in opposite direction to adsorbed methane) of $[Al_{13}O]^-$cluster in singlet state, (b) site-pairs (conf. B1, orientation of oxygen is in parallel direction to adsorbed methane and conf. B2, oxygen oriented in opposite direction to adsorbed methane) of $[Al_{13}O]^-$ cluster in triplet state. {Obtained using Pople 6-311G(d)/MO6-2x}

The activation barriers for each site pair are depicted in Figure 19. We found that the activation barriers for the two conformers (conf B1 and conf B2) in triplet state (radical pathway) were higher than the activation barriers for conf A1 and conf A2 in singlet state (polar pathway) (Figure 19a-b). However, the comparative analysis between free activation barrier of $[Al_{13}O]^-$ cluster (Figure 19a-b) and γ-Al_2O_3 (Figure 8a) suggest that the site-pairs of γ-Al_2O_3 are energetically more preferred site pairs than the site-pairs of $[Al_{13}O]^-$ cluster. This can be attributed to the high surface coordination number and less Lewis acidity of $[Al_{13}O]^-$ cluster compared to γ-Al_2O_3. To quantify the acidity of different Al-sites, we computed NBO charges for Al-sites of $[Al_{13}O]^-$ cluster (Table 2*). The low NBO charges for Al-sites (Table 2*) confirm the lower Lewis acidity of Al in $[Al_{13}O]^-$ compared to γ-Al_2O_3. On the other hand, site-pairs of $[Al_{13}O]^-$ show higher proton affinity compared to pristine γ-Al_2O_3 (due to lower surface coordination of oxygen on $[Al_{13}O]^-$). These results highlight the high catalytic activity of γ-Al_2O_3 for the C-H bond activation

Table 2* The Natural Bond Orbital (NBO) analysis and Proton Affinity for Al site of different site pairs, conf. A1, conf. A2 (singlet state, polar pathway) Al sites of conf. B1, conf. B2 (triplet state, radical pathway) of $[Al_{13}O]$- and site pairs Al^{IV}-O^{II}, Al^{IV}-OI^{II}, Al^{III}-O^{III} and Al^{III}-OI^{I} of γ-Al_2O_3 system. QM (charges on the Al) (electron acceptor) have been presented in the table.

$[Al_{13}O]^-$	NBO	Proton Affinity	γ-Al_2O_3	NBO	Proton Affinity
	Q_{Al}	PA		Q_{Al}	PA(kJ/mol)
conf A1	0.834	-1392.163499	Al^{IV}-O^{II}	2.0834	-880.624
conf A2	0.834	-1392.163499	Al^{IV}-O^{III}	2.034	-778.400
conf B1	0.826	-1443.909478	Al^{III}-O^{III}	2.06	-778.400
conf B2	0.825	-1443.909478	Al^{III}-O^{II}	2.059	-880.624

4.1 Summary

We conducted Natural Bond Orbital (NBO) charge analysis to investigate charge localization at different metal centers (Al, B, Ga) in pristine and doped γ-Al_2O_3. The analysis revealed higher charge localization at all Al-O site pairs (Al^{IV}-O^{II}, Al^{IV}-O^{III}, Al^{III}-O^{II}, Al^{III}-O^{III}) in pristine γ-Al_2O_3 compared to B- and Ga-doped γ-Al_2O_3. Specifically, the tricoordinated aluminium sites (Al^{III}) in pristine γ-Al_2O_3showed higher electron deficiency, indicating stronger acidity, compared to Ga^{III} and B^{III} sites.

Proton affinity (PA) was used as a descriptor for basicity. The non-local O^{II} and O^{III} sites in Ga- and B-doped γ-Al_2O_3showed significantly higher PA than those in pristine γ-Al_2O_3, suggesting enhanced catalytic activity due to dopant incorporation.

Examining the frontier molecular orbitals (HOMO and LUMO), we observed that in pristine γ-Al_2O_3, the lowest energy orbitals (LUMO) were on Al^{III} sites, while the highest occupied molecular orbitals (HOMO) were mostly on O^{II} and partly on O^{III} sites. This indicates higher acidity and basicity at Al^{III}-O^{II} site pairs.

For Ga-doped γ-Al_2O_3, the LUMO was localized on the Ga^{III} site, whereas in B-doped γ-Al_2O_3, the LUMO was more localized on neighbouring Al-O site pairs. This suggests that while both Al and Ga exhibit similar acidity, the difference in atomic size affects

the localization of the lowest unoccupied orbitals, leading to lower activation energy barriers for M^{IV}-O^{III} (M=Al/Ga) site pairs, in agreement with PA values.

We further explored methane activation mechanisms on a 13-atom aluminium cluster with a pre-adsorbed oxygen atom $[Al_{13}O]$-. Two conformers (A1, A2) in the singlet state and two conformers (B1, B2) in the triplet state were considered. The activation barriers for the triplet state conformers (radical pathway) were higher than those for the singlet state conformers (polar pathway). A comparative analysis showed that the activation barriers for site pairs in γ-Al_2O_3were lower than those in $[Al_{13}O]$-, indicating higher catalytic activity in γ-Al_2O_3 due to its higher surface coordination number and lesser Lewis acidity.

The NBO charge analysis and proton affinity measurements suggest that doping γ-Al_2O_3 with Ga and B significantly influences charge localization and catalytic activity. Ga doping enhances acidity and basicity at specific site pairs, while B doping shows a contrasting behaviour with lower charge localization and higher activation free-energy barriers. Methane activation studies confirm that γ-Al_2O_3exhibits superior catalytic activity compared to the $Al_{13}O$ cluster, attributed to its structural and electronic properties. These findings underscore the potential of doped γ-Al_2O_3as an efficient catalyst for various chemical reactions.

Chapter 5: Correlation between activation free energy and H_2 Binding energy

To quantitatively assess the relationship between acidic and basic strength of respective site pairs and catalytic activity, we related the computed activation free energies with H_2 binding energy.[57] As H_2 dissociate to release a proton, H^+ and hydride, H^- ion and these fragments respectively probe the Lewis acidity and basicity of surface acid-base pairs.[57]

Therefore, we calculated the binding energy of H_2 on different site pairs of pristine, boron- and gallium-doped γ-Al_2O_3 (Figure 20).

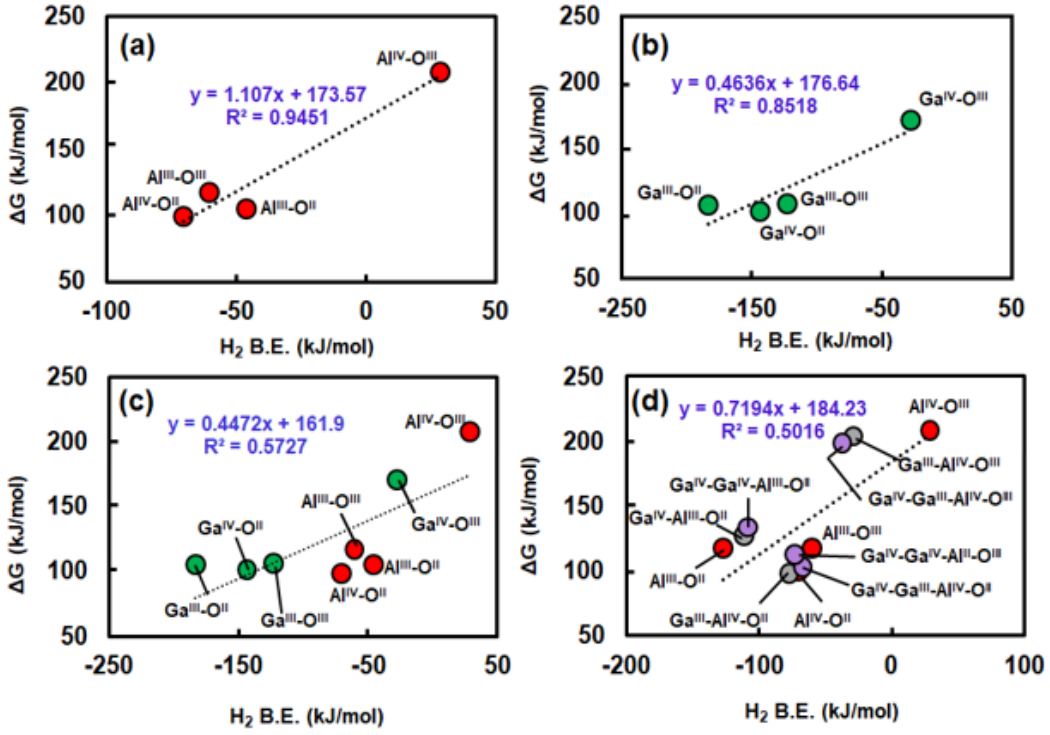

Figure 20: Plot (a) represents the correlation between H_2 binding energy with an activation free energy barrier for site pairs of pristine γ-Al_2O_3. (Al^{III}-O^{II} site pair represents Al^{III*}-O^{II*} site pair on alternative model where sites Al^{III} and O^{II} are adjacent to each other). The activation free-energy barriers v/s H_2 binding energy for different site-pairs of Ga-γ-Al_2O_3 are shown in plot b. Plot c shows the H_2 binding energy correlation with the activation free-energy barrier for all the site pairs of pristine γ-Al_2O_3 and Ga doped γ-Al_2O_3 together. Plot d represents the binding energy correlation for pristine γ-Al_2O_3, neighboring Al sites of single Ga atom doped γ-Al_2O_3 (at tricoordinated Ga^{III} and tetracoordinated sites Ga^{IV}) and adjacent aluminum site pairs of two Ga atom doped γ-Al_2O_3 (Ga^{IV}-Ga^{IV} and Ga^{IV}-Ga^{III}). {Obtained using Pople 6-311G(d)/MO6-2x}

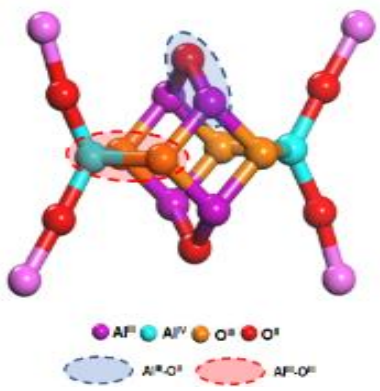

Figure 21: The structure of 20 atom clusters of bulk Al_2O_3 (110) surface with Al^{III}-O^{II} and Al^{III}-O^{III} site pairs adjacent to each other {Obtained using Pople 6-311G(d)/MO6-2x}

For site pair Al^{III}-O^{II}, due to the large separation between the sites (Al^{III} and O^{II}), methane activation on this site pair imparts a large strain in the transition state (as seen by the distortion of the structure of the catalyst in the TS, Figure 4d). Thus, expectedly high activation free energy barrier was noticed which cannot be accounted to the Lewis acidity and basicity of this site pair. To decouple the strain effect with Lewis acidity and basicity (to account for activation energy) on this site pair, we performed C-H bond dissociation calculations on an alternative 20-atom cluster of the Al_2O_3 (110) surface (Figure 21)

In this model Al^{III}-O^{II} site pair is located adjacent to each other. As expected, on this Al^{III*}-O^{II*} (on the new 20 atom model) site pair the C-H activation free energy barrier is significantly low[41]. The plots of H_2 binding energy against the activation free energy barrier are shown in Figure 20 (a-d). In the case of pristine γ-Al_2O_3, the H_2 binding energy shows a linear correlation with activation barrier (Figure 20a) (we excluded highly distant site pair Al^{III}-O^{II} with Al^{III*}-O^{II*} distance of 3.47 Å). Further we examined the Ga - doped γ-Al_2O_3, we found that the binding energy is a good predictive descriptor for activation free energy, as shown by the linear correlation between H_2 binding energies and activation free energies (Figure 20b).

However, in the case of boron-doped systems, we do not observe any correlation between H_2 binding energy and activation barrier. Unlike to that of Gallium doping, we observed that in the case of the boron-doped γ-Al_2O_3 catalyst system, severe reconstructions take place in the structure as a result of doping. Figure 11 shows the structural representation of C-H bond dissociation over(a)B^{IV}-O^{III} (b) B^{III}-O^{II} (c B^{IV}-O^{II} (d) B^{III}-O^{III} site pair of doped γ-Al_2O_3 catalyst surface. The reconstruction in the structure occurs because of the induced strain in the structure as a result of doping. This can be attributed to the preference of boron to the trigonal planar geometry due to the absence of empty d-orbitals

It is important to notice here, due to the lack of d-orbitals boron prefers to be in trigonal planar structure, which imparts severe reconstruction in the catalyst structure as shown in Figure 11.It was observed that the tetracoordinated boron sites get transformed to new tricoordinated ($B^{III'}$-O^{II}, $B^{III'}$-$O^{II'}$) state during optimization whereas original tricoordinated B^{III}-O^{III}, B^{III}-O^{II} site pairs remain in their tricoordinated state).As a result, we noticed that the $B^{III'}$-O^{II}, $B^{III'}$-O^{III} and B^{III}-$O^{II'}$ site pairs show relatively lower activation free-energy barriers (207.1 kJ/mol, 136 kJ/mol, and 206 kJ/mol respectively, Figure 12a) than B^{III}-O^{II} (267.3 kJ/mol) site pairs. The apparently lower coordination number (three) of ($B^{III'}$) enhances the adsorption and activation of the methane as is evident by higher exothermic reaction energy values for methane activation over these sites. However, because boron naturally prefers to achieve tri coordination, the adsorption and activation of methane was substantially less preferred on site pairs comprising tricoordinated (initially existent Boron sites (B^{III}).The above results suggest that on the boron-doped system the methane activation is not primarily driven by Lewis acidity and basicity but other structural factors (such as strain) play a crucial role[41].

In addition to this we also computed H^+ and CH_3^- binding energy over different site-pairs of pristine γ–Al_2O_3 and Ga-doped γ-Al_2O_3 and plotted against activation free-energy barrier for each site-pair (Figure 22). We noted that, all the site-pairs of pristine and Ga-doped γ-Al_2O_3 were in good agreement with activation free-energy barrier

except for site pair Al^{III}-O^{II} of pristine system (Al^{III} and O^{II} sites are highly distant, 3.47 Å) (Figure 22). These analyses suggest that H_2 binding energies and CH_4 binding energies were identified as suitable descriptor to explain the catalytic activity of γ-Al_2O_3.

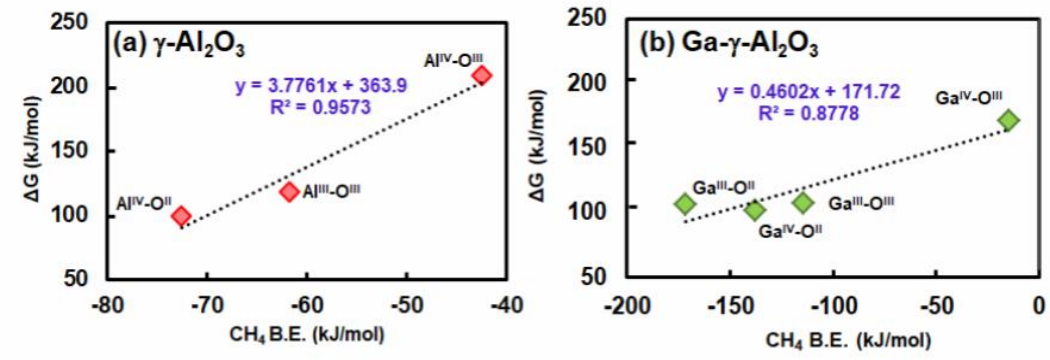

Figure 22: The correlation between CH_4 binding energy with activation energy barrier for (a) pristine γ-Al_2O_3 (b) gallium doped γ-Al_2O_3 site-pairs respectively. Aluminum site pairs are shown in red, gallium site-pairs are shown in green color. {Obtained using Pople 6-311G(d)/MO6-2x}

Al^{IV}-O^{II} and Al^{III}-O^{III} site pairs of Ga^{IV}-doped γ-Al_2O_3 catalyst surface exhibit the lowest activation free energy barrier and respective H_2 binding energy due to the neighboring effect of gallium. Similar results were found when we doped the catalyst with single and double Ga^{III} atom[41]. Moreover, we observed a good correlation between dissociative H_2 binding energy and activation free energy barrier for pristine γ-Al_2O_3 along with Ga-doped γ-Al_2O_3 catalyst surface as explained through Figure 20d.Although the $B^{III'}$ single and double doped system gives the lowest energy barriers ($B^{III'}$-Al^{III}-$O^{II'}$, 88.4 kJ/mol, $B^{III'}$-$B^{III'}$-Al^{III}-$O^{II'}$, 92 kJ/mol), Figure 12 b-c), these boron systems do not show any correlation between H_2 binding energy with activation free energy (Figure 23) due to major reconstruction of the structure

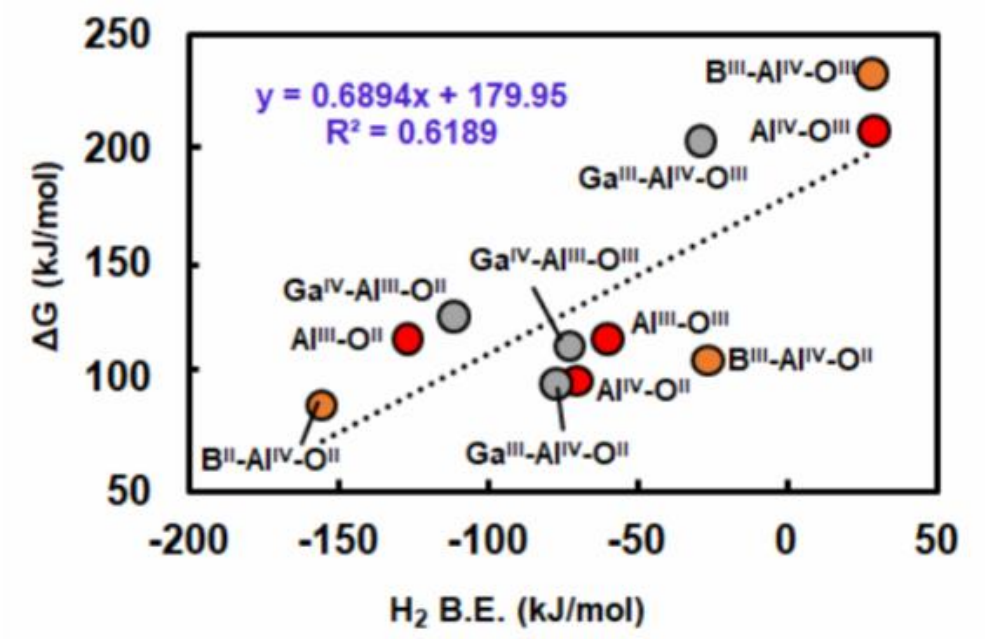

Figure 23: The correlation between CH_4 binding energy with activation energy barrier for (a) pristine γ-Al_2O_3 (b) gallium doped γ-Al_2O_3 site-pairs respectively. Aluminum site pairs are shown in red, gallium site-pairs are shown in green color. {Obtained using Pople 6-311G(d)/MO6-2x}

Along with this, we found that the final state energy (difference between the physiosorbed state and final product), is good descriptor for C-H bond activation in methane through polar mechanism (Figure 24).

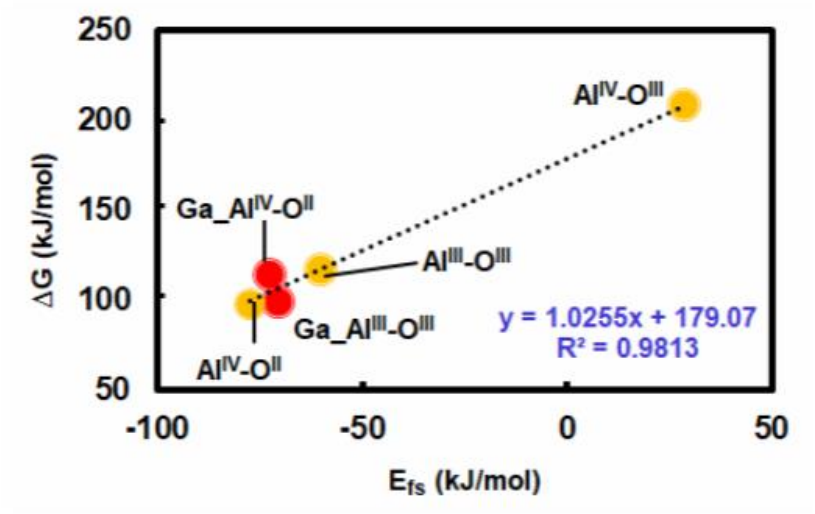

Figure 24: Correlation between activation free-energy barrier and final state energy for Al^{III} and Al^{IV} site pairs of pristine γ-$Al_2O_3$and Ga-doped aluminium catalyst surface. {Obtained using Pople 6-311G(d)/MO6-2x}

5.1 Summary

To assess the relationship between the acidic and basic strengths of site pairs and their catalytic activity, we analysed the correlation between computed activation free energies and H_2 binding energies. This analysis probes the Lewis acidity and basicity of surface acid-base pairs, as H_2 dissociation releases H^+ and H^- ions.We calculated H_2 binding energies for various site pairs in pristine, boron-doped, and gallium-doped γ-Al_2O_3. A linear correlation was observed between H_2 binding energy and activation free energy barriers for pristine γ-Al_2O_3, excluding the distant Al^{III}-O^{II} site pair (Figure 20a). For Ga-Doped γ-Al_2O_3, a similar linear correlation was found,

indicating that H_2 binding energy is a reliable predictor for activation free energy in Ga-doped systems (Figure 20b).

In case of Pristine γ-Al_2O_3, high activation free energy barriers were noted for the distant Al^{III}-O^{II} site pair due to the structural strain induced during methane activation. This was mitigated by modelling an alternative structure with adjacent Al^{III*}-O^{II*} sites, resulting in significantly lower barriers. In case of Ga-Doped γ-Al_2O_3, the binding energy correlation with activation barriers confirmed the predictive power of H_2 binding energies. Al^{IV}-O^{II} and Al^{III}-O^{III} site pairs in Ga-doped γ-Al_2O_3exhibited the lowest activation barriers due to the neighbouring effect of gallium atoms. However, in case of B-doped γ-Al_2O_3, no correlation was found between H_2 binding energy and activation barriers. Structural reconstructions induced by boron doping, due to its preference for trigonal planar geometry, resulted in severe strain and altered the catalytic properties. New tricoordinated $B^{III'}$ sites showed lower activation barriers and higher exothermic reaction energies for methane activation compared to original tricoordinated B^{III} sites (Figure 11, 12).

Additionally, we observed that the plots of CH_4 binding energy against activation free energy barriers showed good agreement for pristine and Ga-doped γ-Al_2O_3, except for the distant Al^{III}-O^{II} site pair in the pristine system (Figure 22). The difference between the physiosorbed state and the final product emerged as a good descriptor for C-H bond activation in methane via the polar mechanism (Figure 24)

The study demonstrates that H_2 binding energy is a reliable descriptor for predicting catalytic activity in pristine and Ga-doped γ-Al_2O_3. However, B-doped systems require consideration of structural factors due to significant reconstruction. Overall, these findings enhance our understanding of how doping affects the catalytic properties of γ-Al_2O_3, paving the way for designing more efficient catalysts for methane activation and other reactions.

Chapter 6: Computational Methods

Density functional theory (DFT) forms the basis of a significant portion of molecular calculations in quantum chemistry. DFT's success can be ascribed to its comparably low computing cost while frequently maintaining a sufficient level of accuracy[87]. The DFT is frequently used to describe the chemistry of molecular systems of hundreds to thousands of atoms.[88] Large ligands, heavy elements, and explicit solvents can all be included in these models. Furthermore, molecular dynamics or Monte Carlo simulations based on DFT can be used to study the impacts of dynamic and finite temperature[89-91]. The accuracy of a particular system is constrained by both fundamental and technical factors. It actually requires much research efforts to account the inherent limitation of the approximate nature of currently used density functionals. Vande Avaondelle focussed on the formulation of a basis set employed to solve the Kohn-Sham equations, which actually restricted the main technical part of calculations[87]. There are numerous different functional forms that are in use, such as Gaussian functions, Slater functions, plane waves, wavelets, numerical basis functions, and many more[92]. The volume of literature on Gaussian basis sets is very large, and this emphasizes their significance[93]. There is a dire need to expand the size and, consequently, the accuracy of the base for each of these functional types. There is frequently no ideal method to achieve this, thus many techniques are employed to produce desirable total energies, geometries, interaction energies, or unique electronic features. One can say that each method aims to strike a balance between accuracy and computing expense[87].

Density functional theory is based on exact principles[94], but even if it were possible, the exact functional would probably be so difficult to use that it would be of little use in comparison to the best wave function theories. The greatest accomplishment of functional development to far is that many electronic structure problems in chemistry and condensed matter physics may be solved with useful levels of accuracy using extremely approximate functionals[95]. Many research groups are in continuous pursuit

of better functionals that are computationally tractable continues. Mardirossian et al describe a promising effort in this direction. Perhaps the most popular technique for developing functionals in the quantum chemistry field is parameterizing empirical density functionals using linear least-squares fitting[96]. Based on the results obtained by B97, a number of semi-empirical density functionals have been created since 1997.These functionals include meta-GGA and meta-NGA functionals in addition to generalized gradient approximation (GGA) and nonseparable gradient approximation (NGA) functionals. GGAs, which stand for Perdew's Jacob's Ladder Rung 2[97] rely on a single inhomogeneity variable that is a function of $\rho\sigma$ and $|\nabla\rho\sigma|$, NGAs, however, also rely on an additional inhomogeneity variable that is exclusively a function of $\rho\sigma$.

Global inclusion of exact exchange, made popular by the B3PW91 density functional in 1993, means that the fraction of exact exchange is constant over all interelectronic distances[98]. Range-separated hybrid (RSH) functionals, which feature a proportion of short-range exact exchange that typically either smoothly raises to 1 (long-range-corrected) or smoothly falls to 0 (screened-exchange), have largely supplanted these global hybrids in more recent times[99]. The majority of contemporary parameterizations simultaneously train a dispersion correction onto the exchange-correlation functional since density functionals are unable to accurately account for long-range correlation.

A damped, atom-atom potential (DFT-D), such as Grimme's DFT-D2 or DFT-D3 models, is the most basic form for a dispersion correction.[100-102]Nonlocal correlation (NLC) functionals like VV10 and vdWDF-2 allow a more thorough analysis of dispersion [103]. However, a post Hartree-Fock correlation (post-HFC) approach like MP2, RPA, or CCSD is the most complex and computationally intensive option for a dispersion correction.[104]

Figure 25 gives a different perspective of the elements that can be combined to define the majority of existing density functionals in light of the aforementioned factors[95].

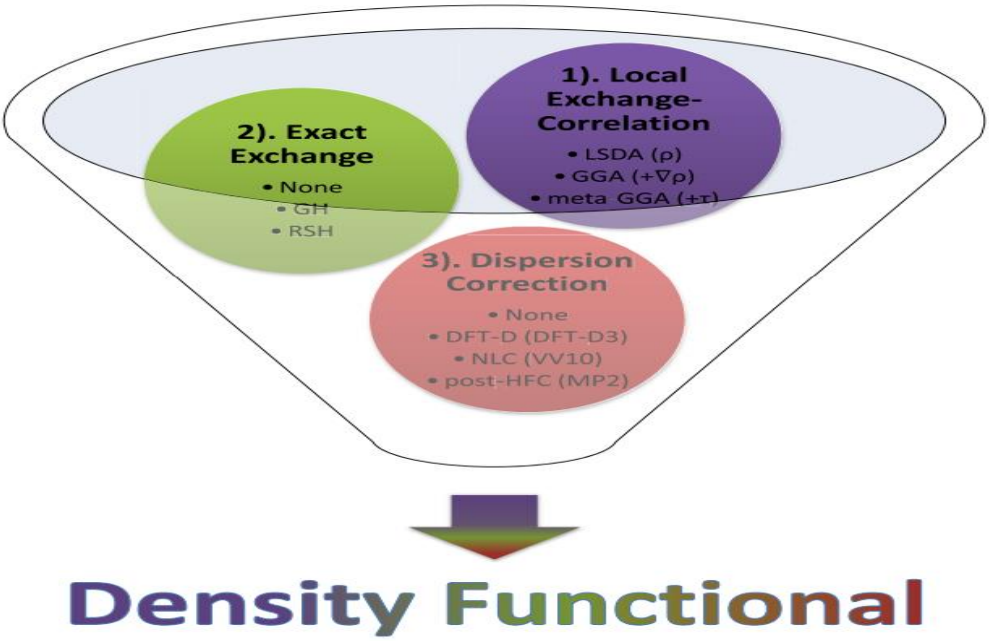

Figure 25: An alternate view of elements that can be combined to define most existing density functionals. Reprinted with copyright permission from reference no. 98

The first component (Local Exchange-Correlation) focuses on the components that make up the functional for local exchange-correlation, with the options available simulating the first three rungs of Jacob's ladder. The second component, "Exact Exchange," deals with the optional utilization of contributions from exact exchanges to define hybrid functionals. The optional treatment of long-range correlation by one of the aforementioned methods is normally accounted for by the third element (Dispersion Correction)[95].

To study the role of metal oxides for C-H activation of methane, we investigated methane activation over γ-Al_2O_3 as a catalyst. In molecular calculations, as it is computationally challenging to study the full γ-Al_2O_3 surface, we utilized the previously reported 20-atom molecular cluster[41]. In order to perform the proposed work, we used a workstation consisting of Linux based High Performance Computing cluster (HPC)to model the reactions and visualize the results. The cluster comprised of 32 processors per node, utilizing a total of 4 nodes. It is noteworthy to mention here that the results obtained are generally independent of the hardware used. We used Gaussian 16 program to optimize and identify the least energy structures of methane activation on γ-Al_2O_3, boron, and gallium doped γ-Al_2O_3 d different site pairs, by performing density functional theory (DFT) calculations[95, 105].

For density functional calculations of molecular structure, properties, and thermochemistry, kinetics, noncovalent interactions, and spectroscopy, the Minnesota family of exchange-correlation functionals, which consists of meta generalized gradient approximations (meta-GGAs) and global-hybrid meta-GGAs, has been successful. We used M06-2X exchange-correlation functional to study the thermodynamic and kinetic properties of different catalysts[106]. Vande Vondele offered a collection of Gaussian basis sets that have been fine-tuned specifically for density functional theory-based calculations on molecules. It targets the gas phase, interfaces, and condensed phase, among other chemical conditions. They focused on the basis sets of contracted Gaussian functions. They deliberated upon the Gaussian basis sets with good performance for

total energies, geometries, and hydrogen bonding energies that may be used in large-scale simulations of molecular systems, including gas phase systems, interfaces, and liquids.

In order to predict the extent of reactivity between the catalyst surface and adsorbent, we employed the Pople 6-311G(d) basis sets[87].M06-2X frequency calculations confirmed the presence of local minima for different site pairs with zero imaginary frequencies while the transition state structures consist of one imaginary frequency. The connectivity between reactant and product with TS structures was verified with the help of intrinsic reaction coordinate (IRC) calculations which follow the minimum energy reaction pathway of the negative frequency. The charge distribution over different site pairs was examined through NBO charge analysis[107]. We calculated the NBO charges using the technique. We calculated the Hydrogen binding energy (BE) through dissociative adsorption on Lewis acid (metal) and base (oxygen) site-pairs of the metal oxide surface as,

$$BE_{H_2} = E_{surface/H_2} - (E_{H_2} + E_{surface})$$

Where E_{H_2} represents the total energy of gas-phase H_2, $E_{surface}$ represents the total energy of clean surface, $E_{surface/H_2}$ is the total energy of a H_2 adsorbed on the surface, respectively. Proton affinity for any compound is computed through following equation,

$$PA_{complex} = E_{complex} - E_{catalyst\ surface} - E_{proton}$$

Where $E_{complex}$ represent the Gibb's free energy of complex (catalyst with adsorbent), $E_{catalyst\ surface}$ is the Gibb's free energy of catalyst surface, E_{proton} is the Gibb's free energy of proton, respectively.

6.1 Summary

Density Functional Theory (DFT) is a widely used method in quantum chemistry for molecular calculations, especially due to its balance between computational cost and accuracy. DFT can handle complex molecular systems with hundreds to thousands of atoms, including large ligands, heavy elements, and explicit solvents. It is also utilized

in molecular dynamics and Monte Carlo simulations to study dynamic and finite temperature effects. Despite its utility, DFT's accuracy is limited by both fundamental and technical constraints, necessitating ongoing research to improve the approximate nature of current density functionals.

Different basis sets like Gaussian functions, Slater functions, and plane waves are used to solve the Kohn-Sham equations in DFT calculations. Numerous functionals, such as meta-GGA, meta-NGA, GGA, and NGA, are developed to optimize total energies, geometries, and electronic properties. These functionals balance accuracy and computational expense. Modern developments include hybrid functionals with exact exchange and range-separated hybrid (RSH) functionals for improved accuracy. Dispersion corrections are added to account for long-range correlations, using methods like Grimme's DFT-D models or more complex post-Hartree-Fock approaches.

To explore the role of metal oxides in methane activation, we studied the activation over γ-Al_2O_3 using a 20-atom molecular cluster model due to computational limitations. The Gaussian 16 program was used for DFT calculations to optimize and identify the least energy structures of methane activation on pristine, boron-doped, and gallium-doped γ-Al_2O_3. The M06-2X exchange-correlation functional was employed for these studies, focusing on thermodynamic and kinetic properties. The Pople 6-311G(d) basis sets were used to predict reactivity. M06-2X frequency calculations ensured the presence of local minima and verified transition states through intrinsic reaction coordinate (IRC) calculations. NBO charge analysis was performed to examine charge distribution over different site pairs.

Hydrogen Binding Energy (BE) was calculated through dissociative adsorption on Lewis acid (metal) and base (oxygen) site pairs of the metal oxide surface using the formula:

$$BE_{H_2} = E_{surface/H_2} - (E_{H_2} + E_{surface})$$

where E_{H_2} is the total energy of gas-phase H_2, $E_{surface}$ is the total energy of the clean surface, and $E_{surface/H_2}$ is the total energy of H_2 adsorbed on the surface.

Proton Affinity (PA), is computed as:

$$PA_{complex} = E_{complex} - E_{catalyst\ surface} - E_{proton}$$

where $E_{complex}$ is the Gibbs free energy of the complex (catalyst with adsorbent), $E_{catalyst\ surface}$ is the Gibbs free energy of the catalyst surface, and, E_{proton} is the Gibbs free energy of the proton.

In nutshell we can say that DFT, with its various functional and basis set developments, remains a crucial tool for studying complex molecular systems and catalytic processes, such as methane activation on γ-Al_2O_3. The continuous improvement in functionals and computational methods promises better accuracy and applicability in quantum chemistry.

Chapter 7: Summary and Conclusions

Alkanes, particularly methane, are abundant yet chemically inert due to their strong C-C and C-H bonds. Their conversion to valuable products is limited by the inefficiency of current industrial processes, which are energy-intensive and commercially unviable. Metal oxides like γ-Al_2O_3can activate methane's C-H bonds through their Lewis acidic (metal) and basic (oxygen) sites, making them potential catalysts for methane conversion. This study focuses on elucidation of the mechanism of C-H bond activation on γ-Al_2O_3surface, Identifying the most active site pairs on γ-$Al_2O_3$for efficient C-H bond activation, Investigation of the effect of doping γ-$Al_2O_3$with trivalent elements Barium and Gallium on the kinetics and thermodynamics of methane activation and determination of the influence of dopants on the catalytic activity of neighbouring site pairs. These insights could lead to more efficient and commercially viable methods for converting methane to methanol, leveraging the enhanced catalytic properties of doped γ-Al_2O_3 surfaces.

Using Density Functional Theory (DFT), we used a cluster model to investigate the C-H activation of methane on different site pairs of γ-Al_2O_3. The activation of the C-H bond on pristine and doped γ-Al_2O_3 clusters was evaluated in this analysis. The C-H activation was investigated using two potential pathways, radical and polar, and it was revealed that the activation barriers are lower for polar pathways on γ-Al_2O_3. Figures suggest that methane C-H activation on γ-Al_2O_3 via a radical pathway encompasses a triplet state (high energy state). For the C-H activation of methane on γ-Al_2O_3, the polar 11q2pathway is more energy efficient than the radical pathway. We also analyse how dopants (boron and gallium) can lower activation free energy barriers and enhance catalytic activity on both local (doped site-pair) and non-local (adjacent) site-pairs of the γ-Al_2O_3 surface. Gallium doping lowers the activation energy barrier on multiple site-pairs of pristine γ-Al_2O_3. Boron doped systems have a higher activation free energy

barrier on doped site-pairs (local), whereas adjacent aluminium site-pairs have a significantly lower energy barrier (non-local). Boron and gallium doping have a noticeable effect on adjacent sites in addition to altering the catalytic activity of dopant sites. Gallium is found to significantly improve the catalytic activity for the most of pristine γ-Al_2O_3 site pairs. In the case of pristine and doped γ-Al_2O_3, we explain the Lewis acidity and basicity of site-pairs with the highest occupied and lowest unoccupied molecular orbital diagrams (HOMO-LUMO). For pristine γ-Al_2O_3, the lowest energy orbitals were found on the Al^{III}- site, whereas the highest occupied molecular orbitals were found primarily over the O^{II}- and partially on the O^{III}- sites. This suggests that the Al^{III}-O^{II} site-pair has a higher acidity and basicity than other Al-O site-pairs in pristine γ-Al_2O_3. We also use molecular H_2 binding energy as a descriptor to explain the effect of doping on C-H bond activation. For the preferred polar pathway, we discovered a relationship between dissociated H_2 binding energies and C-H activation free energies. The H_2 binding energy of pristine γ-Al_2O_3 has a linear correlation with activation barrier. We evaluated Ga doped γ-Al_2O_3 and observed that the binding energy is a good predictor of activation free energy, as evidenced by the linear correlation between H_2 binding energies and activation free energies. In the case of boron-doped systems, however, we encounter no correlation between H_2 binding energy and activation barrier.

A detailed study of reaction mechanism for methane activation will provide fundamental understanding on the impact of multi-functionality of active sites on the reaction efficiency. This will be a major step towards the process of energy conversion and storage and will be used to design a catalyst whose electronic structure can be tuned in such a way so that we achieve higher reactivity and selectivity. γ-Al_2O_3based catalysts require detailed investigation to understand the impact of introduction of different series of dopants that can help us achieve required selectivity and activity. Overall, the impact of doping on the active site and electronic structure of the active site needs to examined in detail so that the C-H activation of methane can be kinetically controlled and the desired selectivity and activity for energy conversion and storage can be achieved. The study aims at the futuristic aspect of comparison of computational results obtained to that of experimental values.

Bibliography

1. Labinger, J. A.; Bercaw, J. E., Understanding and exploiting C–H bond activation. *Nature* **2002,** *417* (6888), 507-514.
2. Tang, P.; Zhu, Q.; Wu, Z.; Ma, D., Methane activation: the past and future. *Energy & Environmental Science* **2014,** *7* (8), 2580-2591.
3. Schwach, P.; Pan, X.; Bao, X., Direct Conversion of Methane to Value-Added Chemicals over Heterogeneous Catalysts: Challenges and Prospects. *Chemical Reviews* **2017,** *117* (13), 8497-8520.
4. Kerr, R. A., Natural Gas From Shale Bursts Onto the Scene. *Science* **2010,** *328* (5986), 1624-1626.
5. McFarland, E., Unconventional chemistry for unconventional natural gas. *Science* **2012,** *338* (6105), 340-342.
6. Bajec, D.; Grom, M.; Lašič Jurković, D.; Kostyniuk, A.; Huš, M.; Grilc, M.; Likozar, B.; Pohar, A., A Review of Methane Activation Reactions by Halogenation: Catalysis, Mechanism, Kinetics, Modeling, and Reactors. *Processes* **2020,** *8* (4), 443.
7. Guerrero, F.; Espinoza, L.; Ripoll, N.; Lisbona, P.; Arauzo, I.; Toledo, M., Syngas Production From the Reforming of Typical Biogas Compositions in an Inert Porous Media Reactor. *Frontiers in Chemistry* **2020,** *8* (145).
8. York, A. P. E.; Xiao, T.; Green, M. L. H., Brief Overview of the Partial Oxidation of Methane to Synthesis Gas. *Topics in Catalysis* **2003,** *22* (3), 345-358.
9. Choudhary, T. V.; Choudhary Vasant, R., Energy-Efficient Syngas Production through Catalytic Oxy-Methane Reforming Reactions. *Angew. Chem., Int. Ed.* **2008,** *47*, 1828.
10. Choudhary, T. V.; Choudhary, V. R., Energy-Efficient Syngas Production through Catalytic Oxy-Methane Reforming Reactions. *Angewandte Chemie International Edition* **2008,** *47* (10), 1828-1847.
11. Wang, B.; Albarracín-Suazo, S.; Pagán-Torres, Y.; Nikolla, E., Advances in methane conversion processes. *Catalysis Today* **2017,** *285*, 147-158.
12. Senanayake, S. D.; Rodriguez, J. A.; Weaver, J. F., Low Temperature Activation of Methane on Metal-Oxides and Complex Interfaces: Insights from Surface Science. *Accounts of Chemical Research* **2020,** *53* (8), 1488-1497.
13. Liang, Z.; Li, T.; Kim, M.; Asthagiri, A.; Weaver, J. F., Low-temperature activation of methane on the IrO₂(110) surface. *Science* **2017,** *356* (6335), 299-303.
14. Tsuji, Y.; Yoshizawa, K., Adsorption and Activation of Methane on the (110) Surface of Rutile-type Metal Dioxides. *The Journal of Physical Chemistry C* **2018,** *122* (27), 15359-15381.
15. Zhang, T.; Holiharimanana, D.; Yang, X.; Ge, Q., DFT Study of Methane Activation and Coupling on the (0001) and (11$\bar{2}$0) Surfaces of α-WC. *The Journal of Physical Chemistry C* **2020,** *124* (49), 26722-26729.
16. Ren, Y.; Liu, X.; Zhang, Z.; Shen, X., Methane activation on single-atom Ir-doped metal nanoparticles from first principles. *Physical Chemistry Chemical Physics* **2021,** *23* (29), 15564-15573.
17. Carstens, J. N.; Bell, A. T., Methane activation and conversion to higher hydrocarbons on supported ruthenium. *Journal of Catalysis* **1996,** *161* (1), 423-429.

18. Kumar, G.; Lau, S. L. J.; Krcha, M. D.; Janik, M. J., Correlation of Methane Activation and Oxide Catalyst Reducibility and Its Implications for Oxidative Coupling. *ACS Catalysis* **2016,** *6* (3), 1812-1821.
19. Derk, A. R.; Li, B.; Sharma, S.; Moore, G. M.; McFarland, E. W.; Metiu, H., Methane Oxidation by Lanthanum Oxide Doped with Cu, Zn, Mg, Fe, Nb, Ti, Zr, or Ta: The Connection Between the Activation Energy and the Energy of Oxygen-Vacancy Formation. *Catalysis Letters* **2013,** *143* (5), 406-410.
20. Deshlahra, P.; Iglesia, E., Reactivity and selectivity descriptors for the activation of C–H bonds in hydrocarbons and oxygenates on metal oxides. *The Journal of Physical Chemistry C* **2016,** *120* (30), 16741-16760.
21. Afanasiev, P.; Bezverkhyy, I. J. A. C. A. G., Ternary transition metals sulfides in hydrotreating catalysis. **2007,** *322*, 129-141.
22. Deshlahra, P.; Iglesia, E., Toward More Complete Descriptors of Reactivity in Catalysis by Solid Acids. *ACS Catalysis* **2016,** *6* (8), 5386-5392.
23. Fornaciari, J. C.; Primc, D.; Kawashima, K.; Wygant, B. R.; Verma, S.; Spanu, L.; Mullins, C. B.; Bell, A. T.; Weber, A. Z., A Perspective on the Electrochemical Oxidation of Methane to Methanol in Membrane Electrode Assemblies. *ACS Energy Letters* **2020,** *5* (9), 2954-2963.
24. Senftle, T. P.; van Duin, A. C. T.; Janik, M. J., Role of Site Stability in Methane Activation on PdxCe1–xOδ Surfaces. *ACS Catalysis* **2015,** *5* (10), 6187-6199.
25. Senftle, T. P.; van Duin, A. C. T.; Janik, M. J., Methane Activation at the Pd/CeO2 Interface. *ACS Catalysis* **2017,** *7* (1), 327-332.
26. Zou, X.; Rui, Z.; Ji, H., Core–Shell NiO@PdO Nanoparticles Supported on Alumina as an Advanced Catalyst for Methane Oxidation. *ACS Catalysis* **2017,** *7* (3), 1615-1625.
27. Wen, J.-H.; Guo, D.; Wang, G.-C., Structure-sensitivity of direct oxidation methane to methanol over Rhn/ZrO2-x (101) (n = 1, 4, 10) surfaces: A DFT study. *Applied Surface Science* **2021,** *555*, 149690.
28. Sharma, R.; Poelman, H.; Marin, G. B.; Galvita, V. V., Approaches for Selective Oxidation of Methane to Methanol. *Catalysts* **2020,** *10* (2), 194.
29. Su, Y.-Q.; Filot, I. A. W.; Liu, J.-X.; Hensen, E. J. M., Stable Pd-Doped Ceria Structures for CH4 Activation and CO Oxidation. *ACS Catalysis* **2018,** *8* (1), 75-80.
30. Cui, Q.; Musaev, D. G.; Morokuma, K., Molecular Orbital Study of H2 and CH4 Activation on Small Metal Clusters. 2. Pd3 and Pt3. *The Journal of Physical Chemistry A* **1998,** *102* (31), 6373-6384.
31. Xu, Y.; Bao, X.; Lin, L., Direct conversion of methane under nonoxidative conditions. *Journal of Catalysis* **2003,** *216* (1), 386-395.
32. Gunsalus, N. J.; Koppaka, A.; Park, S. H.; Bischof, S. M.; Hashiguchi, B. G.; Periana, R. A., Homogeneous Functionalization of Methane. *Chemical Reviews* **2017,** *117* (13), 8521-8573.
33. Caballero, A.; Pérez, P. J., Methane as raw material in synthetic chemistry: the final frontier. *Chemical Society Reviews* **2013,** *42* (23), 8809-8820.
34. Latimer, A. A.; Kulkarni, A. R.; Aljama, H.; Montoya, J. H.; Yoo, J. S.; Tsai, C.; Abild-Pedersen, F.; Studt, F.; Nørskov, J. K., Understanding trends in C–H bond activation in heterogeneous catalysis. *Nature materials* **2017,** *16* (2), 225-229.
35. Mazzone, G.; Russo, N.; Sicilia, E., Dimethylplatinum(II) Complexes: Computational Insights into Pt-C Bond Protonolysis. *Inorg. Chem.* **2011,** *50*, 10091.

36. Cholewinski, M. C.; Dixit, M.; Mpourmpakis, G., Computational Study of Methane Activation on γ-Al2O3. *ACS Omega* **2018,** *3* (12), 18242-18250.
37. Metiu, H.; Chrétien, S.; Hu, Z.; Li, B.; Sun, X., Chemistry of Lewis Acid–Base Pairs on Oxide Surfaces. *The Journal of Physical Chemistry C* **2012,** *116* (19), 10439-10450.
38. Sattler, J. J. H. B.; Ruiz-Martinez, J.; Santillan-Jimenez, E.; Weckhuysen, B. M., Catalytic Dehydrogenation of Light Alkanes on Metals and Metal Oxides. *Chemical Reviews* **2014,** *114* (20), 10613-10653.
39. Coperet, C., C−H Bond Activation and Organometallic Intermediates on Isolated Metal Centers on Oxide Surfaces. *Chemical Reviews* **2010,** *110* (2), 656-680.
40. Bañares, M. A., Supported metal oxide and other catalysts for ethane conversion: a review. *Catalysis Today* **1999,** *51* (2), 319-348.
41. Singh, P.; Gogoi, A.; Aien, Q. U.; Dixit, M. J. C., Assessing the Effect of Dopants on the C− H Activation Activity of γ-Al2O3 using First-Principles Calculations. **2023,** *24* (5), e202200670.
42. Digne, M.; Sautet, P.; Raybaud, P.; Euzen, P.; Toulhoat, H., Hydroxyl Groups on γ-Alumina Surfaces: A DFT Study. *Journal of Catalysis* **2002,** *211* (1), 1-5.
43. Raynes, S.; Shah, M. A.; Taylor, R. A. J. D. T., Direct conversion of methane to methanol with zeolites: towards understanding the role of extra-framework d-block metal and zeolite framework type. **2019,** *48* (28), 10364-10384.
44. Weaver, J. F.; Carlsson, A. F.; Madix, R. J. J. S. S. R., The adsorption and reaction of low molecular weight alkanes on metallic single crystal surfaces. **2003,** *50* (4-5), 107-199.
45. Figueras, M.; Gutiérrez, R. A.; Prats, H.; Viñes, F.; Ramírez, P. J.; Illas, F.; Rodriguez, J. A. J. P. C. C. P., Boosting the activity of transition metal carbides towards methane activation by nanostructuring. **2020,** *22* (13), 7110-7118.
46. Sattler, J. J.; Ruiz-Martinez, J.; Santillan-Jimenez, E.; Weckhuysen, B. M. J. C. r., Catalytic dehydrogenation of light alkanes on metals and metal oxides. **2014,** *114* (20), 10613-10653.
47. Coperet, C. J. C. r., C− H bond activation and organometallic intermediates on isolated metal centers on oxide surfaces. **2010,** *110* (2), 656-680.
48. Pantaleo, G.; La Parola, V.; Deganello, F.; Singha, R. K.; Bal, R.; Venezia, A. M., Ni/CeO2 catalysts for methane partial oxidation: synthesis driven structural and catalytic effects. *Appl. Catal., B* **2016,** *189*, 233.
49. Wu, H.; La Parola, V.; Pantaleo, G.; Puleo, F.; Venezia, A. M.; Liotta, L. F. J. C., Ni-based catalysts for low temperature methane steam reforming: recent results on Ni-Au and comparison with other bi-metallic systems. **2013,** *3* (2), 563-583.
50. Fan, M.-S.; Abdullah, A. Z.; Bhatia, S. J. i. j. o. h. e., Hydrogen production from carbon dioxide reforming of methane over Ni–Co/MgO–ZrO2 catalyst: Process optimization. **2011,** *36* (8), 4875-4886.
51. Nolan, M. J. T. J. o. c. p., Charge transfer and formation of reduced Ce3+ upon adsorption of metal atoms at the ceria (110) surface. **2012,** *136* (13).
52. Calle-Vallejo, F.; Loffreda, D.; Koper, M. T.; Sautet, P. J. N. c., Introducing structural sensitivity into adsorption–energy scaling relations by means of coordination numbers. **2015,** *7* (5), 403-410.
53. Digne, M.; Sautet, P.; Raybaud, P.; Euzen, P.; Toulhoat, H. J. J. o. C., Hydroxyl groups on γ-alumina surfaces: a DFT study. **2002,** *211* (1), 1-5.

54. Digne, M.; Sautet, P.; Raybaud, P.; Euzen, P.; Toulhoat, H. J. J. o. C., Use of DFT to achieve a rational understanding of acid–basic properties of γ-alumina surfaces. **2004,** *226* (1), 54-68.
55. Kostetskyy, P.; Mpourmpakis, G., Structure-Activity Relationships in the Production of Olefins from Alcohols and Ethers: a First-Principles Theoretical Study. *Catal. Sci. Technol.* **2015,** *5*, 4547.
56. Dixit, M.; Kostetskyy, P.; Mpourmpakis, G. J. A. C., Structure–activity relationships in alkane dehydrogenation on γ-Al2O3: site-dependent reactions. **2018,** *8* (12), 11570-11578.
57. Dixit, M.; Kostetskyy, P.; Mpourmpakis, G., Structure–Activity Relationships in Alkane Dehydrogenation on γ-Al2O3: Site-Dependent Reactions. *ACS Catalysis* **2018,** *8* (12), 11570-11578.
58. Antony, A.; Asthagiri, A.; Weaver, J. F., Pathways and kinetics of methane and ethane C–H bond cleavage on PdO(101). *The Journal of Chemical Physics* **2013,** *139* (10), 104702.
59. Ricciarelli, D.; Meggiolaro, D.; Belanzoni, P.; Alothman, A. A.; Mosconi, E.; De Angelis, F., Energy vs Charge Transfer in Manganese-Doped Lead Halide Perovskites. *ACS Energy Letters* **2021,** *6*, 1869-1878.
60. Lunsford, J. H., The catalytic oxidative coupling of methane. *Angewandte Chemie International Edition in English* **1995,** *34* (9), 970-980.
61. Dai, Y.; Zhang, X.; Cui, Y.; Li, M.; Luo, Y.; Jiang, F.; Zhao, R.; Huang, Y., Theoretical insights into strong intrinsic piezoelectricity of blue-phosphorus-like group-IV monochalcogenides. *Nano Research* **2021**, 1-8.
62. Maciel, L.; Burimova, A.; Pereira, L.; Ferreira, W.; Sales, T.; Gonçalves, V.; Cabrera-Pasca, G.; Saxena, R.; Carbonari, A., DFT-based calculations of the magnetic hyperfine interactions at Cd sites in RCd (R= rare earth) compounds with the FP-LAPW ELK code. *AIP Advances* **2021,** *11* (2), 025010.
63. Valla, M.; Wischert, R.; Comas-Vives, A.; Conley, M. P.; Verel, R.; Copéret, C.; Sautet, P., Role of Tricoordinate Al Sites in CH3ReO3/Al2O3 Olefin Metathesis Catalysts. *Journal of the American Chemical Society* **2016,** *138* (21), 6774-6785.
64. Meyet, J.; Ashuiev, A.; Noh, G.; Newton, M. A.; Klose, D.; Searles, K.; van Bavel, A. P.; Horton, A. D.; Jeschke, G.; van Bokhoven, J. A., Methane-to-Methanol on Mononuclear Copper (II) Sites Supported on Al2O3: Structure of Active Sites from Electron Paramagnetic Resonance. *Angewandte Chemie International Edition* **2021,** *60* (29), 16200-16207.
65. Wischert, R.; Copéret, C.; Delbecq, F.; Sautet, P., Optimal Water Coverage on Alumina: A Key to Generate Lewis Acid–Base Pairs that are Reactive Towards the C□H Bond Activation of Methane. *Angewandte Chemie* **2011,** *123* (14), 3260-3263.
66. Wischert, R.; Laurent, P.; Copéret, C.; Delbecq, F. o.; Sautet, P., γ-Alumina: the essential and unexpected role of water for the structure, stability, and reactivity of "defect" sites. *Journal of the American Chemical Society* **2012,** *134* (35), 14430-14449.
67. Joubert, J.; Delbecq, F.; Sautet, P., Alkane metathesis by a tungsten carbyne complex grafted on gamma alumina: Is there a direct chemical role of the support? *Journal of Catalysis* **2007,** *251* (2), 507-513.
68. Joubert, J.; Salameh, A.; Krakoviack, V.; Delbecq, F.; Sautet, P.; Copéret, C.; Basset, J. M., Heterolytic Splitting of H2 and CH4 on γ-Alumina as a Structural Probe for Defect Sites. *The Journal of Physical Chemistry B* **2006,** *110* (47), 23944-23950.

69. Sader, S.; Miliordos, E., Methane to Methanol Conversion Facilitated by Anionic Transition Metal Centers: The Case of Fe, Ni, Pd, and Pt. *The Journal of Physical Chemistry A* **2021,** *125* (11), 2364-2373.
70. Martin, R.; Kim, M.; Asthagiri, A.; Weaver, J. F., Alkane Activation and Oxidation on Late-Transition-Metal Oxides: Challenges and Opportunities. *ACS Catalysis* **2021,** *11*, 4682-4703.
71. wwAbdelgaid, M.; Dean, J.; Mpourmpakis, G., Improving alkane dehydrogenation activity on γ-Al2O3 through Ga doping. *Catalysis Science & Technology* **2020,** *10* (21), 7194-7202.
72. Batchu, S. P.; Wang, H.-L.; Chen, W.; Zheng, W.; Caratzoulas, S.; Lobo, R. F.; Vlachos, D. G., Ethane Dehydrogenation on Single and Dual Centers of Ga-modified γ-Al2O3. *ACS Catalysis* **2021,** *11* (3), 1380-1391.
73. Hargreaves, J.; Hutchings, G. J.; Joyner, R.; Taylor, S. H. J. A. C. A. G., A study of the methane–deuterium exchange reaction over a range of metal oxides. **2002,** *227* (1-2), 191-200.
74. Quanzhi, L.; Amenomiya, Y. J. A. c., Exchange reaction of methane on some oxide catalysts. **1986,** *23* (1), 173-182.
75. Weller, S.; Hindin, S. J. T. J. o. P. C., The Effect of Pretreatment on the Activity of Gamma-Alumina. II. Hydrogen–Deuterium Exchange. **1956,** *60* (11), 1506-1512.
76. Roy, S.; Mpourmpakis, G.; Hong, D.-Y.; Vlachos, D. G.; Bhan, A.; Gorte, R. J., Mechanistic Study of Alcohol Dehydration on γ-Al2O3. *ACS Catalysis* **2012,** *2* (9), 1846-1853.
77. Kostetskyy, P.; Nolan, C. M.; Dixit, M.; Mpourmpakis, G., Understanding Alkane Dehydrogenation through Alcohol Dehydration on γ-Al2O3. *Industrial & Engineering Chemistry Research* **2018,** *57* (49), 16657-16663.
78. Tsai, C.; Abild-Pedersen, F.; Studt, F.; Nørskov, J. K., Understanding trends in C–H bond activation in heterogeneous catalysis. **2017**.
79. Wang, C.-C.; Siao, S. S.; Jiang, J.-C., C–H bond activation of methane via σ–d interaction on the IrO2 (110) surface: density functional theory study. *The Journal of Physical Chemistry C* **2012,** *116* (10), 6367-6370.
80. Yoo, J. S.; Khan, T. S.; Abild-Pedersen, F.; Nørskov, J. K.; Studt, F., On the role of the surface oxygen species during A–H (A= C, N, O) bond activation: a density functional theory study. *Chemical communications* **2015,** *51* (13), 2621-2624.
81. Antony, A.; Asthagiri, A.; Weaver, J. F., Pathways and kinetics of methane and ethane C–H bond cleavage on PdO (101). *The Journal of chemical physics* **2013,** *139* (10).
82. Zhao, Z.-J.; Kulkarni, A.; Vilella, L.; Nørskov, J. K.; Studt, F., Theoretical insights into the selective oxidation of methane to methanol in copper-exchanged mordenite. *ACS Catalysis* **2016,** *6* (6), 3760-3766.
83. Latimer, A. A.; Aljama, H.; Kakekhani, A.; Yoo, J. S.; Kulkarni, A.; Tsai, C.; Garcia-Melchor, M.; Abild-Pedersen, F.; Nørskov, J. K., Mechanistic insights into heterogeneous methane activation. *Physical Chemistry Chemical Physics* **2017,** *19* (5), 3575-3581.
84. Wang, S.; Petzold, V.; Tripkovic, V.; Kleis, J.; Howalt, J. G.; Skulason, E.; Fernández, E.; Hvolbæk, B.; Jones, G.; Toftelund, A., Universal transition state scaling relations for (de) hydrogenation over transition metals. *Physical Chemistry Chemical Physics* **2011,** *13* (46), 20760-20765.

85. Tsai, C.; Latimer, A. A.; Yoo, J. S.; Studt, F.; Abild-Pedersen, F., Predicting promoter-induced bond activation on solid catalysts using elementary bond orders. *The Journal of Physical Chemistry Letters* **2015,** *6* (18), 3670-3674.
86. Hibbitts, D.; Neurock, M., Promotional effects of chemisorbed oxygen and hydroxide in the activation of C–H and O–H bonds over transition metal surfaces. *Surface Science* **2016,** *650*, 210-220.
87. VandeVondele, J.; Hutter, J., Gaussian basis sets for accurate calculations on molecular systems in gas and condensed phases. *The Journal of Chemical Physics* **2007,** *127* (11), 114105.
88. VandeVondele, J.; Hutter, J. J. T. J. o. c. p., An efficient orbital transformation method for electronic structure calculations. **2003,** *118* (10), 4365-4369.
89. Kuo, I.-F. W.; Mundy, C. J.; McGrath, M. J.; Siepmann, J. I.; VandeVondele, J.; Sprik, M.; Hutter, J.; Chen, B.; Klein, M. L.; Mohamed, F. J. T. J. o. P. C. B., Liquid water from first principles: Investigation of different sampling approaches. **2004,** *108* (34), 12990-12998.
90. VandeVondele, J.; Mohamed, F.; Krack, M.; Hutter, J.; Sprik, M.; Parrinello, M. J. T. J. o. c. p., The influence of temperature and density functional models in ab initio molecular dynamics simulation of liquid water. **2005,** *122* (1).
91. McGrath, M. J.; Siepmann, J. I.; Kuo, I.-F. W.; Mundy, C. J.; VandeVondele, J.; Hutter, J.; Mohamed, F.; Krack, M. J. T. J. o. P. C. A., Simulating fluid-phase equilibria of water from first principles. **2006,** *110* (2), 640-646.
92. Ihm, J.; Zunger, A.; Cohen, M. L. J. J. o. P. C. S. S. P., Momentum-space formalism for the total energy of solids. **1979,** *12* (21), 4409.
93. Huzinaga, S.; Andzelm, J.; Radzio-Andzelm, E.; Sakai, Y.; Tatewaki, H.; Klobukowski, M., *Gaussian basis sets for molecular calculations*. Elsevier: 2012.
94. Kohn, W.; Sham, L. J. J. P. r., Self-consistent equations including exchange and correlation effects. **1965,** *140* (4A), A1133.
95. Mardirossian, N.; Head-Gordon, M., ωB97M-V: A combinatorially optimized, range-separated hybrid, meta-GGA density functional with VV10 nonlocal correlation. *The Journal of Chemical Physics* **2016,** *144* (21), 214110.
96. Becke, A. D. J. T. J. o. c. p., Density-functional thermochemistry. V. Systematic optimization of exchange-correlation functionals. **1997,** *107* (20), 8554-8560.
97. Perdew, J. P.; Ruzsinszky, A.; Tao, J.; Staroverov, V. N.; Scuseria, G. E.; Csonka, G. I. J. T. J. o. c. p., Prescription for the design and selection of density functional approximations: More constraint satisfaction with fewer fits. **2005,** *123* (6).
98. Becke, A. D. J. T. J. o. c. p., Density-functional thermochemistry. I. The effect of the exchange-only gradient correction. **1992,** *96* (3), 2155-2160.
99. Gill, P. M.; Adamson, R. D.; Pople, J. A. J. M. P., Coulomb-attenuated exchange energy density functionals. **1996,** *88* (4), 1005-1009.
100. Grimme, S.; Antony, J.; Ehrlich, S.; Krieg, H. J. T. J. o. c. p., A consistent and accurate ab initio parametrization of density functional dispersion correction (DFT-D) for the 94 elements H-Pu. **2010,** *132* (15).
101. Grimme, S.; Ehrlich, S.; Goerigk, L. J. J. o. c. c., Effect of the damping function in dispersion corrected density functional theory. **2011,** *32* (7), 1456-1465.
102. Grimme, S. J. J. o. c. c., Semiempirical GGA-type density functional constructed with a long-range dispersion correction. **2006,** *27* (15), 1787-1799.

103. Lee, K.; Murray, É. D.; Kong, L.; Lundqvist, B. I.; Langreth, D. C. J. P. R. B., Higher-accuracy van der Waals density functional. **2010,** *82* (8), 081101.
104. Vydrov, O. A.; Van Voorhis, T. J. T. J. o. c. p., Nonlocal van der Waals density functional: The simpler the better. **2010,** *133* (24).
105. Gilbert, T. L., Hohenberg-Kohn theorem for nonlocal external potentials. *Physical Review B* **1975,** *12* (6), 2111-2120.
106. Peverati, R.; Truhlar, D., Improving the Accuracy of Hybrid Meta-GGA Density Functionals by Range Separation. *The Journal of Physical Chemistry Letters* **2011,** *2*.
107. Weinhold, F., Natural bond orbital analysis: A critical overview of relationships to alternative bonding perspectives. *Journal of Computational Chemistry* **2012,** *33* (30), 2363-2379.

Appendices

The relaxed Cartesian coordinates of relevant structures:

Table 1: Initial state (IS) for the C-H bond activation on Al^{IV}-O^{II} site pair of γ-Al_2O_3 through the polar mechanism.

O	0.21151000	3.24620000	-0.48193200
Al	1.29215000	2.08293600	0.26638400
O	2.43037600	-1.97046400	-0.18593400
O	-0.27280500	-1.62309400	-1.19218600
A	0.77175000	-2.39107300	0.19255800
O	-1.89411700	-0.64436200	1.07635500
O	0.89607800	-0.97365000	1.43792200
O	-0.22682400	1.62388100	1.30118900
O	-3.14799500	-1.29313700	-0.92817000
O	-1.37758100	0.97508600	-1.33875500
Al	-0.01715600	-0.00039700	-1.61863300
Al	2.33946300	-0.30607100	0.38027000
Al	-0.46357200	-0.00154800	1.72777300
Al	-2.80794200	0.30469700	-0.28859300
O	-2.92743900	1.95751600	0.28665600
Al	-1.26797100	2.39106600	-0.08319700
O	-0.70643200	-3.24798800	0.59246000
Al	-1.78966300	-2.08531700	-0.14981800
C	4.89004700	0.01320800	-1.06841800
H	4.62545900	-1.04440100	-1.03830700
H	5.02881900	0.41675300	-0.06391100
H	5.82356500	0.13087300	-1.61701700
H	4.11316600	0.58109800	-1.58410000

Table 2: Initial state (IS) for the C-H bond activation on Al^{IV}-O^{III} site pair of γ-Al_2O_3 through the polar mechanism.

O	2.66666200	1.22618800	1.06917400
O	-0.19537300	1.61945700	1.30770400
Al	1.33748800	2.04879500	0.28033300
O	-1.34981800	1.00337900	-1.33902500
O	1.43250900	0.61428700	-0.96359300
O	-0.30138500	-1.61848600	-1.19492100
O	-2.88368300	2.01424300	0.28402100
O	-1.91101800	-0.61182100	1.06990100
Al	-0.46973700	-0.00151200	1.72864400
Al	2.33079400	-0.36243300	0.39174100

Al	-0.00962200	-0.00046200	-1.61607700
Al	-2.79811700	0.36105500	-0.29608400
O	-3.16999500	-1.22720000	-0.94186100
Al	-1.83234700	-2.05069800	-0.16035300
O	0.28525000	3.23751300	-0.46834300
Al	-1.21387200	2.41311300	-0.07841000
C	4.86880100	0.01415300	-1.10486300
H	5.06744200	0.39822600	-0.10363700
H	5.80088100	0.00530500	-1.66823600
H	4.48176700	-1.00695200	-1.07048300
H	4.15753100	0.67087800	-1.60706400

Table 3: Initial state (IS) for the C-H bond activation on Al^{III}-O^{II} site pair of γ-Al_2O_3 through the polar mechanism.

O	0.21151000	3.24620000	-0.48193200
Al	1.29215000	2.08293600	0.26638400
O	2.43037600	-1.97046400	-0.18593400
O	-0.27280500	-1.62309400	-1.19218600
Al	0.77175000	-2.39107300	0.19255800
O	-1.89411700	-0.64436200	1.07635500
O	0.89607800	-0.97365000	1.43792200
O	-0.22682400	1.62388100	1.30118900
O	-3.14799500	-1.29313700	-0.92817000
O	-1.37758100	0.97508600	-1.33875500
Al	-0.01715600	-0.00039700	-1.61863300
Al	2.33946300	-0.30607100	0.38027000
Al	-0.46357200	-0.00154800	1.72777300
Al	-2.80794200	0.30469700	-0.28859300
O	-2.92743900	1.95751600	0.28665600
Al	-1.26797100	2.39106600	-0.08319700
O	-0.70643200	-3.24798800	0.59246000
Al	-1.78966300	-2.08531700	-0.14981800
C	4.89004700	0.01320800	-1.06841800
H	4.62545900	-1.04440100	-1.03830700
H	5.02881900	0.41675300	-0.06391100
H	5.82356500	0.13087300	-1.61701700
H	4.11316600	0.58109800	-1.58410000

Table 4 Initial state (IS) for the C-H bond activation on Al^{III}-O^{III} site pair of γ-Al_2O_3 through the polar mechanism.

O	-1.44345000	-2.92851200	0.40336100
O	-0.72247000	-1.47313900	-1.44119700

O	1.82219800	-2.72317300	-0.78297900
Al	0.17315800	-2.58402400	-0.19331000
O	-3.26554800	-0.21690800	-0.79424000
O	-0.90864800	1.36130700	-1.44462900
Al	-2.32325900	1.14178000	-0.20183100
O	0.71390600	1.45186300	1.01939800
O	-1.61517300	-0.10534500	1.01749500
O	0.89835900	-1.34400200	1.02329300
O	1.44929900	2.93542500	-0.79072800
O	1.63911100	0.10535000	-1.43908300
Al	0.00333300	-0.00261700	-1.88085900
Al	-2.15299700	-1.43835200	-0.19853600
Al	-0.00198000	0.00142200	1.58704600
Al	2.15248400	1.44031100	-0.19506400
O	3.25792400	0.21495000	0.40703800
Al	2.32327300	-1.14668000	-0.19191300
O	-1.81543100	2.71435300	0.39533800
Al	-0.16737800	2.58298200	-0.20050900
C	-0.01649400	0.01286600	3.83657600
H	-1.06899000	-0.09106700	3.54235000
H	-0.02363100	0.01781800	4.92496500
H	0.60153600	-0.85017800	3.55657900
H	0.42317900	0.97620700	3.54681100

Table 5: Transition state (TS) for the C-H bond activation on Al^{IV}-O^{II} site pair of γ-Al_2O_3 through the polar mechanism.

O	-0.40751300	3.26114600	0.46440100
O	-0.27480100	1.57564000	-1.31738900
O	-3.06863600	0.99295500	-0.83528600
Al	-1.66808600	2.14850200	-0.11381900
O	2.57665000	1.99628100	-0.69868000
O	1.52923700	-0.64289900	-1.20111900
Al	2.58937300	0.38437700	-0.01770500
O	0.23241700	-1.53227000	1.27402800
O	1.27244000	1.05840700	1.16454000
O	-1.58362000	0.67004700	1.10662900
O	0.55662900	-3.29147500	-0.41803700
O	-1.22296200	-1.12587900	-1.22251900
Al	0.01126700	-0.05616900	-1.69511900
Al	0.97300100	2.41157200	-0.12498600
Al	-0.05440400	0.10807700	1.62270100
Al	-0.89924800	-2.46542400	0.08945000
O	-2.51802000	-2.07900100	0.64013000
Al	-2.53727600	-0.47696100	-0.06153800
O	3.07263400	-1.16451600	0.64370700
Al	1.64911800	-2.02280100	0.09788400

C	-3.37052600	3.41356100	0.06717700
H	-3.18286500	3.65489500	1.11678700
H	-2.98279500	4.23064000	-0.54659800
H	-4.45671400	3.42774500	-0.06102500
H	-3.47066600	2.11470100	-0.40839700

Table 6: Transition state (TS) for the C-H bond activation on Al^{IV}-O^{III} site pair of γ-Al_2O_3 through the polar mechanism.

O	-0.19183600	3.33904700	-0.01303900
O	0.08131700	1.41745600	-1.46270700
O	-2.57620700	0.92693400	-1.05808300
Al	-1.48554600	2.21100200	-0.48247700
O	2.85429500	1.88191900	-0.55974700
O	1.86821600	-0.79625200	-1.06661200
Al	2.75852200	0.30612500	0.17757700
O	0.34421500	-1.62359400	1.33871800
O	1.26220800	1.03692700	1.13297300
O	-1.60088100	0.41209100	1.29972200
O	0.81677100	-3.41573900	-0.27134400
O	-0.85817400	-1.27192300	-1.24974400
Al	0.39450300	-0.22576700	-1.70527200
Al	1.18915100	2.33873600	-0.27319600
Al	0.02786400	0.00623300	1.66796200
Al	-0.69034100	-2.59197600	0.07841100
O	-2.36167300	-2.19270300	0.42750900
Al	-2.28747600	-0.57737800	-0.26637800
O	3.16832400	-1.19074000	0.98637200
Al	1.84914400	-2.11832400	0.29581800
C	-2.73378100	2.83178300	1.06895800
H	-2.29528400	3.41309700	1.88039700
H	-3.06812700	3.59533400	0.34307800
H	-3.67770700	2.38259400	1.39030400
H	-2.06919300	1.41599400	1.30038300

Table 7: Transition state (TS) for the C-H bond activation on Al^{III}-O^{III} site pair of γ-Al_2O_3 through the polar mechanism.

O	-0.31990700	1.54895500	1.66682900
O	0.36601900	0.08581500	-0.18309500
O	-2.48057300	-0.51135800	-0.12679700
Al	-1.24861500	0.32614500	0.80095900
O	2.95425200	0.59463000	1.02281000
O	2.22348300	-2.02992700	0.02809000
Al	2.96523900	-1.09951800	1.47111500

O	0.54852800	-3.25814500	2.10318000
O	1.41015100	-0.61480200	2.50190500
O	-1.27143200	-1.18384000	1.89626400
O	1.24896900	-4.75735100	0.29506300
O	-0.50670100	-2.60381300	-0.57480300
Al	0.76734400	-1.49347300	-0.66308200
Al	1.24118400	0.86346800	1.27601400
Al	0.04835900	-1.77934700	2.82368700
Al	-0.32430200	-4.05214200	0.64165700
O	-2.03687800	-3.79826500	0.93178200
Al	-2.02943700	-2.11041000	0.44945800
O	3.39358300	-2.67939300	2.08782000
Al	2.14813400	-3.54198900	1.18650900
C	0.35625600	-1.30955100	4.79951100
H	0.53970400	-2.30689400	5.21014700
H	1.02778300	-0.65645900	5.37027800
H	-0.64601400	-0.96646400	5.07317600
H	1.14555300	-0.72289600	3.73473100

Table 8: Transition state (TS) for the C-H bond activation on Al^{III}-O^{II} site pair of γ-Al_2O_3 through the polar mechanism.

O	-0.10047100	0.92413000	2.50182800
O	0.29385100	0.19247400	0.15942000
O	-2.53107500	-0.56467900	0.37109700
Al	-1.19271400	0.08029300	1.29010300
O	3.08961500	0.54095100	0.97127000
O	2.20698300	-1.95152300	-0.21363700
Al	3.18838000	-1.21997500	1.20622300
O	0.80685000	-3.41744300	2.00873500
O	1.79005900	-0.97049600	2.38692300
O	-1.07692200	-1.53533100	2.08000400
O	1.28296200	-4.72679100	-0.04108700
O	-0.55735100	-2.49509100	-0.50885800
Al	0.67262300	-1.33409900	-0.57368200
Al	1.45052800	0.60080100	1.57193900
Al	0.42217500	-1.93510500	2.87551200
Al	-0.22431700	-4.08095900	0.56353100
O	-1.93524800	-3.96862600	0.92338100
Al	-2.00849300	-2.24218000	0.65094200
O	3.71371800	-2.85731700	1.52718500
Al	2.28134100	-3.58808300	0.83110300
C	0.01623300	-0.81633100	4.61019700
H	0.19119700	-1.87721500	4.93171800
H	0.76695700	-0.28837800	5.19842800
H	-0.98082400	-0.63329200	5.01112300

H	-0.04537700	0.10724500	3.48980900

Table 9: Final state (FS) for the C-H bond activation on Al^{IV}-O^{II} site pair of γ-Al_2O_3 through the polar mechanism.

O	-3.51866800	1.77580300	-0.31967100
O	-1.55485400	0.14362100	1.00043600
O	-0.92122200	3.11939400	0.76132200
Al	-1.89066200	1.80722600	0.14269700
O	-1.41820200	-2.89073600	0.80564500
O	0.93437900	-1.43915900	1.18882500
Al	0.10820500	-2.66752100	0.04641900
O	1.73466100	-0.14343400	-1.23944300
O	-0.79994500	-1.41647200	-1.14259500
O	-0.54649200	1.52696900	-1.15264700
O	3.54616200	-0.28810800	0.45430700
O	1.14985800	1.28561800	1.17506100
Al	0.09667900	-0.00234900	1.53917900
Al	-2.22176700	-1.48469000	0.13081600
Al	0.06860200	-0.01198000	-1.58100200
Al	2.59006900	1.07147800	-0.06553500
O	2.17284500	2.67226200	-0.61831800
Al	0.55700800	2.63103700	0.02185400
O	1.69395400	-2.98498300	-0.60039000
Al	2.38015100	-1.47841500	-0.05524000
C	-4.05783700	-1.30646000	-0.43091300
H	-4.15903800	-0.60714800	-1.26278100
H	-4.06494300	2.50172600	-0.61257200
H	-4.68929500	-0.91183600	0.36845100
H	-4.46721300	-2.27239500	-0.73732500

Table 10: Final state (FS) for the C-H bond activation on Al^{IV}-O^{III} site pair of γ-Al_2O_3 through the polar mechanism.

O	3.20361700	-0.76972400	-0.55496700
O	1.63380900	-0.31808000	1.36745800
O	1.04911500	-3.16305500	0.60891600
Al	1.92425000	-1.75494300	0.06076400
O	1.09603200	1.42527200	-0.73642800
O	-0.64451300	1.55146600	1.53286700
Al	-0.09957100	2.39392900	0.06368500
O	-1.46292300	0.41457000	-0.80442000
O	0.13333200	0.56328300	-3.37048200
O	0.48710600	-1.37051200	-1.01003300
O	-3.46561500	0.36823800	0.72601900
O	-1.09938500	-1.31011300	1.38686000

Al	-0.01021500	-0.04774400	1.71205100
Al	2.65083100	0.71910700	0.16342500
Al	0.06155300	0.16145500	-1.73098500
Al	-2.44377800	-0.93834900	0.13216000
O	-2.12748700	-2.49846400	-0.55568500
Al	-0.48666900	-2.55084600	0.04410300
O	-1.62660900	3.09952500	-0.26196500
Al	-2.37118600	1.59611900	0.25054400
C	3.55106200	2.28009700	0.88848300
H	3.97421400	2.92062400	0.11002800
H	4.37291500	2.00750400	1.55500000
H	2.88028600	2.91259300	1.48540800
H	0.12659400	0.01597000	-4.15116200

Table 11: Final state (FS) for the C-H bond activation on Al^{III}-O^{III} site pair of γ-Al_2O_3 through the polar mechanism.

O	-3.24304900	0.08165600	0.45831200
O	-1.71647300	0.04424000	-1.47601500
O	-1.71914100	-2.79628400	-0.77716500
Al	-2.26700900	-1.23417200	-0.16928200
O	-1.57590000	2.88062700	-0.77337700
O	0.84073300	1.38216800	-1.47361300
Al	0.04476100	2.58274800	-0.17865400
O	1.63081200	-0.04212600	1.12689500
O	-0.70574400	1.35704800	0.94470100
O	-0.77363000	-1.32177900	0.94385200
O	3.24901900	-0.08120100	-0.74650900
O	0.76974700	-1.41935100	-1.47432000
Al	-0.07735800	0.00381300	-1.86552600
Al	-2.20193800	1.34693700	-0.16841800
Al	-0.12516300	0.00174900	1.89718800
Al	2.18985800	-1.39840500	-0.31860000
O	1.57964600	-2.88103200	0.33885700
Al	-0.08547700	-2.58136000	-0.18250000
O	1.72287100	2.79712600	0.34329500
Al	2.25805200	1.28752700	-0.31767900
C	0.06424900	-0.00651500	3.82269800
H	0.62039100	0.85924400	4.19481100
H	0.57036300	-0.90429600	4.19038300
H	-0.91036500	0.01989000	4.31775400
H	2.29855200	-0.05935800	1.82667900

Table 12: Final state (TS) for the C-H bond activation on Al^{III}-O^{II} site pair of γ-Al_2O_3 through the polar mechanism.

O	-2.84001700	-1.66857100	0.41969200
O	-1.44885900	-0.81699100	-1.44338800
O	-0.00084800	-3.28336100	-0.76407700
Al	-1.27780600	-2.24434300	-0.14907400
O	-2.90624400	1.58359500	-0.82306600
O	0.00044200	1.67198200	-1.43770100
Al	-1.35991800	2.11805700	-0.26825000
O	1.35541500	0.82022600	0.95220200
O	-1.35498800	0.82092400	0.95216900
O	-0.00042600	-1.52680100	0.96214400
O	2.90710800	1.58209800	-0.82300300
O	1.44844300	-0.81772800	-1.44341100
Al	-0.00001400	-0.02979000	-1.80414400
Al	-2.60606800	-0.04639000	-0.16353800
Al	-0.00002700	0.01121900	1.84208000
Al	2.60604700	-0.04773800	-0.16352300
O	2.83913100	-1.67004100	0.41969000
Al	1.27664400	-2.24499400	-0.14908400
O	0.00088100	3.29288800	0.30855100
Al	1.36104900	2.11732800	-0.26819900
C	-0.00000200	0.11184300	3.77915700
H	0.00099800	3.80452300	1.12184200
H	0.00015400	1.14065100	4.15292700
H	-0.87801500	-0.37758800	4.21014400
H	0.87777900	-0.37791500	4.21023200

Table 13: Initial state (IS) for the C-H bond activation on B^{IV}-O^{II} site pair of γ-Al_2O_3 through the polar mechanism.

O	-2.37559400	-1.87391400	-0.06979800
O	-0.83451200	-1.31443800	-1.61599500
O	0.83714400	-3.26435800	-0.18091300
Al	-0.67243900	-2.40947300	-0.05461800
O	-2.50605900	0.42120000	-1.10182800
O	0.01051100	1.34032400	-1.35420300
Al	-1.52983800	1.72433200	-0.27076900
O	1.19684200	1.19922200	1.25166100
O	-1.64265900	0.98103800	1.33632600
O	0.15587200	-1.35079900	1.19886400
O	2.65301300	2.07924300	-0.51437900
O	1.91453500	-0.69679600	-1.00568100
Al	0.48098500	-0.21513500	-1.76610800
Al	-0.17887200	0.27082100	1.68110800

Al	2.64697700	0.52479100	0.30300900
O	3.06167300	-0.96181400	1.15421100
Al	1.80902300	-1.92245100	0.41661500
O	-0.59730800	3.21366300	0.02675500
Al	0.96372200	2.44673300	-0.17302500
C	-5.01617300	0.05725100	0.98568600
H	-4.06996200	0.40194700	1.40057500
H	-5.30139800	0.69415800	0.14862000
H	-4.88546900	-0.96345000	0.62957200
H	-5.79543600	0.08663300	1.74705400
B	-2.11852100	-0.83967900	-0.92217500

Table 14: Initial state (IS) for the C-H bond activation on B^{IV}-O^{III} site pair of γ-Al_2O_3 through the polar mechanism.

O	-2.12591100	1.77964700	0.02870400
O	-0.32467000	1.58863600	1.95984300
O	1.14676600	3.18384800	0.20468500
Al	-0.42442100	2.35719700	0.36658000
O	-2.77047600	-0.39967400	1.11701900
O	-0.04249500	-1.28726300	1.36959000
Al	-1.65128400	-1.67706600	0.57025000
O	0.93581700	-1.30992800	-1.35577100
O	-1.78883700	-0.47517400	-0.91142200
O	0.26160100	1.41253000	-1.16117600
O	2.47163800	-2.32393900	0.27627700
O	2.04229200	0.43857900	0.86604500
Al	0.63104700	0.23563000	1.81905800
Al	-0.24890800	-0.12446500	-1.59384100
Al	2.56234000	-0.73438300	-0.47970200
O	3.03674100	0.70963500	-1.35958500
Al	1.96735400	1.79521900	-0.47481400
O	-0.89050700	-3.12763700	-0.01660300
Al	0.74540400	-2.48532000	0.09943500
C	-5.03516100	0.43458000	-1.28829300
H	-5.21680100	0.22626200	-0.23461700
H	-5.98711700	0.52536400	-1.80908300
H	-4.48265200	1.36944000	-1.38317000
H	-4.46044700	-0.38090200	-1.72762700
B	-2.36352000	0.47394500	0.15057200

Table 15: Initial state (IS) for the C-H bond activation on B^{III}-O^{III} site pair of γ-Al_2O_3 through the polar mechanism.

O	-3.28179100	-0.11945300	0.45584300

O	-1.64672700	-0.05548100	-1.41035800
O	-1.53596900	-2.89806900	-0.57862400
Al	-2.19415400	-1.35062200	-0.12392500
O	-1.74231500	2.78308900	-0.56642300
O	0.77607400	1.46211600	-1.40421200
Al	-0.07253700	2.57625200	-0.11264200
O	1.36006500	0.04722200	0.98258800
O	-0.72374300	1.15226700	0.98197000
O	-0.63929400	-1.20495100	0.97781600
O	3.28161100	0.12091200	-0.56494600
O	0.87884100	-1.39338800	-1.40738500
Al	0.00328800	0.00532000	-1.83814600
Al	-2.28537000	1.19002800	-0.11677800
Al	2.26765300	-1.22384200	-0.11577600
O	1.74444800	-2.78360900	0.45708700
Al	0.11432700	-2.57382600	-0.12196100
O	1.53732700	2.89993700	0.47010000
Al	2.17420000	1.38673200	-0.11084400
C	-0.01580300	-0.02030600	4.02215100
H	-1.04454100	-0.05914200	3.66270500
H	-0.02107800	-0.02174400	5.11096900
H	0.53533300	-0.89219900	3.66918400
H	0.46737400	0.89208800	3.67178800
B	-0.00136000	-0.00249100	1.12514500

Table 16: Initial state (IS) for the C-H bond activation on B^{III}-O^{II} site pair of γ-Al_2O_3 through the polar mechanism.

O	3.22009000	-0.00158800	-0.19542800
O	1.23706200	-0.00082900	-1.68686600
O	1.40103400	2.84273300	-0.86590800
Al	2.08102100	1.27109000	-0.54758300
O	1.39839800	-2.84438800	-0.86524600
O	-1.18732900	-1.42815600	-1.17720900
Al	-0.13562300	-2.57985000	-0.08205000
O	-1.21887900	0.00067300	1.27602300
O	0.77682400	-1.17987100	0.84627100
O	0.77792700	1.17930300	0.84610400
O	-3.41697300	0.00154300	0.15226300
O	-1.18597700	1.42891800	-1.17757600
Al	-0.46721100	-0.00003300	-1.76905300
Al	2.07989400	-1.27332600	-0.54729500
Al	-2.28673800	1.30834200	0.37467000
O	-1.60085200	2.84717600	0.81579600
Al	-0.13318800	2.57992900	-0.08254600
O	-1.60346000	-2.84560900	0.81648600

Al	-2.28794900	-1.30623300	0.37513300
B	0.14152100	0.00003100	1.12485000
C	2.54557200	0.00017000	3.37125700
H	1.93115700	0.89284300	3.48899500
H	1.92729800	-0.88983600	3.48888700
H	3.00248300	-0.00078400	2.38166500
H	3.32240400	-0.00158000	4.13439900

Table 17: Transition state (TS) for the C-H bond activation on B^{IV}-O^{II} site pair of γ-Al_2O_3 through the polar mechanism.

O	-0.92473600	2.79735400	0.86110200
O	-0.30766400	1.90167600	-1.47498300
O	-2.84608700	1.20828500	0.32538300
O	2.32133100	2.22359000	-0.40017400
O	1.42191600	-0.42670500	-1.40842000
Al	2.44560600	0.49910800	-0.11006600
O	0.45367000	-1.87969900	1.14440500
O	0.99524700	0.82013900	1.07928700
O	-1.55736000	-0.11797200	2.20401100
O	0.48715600	-3.08500000	-1.00311500
O	-1.26002200	-0.74750000	-0.77118500
Al	-0.14098600	0.23700200	-1.60326000
Al	0.60647700	2.29657300	0.01658600
Al	0.06266400	-0.37217500	1.86834000
Al	-0.86446600	-2.48258400	-0.07157700
O	-2.45929400	-2.32405600	0.64070400
Al	-2.37269500	-0.56168300	0.71338500
O	3.06240100	-1.08489100	0.30402400
Al	1.64609000	-1.94404600	-0.30950800
C	-3.04563300	3.52229800	-0.49877700
H	-3.17086400	4.30421300	0.24878300
H	-2.34091700	3.80381300	-1.27958100
H	-4.02575400	3.41901300	-0.99165800
H	-3.35749600	2.21526500	-0.29322400
B	-2.06395100	2.36913300	0.37473200

Table 18: Transition state (TS) for the C-H bond activation on B^{IV}-O^{III} site pair of γ-Al_2O_3 through the polar mechanism.

O	-0.58541800	2.85575600	-0.24065900
O	0.62120100	1.39499200	-2.16589100
O	-2.36640700	1.20095100	-0.82728400
O	2.78797600	1.96567900	-0.44123100
O	2.01697200	-0.87728200	-1.06424800

Al	2.70636500	0.34732200	0.21068600
O	0.30140500	-1.71830700	1.43141200
O	1.00255200	0.92231300	0.83333500
O	-1.73183200	0.34081900	1.50508700
O	0.81010000	-3.35159500	-0.33238700
O	-0.71951700	-1.00964200	-1.09558800
Al	0.62163800	-0.23815400	-1.83736500
Al	1.03127200	2.15072500	-0.62431900
Al	-0.08174900	-0.08074400	1.65493000
Al	-0.68679000	-2.53219900	0.04048400
O	-2.38319900	-2.13498900	0.27256700
Al	-2.18316700	-0.43793300	-0.14190300
O	3.05629200	-1.09060700	1.15455300
Al	1.83766300	-2.08734300	0.35411600
C	-2.68317000	2.79436600	1.20155500
H	-2.18039700	3.40249500	1.94969700
H	-2.96939800	3.49109800	0.39523100
H	-3.64418300	2.41398500	1.55245900
H	-2.12142200	1.58673600	1.36857300
B	-1.73848300	2.20243400	-0.17422600

Table 19: Transition state (TS) for the C-H bond activation on B^{III}-O^{III} site pair of γ-Al_2O_3 through the polar mechanism.

O	-0.26159600	1.63868700	1.64508800
O	0.32107500	0.08044800	-0.19644900
O	-2.53504000	-0.55064700	0.25567200
Al	-1.19776000	0.34402200	0.93129600
O	2.97018600	0.67558600	0.94881100
O	2.23475400	-2.02430700	0.02303800
Al	3.02052200	-1.00949500	1.39562300
O	0.65231600	-2.91133100	2.20801300
O	1.40315800	-0.60219800	2.36085600
O	-0.94151900	-1.15883400	2.02489000
O	1.27769400	-4.74355100	0.69441100
O	-0.54994200	-2.66293100	-0.36298300
Al	0.70930800	-1.53828800	-0.56118000
Al	1.26166700	0.92480100	1.19407700
Al	-0.27604300	-3.99537400	0.97102300
O	-1.96432200	-3.76994900	1.35240400
Al	-1.97900300	-2.12273900	0.77493400
O	3.52800100	-2.52833200	2.08037400
Al	2.22708100	-3.42193900	1.32476500
C	0.18308000	-1.49874800	4.37917000
H	-0.62255600	-2.23788300	4.39885500
H	0.98803100	-1.91960500	4.98451600

H	-0.22611300	-0.59806400	4.84023000
H	1.06151800	-0.79166200	3.52137900
B	0.23618300	-1.63468900	2.63439100

Table 20: Transition state (TS) for the C-H bond activation on B^{III}-O^{II} site pair of γ-Al_2O_3 through the polar mechanism.

O	-0.08330300	1.00460300	2.50274200
O	0.30918000	0.27185600	0.09330300
O	-2.55205800	-0.48423500	0.49191500
Al	-1.15234700	0.19760900	1.26544800
O	3.10713000	0.55501900	1.09752700
O	2.20748000	-1.99650800	-0.14067200
Al	3.14988200	-1.20314400	1.27087200
O	0.70763700	-3.13106400	2.21290900
O	1.57045700	-0.97797400	2.22545100
O	-0.83919700	-1.42070600	1.96638500
O	1.20028300	-4.75097900	0.38522600
O	-0.58035200	-2.50858100	-0.43935900
Al	0.66780800	-1.35162800	-0.47363200
Al	1.43034900	0.67173500	1.54171500
Al	-0.29862600	-3.99359400	0.83251100
O	-2.01011500	-3.83904400	1.13113200
Al	-2.00870600	-2.15033900	0.71801900
O	3.66021500	-2.79807500	1.73745900
Al	2.21221100	-3.53265700	1.10048000
C	0.11405700	-1.10902200	4.27603500
H	0.28926900	-2.18487100	4.46267000
H	0.88594900	-0.64159300	4.89061400
H	-0.88135900	-0.96327100	4.70034600
H	0.00015900	0.04296900	3.37091700
B	0.41467700	-1.76353200	2.60319200

Table 21: Final state (FS) for the C-H bond activation on B^{IV}-O^{II} site pair of γ-Al_2O_3 through the polar mechanism.

O	-2.81504100	3.04181900	0.11013000
O	-1.09553800	1.37388400	-1.53504900
O	-3.50127800	0.05427100	-0.40486900
Al	-2.41992600	1.44550700	-0.33716200
O	2.85123600	2.31893200	-0.51230000
O	1.41469200	-0.31097500	-1.27814500
Al	2.69068800	0.58282700	-0.35234200
O	0.72495000	-1.34376200	1.21161400

O	1.47761600	1.34605900	1.01396300
O	-1.47056900	0.44498700	1.05596900
O	1.08498900	-3.26577700	-0.36640900
O	-1.07404800	-1.46319900	-1.00093800
Al	-0.27448200	-0.07849800	-1.63960400
Al	0.17234600	0.26585200	1.39601100
Al	-0.39575200	-2.61598000	0.29183500
O	-1.93599800	-2.54200000	1.08610700
Al	-2.42336700	-1.07703700	0.27790700
O	3.42338300	-0.88781300	0.14813300
Al	1.98266300	-1.82434600	-0.08190200
C	1.19761300	3.94184300	0.75316200
H	0.14475900	3.91254200	0.44796200
H	-3.60623100	3.31383700	0.57035300
H	1.66836400	4.79054500	0.25936400
H	1.20455100	4.11516300	1.83251500
B	1.88190200	2.60144500	0.38670700

Table 22: Final state (FS) for the C-H bond activation on B^{IV}-O^{III} site pair of γ-Al_2O_3 through the polar mechanism.

O	-3.83800700	0.59527500	0.59043300
O	-2.28229100	0.54807700	-1.10063400
O	-2.27850100	-2.17646900	0.43947100
Al	-2.45451400	-0.47023200	0.63365800
O	1.08807200	2.14851600	1.63802900
O	0.85177000	1.47983000	-1.16813400
Al	1.73425600	2.38945800	0.11236200
O	1.80775600	-0.36798100	0.51954700
O	0.64450900	-0.37120200	3.32494500
O	-0.81486200	0.17253800	0.92232400
O	2.76708000	-1.09770800	-1.72941100
O	-0.12274500	-1.25126100	-1.29273100
Al	-0.51926900	0.43098900	-0.88931600
Al	0.74989400	0.41404700	1.82260600
Al	1.58908600	-1.79057100	-0.64754800
O	0.79828100	-3.21303700	0.00863800
Al	-0.74996100	-2.52698800	-0.19664800
O	3.28533300	1.97196800	-0.49378500
Al	2.65588300	0.42508300	-0.95580500
C	-4.19032000	2.31480400	-1.35419600
H	-5.07654800	2.66544600	-0.82707900
H	-4.48794000	1.98038900	-2.35192600
H	-3.51884200	3.16462300	-1.50745000
H	1.24393800	-0.35925100	4.06632000
B	-3.46794800	1.16367600	-0.59104200

Table 23: Final state (FS) for the C-H bond activation on B^{III}-O^{III} site pair of γ-Al_2O_3 through the polar mechanism.

O	-3.28531500	-0.00678600	0.47785400
O	-1.69530800	-0.00335100	-1.42941500
O	-1.62069300	-2.84552000	-0.57117200
Al	-2.23376800	-1.27335500	-0.10289800
O	-1.63246300	2.83915400	-0.57011500
O	0.84032200	1.41256600	-1.36034200
Al	0.00213400	2.54319900	-0.03587300
O	1.45696000	0.00227000	1.14401600
O	-0.70235700	1.17251000	0.97280300
O	-0.69820800	-1.17613300	0.97342200
O	3.28521000	0.00660300	-0.54552800
O	0.84646200	-1.40784200	-1.35918800
Al	-0.03332800	0.00027700	-1.74767100
Al	-2.23889300	1.26409300	-0.10262700
Al	2.23803000	-1.32717000	-0.15364500
O	1.65954800	-2.81922500	0.51188100
Al	0.01265000	-2.54265500	-0.03685200
O	1.64827600	2.82477600	0.51262300
Al	2.23196900	1.33592600	-0.15564400
C	-0.15742800	0.00016700	3.21600200
H	0.32674100	0.89138900	3.62810700
H	0.33012100	-0.88859400	3.62944400
H	-1.18157300	-0.00152000	3.59985700
H	1.93561200	0.00577000	1.98386200
B	-0.20202500	-0.00086600	1.63314500

Table 24: Final state (FS) for the C-H bond activation on B^{III}-O^{II} site pair of γ-Al_2O_3 through the polar mechanism.

O	-3.28531500	-0.00678600	0.47785400
O	-1.69530800	-0.00335100	-1.42941500
O	-1.62069300	-2.84552000	-0.57117200
Al	-2.23376800	-1.27335500	-0.10289800
O	-1.63246300	2.83915400	-0.57011500
O	0.84032200	1.41256600	-1.36034200
Al	0.00213400	2.54319900	-0.03587300
O	1.45696000	0.00227000	1.14401600
O	-0.70235700	1.17251000	0.97280300
O	-0.69820800	-1.17613300	0.97342200
O	3.28521000	0.00660300	-0.54552800
O	0.84646200	-1.40784200	-1.35918800

Al	-0.03332800	0.00027700	-1.74767100
Al	-2.23889300	1.26409300	-0.10262700
Al	2.23803000	-1.32717000	-0.15364500
O	1.65954800	-2.81922500	0.51188100
Al	0.01265000	-2.54265500	-0.03685200
O	1.64827600	2.82477600	0.51262300
Al	2.23196900	1.33592600	-0.15564400
C	-0.15742800	0.00016700	3.21600200
H	0.32674100	0.89138900	3.62810700
H	0.33012100	-0.88859400	3.62944400
H	-1.18157300	-0.00152000	3.59985700
H	1.93561200	0.00577000	1.98386200
B	-0.20202500	-0.00086600	1.63314500

Table 25: Initial state (IS) for the C-H bond activation on Ga^{IV}-O^{II} site pair of γ-Al_2O_3 through the polar mechanism.

O	-2.42536800	1.51735000	-0.96986600
O	-1.16751000	0.80521200	1.07697100
O	0.18944000	3.30303400	0.45738500
Al	-0.98261300	2.17662600	-0.20433700
O	-2.32927500	-1.91766200	0.27656200
O	0.40580800	-1.56982400	1.19879900
Al	-0.67342300	-2.34498000	-0.15217900
O	2.04664600	-0.73571000	-1.07992100
O	-0.76735800	-0.98285200	-1.43419000
O	0.46087800	1.58283600	-1.26891400
O	3.30381700	-1.41055700	0.91766300
O	1.66656500	0.95012100	1.32304200
Al	0.25221400	0.06341000	1.63785700
Al	0.62172200	-0.05101600	-1.70491600
Al	3.03025700	0.18881400	0.24916900
O	3.22053500	1.82151100	-0.36530100
Al	1.59839000	2.34560200	0.04381300
O	0.76083500	-3.28626900	-0.51932200
Al	1.89712000	-2.14713700	0.17412300
C	-4.69649900	0.19606800	1.18275600
H	-4.47876400	-0.86951900	1.08736300
H	-4.82755800	0.67314500	0.20897900
H	-5.62544700	0.30777000	1.74064200
H	-3.90031300	0.69910900	1.73574100
Ga	-2.27666800	-0.18101900	-0.30123900

Table 26: Initial state (IS) for the C-H bond activation on Ga^{IV}-O^{III} site pair of γ-Al_2O_3 through the polar mechanism.

O	-2.33229900	-1.91531100	0.26991600
O	-0.76594300	-0.98196700	-1.43699000
O	0.75842300	-3.28672700	-0.51918900
Al	-0.67578000	-2.34442900	-0.15482200
O	-2.42353000	1.51958900	-0.97544100
O	0.46366200	1.58268000	-1.26960900
Al	-0.98134700	2.17767800	-0.20752500
O	1.66434800	0.94908300	1.32465800
O	-1.16934100	0.80638600	1.07324900
O	0.40157200	-1.56990500	1.19814200
O	3.22189000	1.81906400	-0.36107500
O	2.04747600	-0.73722100	-1.07761400
Al	0.62434400	-0.05130400	-1.70533600
Al	0.24865500	0.06355200	1.63676600
Al	3.02916900	0.18661600	0.25339400
O	3.30015200	-1.41292400	0.92251300
Al	1.89424900	-2.14834500	0.17637700
O	0.19051300	3.30300200	0.45630600
Al	1.59948700	2.34452700	0.04509500
C	-4.68307200	0.19417800	1.20784100
H	-4.82891600	0.63773100	0.22009000
H	-5.61062500	0.30960200	1.76729500
H	-4.44830400	-0.86998200	1.14366400
H	-3.89146300	0.72752300	1.73821000
Ga	-2.27683000	-0.17883100	-0.30730900

Table 27: Initial state (IS) for the C-H bond activation on Ga^{III}-O^{III} site pair of γ-Al_2O_3 through the polar mechanism.

O	2.85054100	-1.59363800	0.25984000
O	1.43005800	-0.79631800	-1.57214200
O	2.81032100	1.67447100	-0.95344100
Al	2.59907800	0.03968400	-0.33944300
O	0.04688300	-3.26911100	-0.95833300
O	-1.40332800	-0.83753400	-1.57529900
Al	-1.26395000	-2.27047800	-0.34444700
O	-1.46778200	0.81915300	0.89418500
O	0.02356400	-1.68235000	0.89499700
O	1.44377700	0.86112100	0.89732100
O	-2.85411500	1.59484700	-0.95992700
O	-0.02173300	1.63837900	-1.57327100
Al	0.00157200	0.00194600	-2.02093600

Al	1.32792300	-2.23377600	-0.34221600
Al	-1.33420100	2.22956200	-0.34314600
O	-0.04636600	3.26477800	0.25803900
Al	1.27201400	2.26676200	-0.34113800
O	-2.80487700	-1.67260100	0.25476600
Al	-2.59782400	-0.03251600	-0.34452600
C	-0.01046200	-0.00003000	3.89086600
H	0.00520700	-1.05838400	3.60288700
H	-0.01513800	0.00230900	4.98137700
H	0.89949900	0.54248900	3.60488900
H	-0.93313800	0.51581200	3.59763600
Ga	-0.00029600	-0.00087100	1.51355600

Table 28: Initial state (IS) for the C-H bond activation on Ga^{III}-O^{II} site pair of γ-Al_2O_3 through the polar mechanism.

O	0.30274800	-1.59678900	-1.58535200
O	3.08575000	-1.02358100	-1.01060700
Al	1.72111900	-1.93551800	-0.37852700
O	-2.46178200	-2.17081000	-0.92478600
O	-1.58023500	0.51954300	-1.54522700
Al	-2.55335500	-0.52795400	-0.30266600
O	-0.33108900	1.64719500	0.90963200
O	-1.24581500	-1.11983700	0.91197300
O	1.60533800	-0.53013300	0.86596400
O	-0.68092900	3.20599600	-0.93567800
O	1.19317800	1.09430900	-1.58805000
Al	-0.03488600	0.00736100	-2.02256100
Al	-0.82989000	-2.46266300	-0.33743100
Al	0.80344400	2.46943200	-0.34577200
O	2.43925900	2.17153100	0.22713400
Al	2.53643300	0.52432900	-0.38159600
O	-3.10003900	1.02652500	0.31013700
Al	-1.73367500	1.94492000	-0.30673800
C	0.14717900	-0.03770600	3.88717500
H	1.13563300	-0.39673400	3.58269100
H	-0.03760900	1.00704700	3.60616900
H	-0.66558200	-0.72089900	3.60637200
H	0.14844600	-0.03867400	4.97735300
Ga	0.01980000	-0.00313100	1.51325100

Table 29: Transition state (TS) for the C-H bond activation on Ga^{IV}-O^{II} site pair of γ-Al_2O_3 through the polar mechanism.

O	0.66145900	-3.19723100	0.23640600

O	-0.29127700	3.33723000	0.42963400
O	-0.17371200	1.59300700	-1.36712900
O	-3.11746400	0.98568200	-0.81992300
O	2.66250800	1.95588600	-0.67146900
O	1.57037800	-0.67364100	-1.19456500
Al	2.62471100	0.34293800	0.00229100
O	0.24241800	-1.56107200	1.27659700
O	1.27500200	1.03531600	1.14214900
O	-1.58246700	0.64693700	1.14198600
O	0.55434400	-3.30348800	-0.43573300
O	-1.19245000	-1.09206900	-1.20882300
Al	0.06520600	-0.05606000	-1.69400600
Al	1.04633300	2.39584500	-0.15408500
Al	-0.04422100	0.08038600	1.61776700
Al	-0.89484900	-2.46649800	0.07384500
O	-2.51672100	-2.08801400	0.61173600
Al	-2.53284200	-0.46995200	-0.05742200
O	3.08050800	-1.20848600	0.67513200
Al	1.65772500	-2.05348700	0.10338100
C	-3.48000700	3.44173300	0.07059500
H	-3.27546800	3.70241100	1.11169200
H	-3.14300200	4.25212600	-0.57895500
H	-4.56993800	3.40719300	-0.02534100
H	-3.53538900	2.16485100	-0.36976100
Ga	-1.66469500	2.22237500	-0.11438000

Table 30: Transition state (TS) for the C-H bond activation on Ga^{IV}-O^{III} site pair of γ-Al_2O_3 through the polar mechanism.

O	-0.09725000	3.22752200	-0.15852000
O	0.74955800	1.46052800	-1.97454500
O	-2.59070100	1.07416900	-1.22311900
O	3.02656100	1.80872900	-0.23700900
O	2.07172600	-0.93416700	-0.96406000
Al	2.76338100	0.20360100	0.38128200
O	0.16186900	-1.74574500	1.36671300
O	1.05850500	0.88813400	0.90705700
O	-1.77683600	0.41306900	1.18196900
O	0.75014500	-3.40534700	-0.35525400
O	-0.65483700	-0.99342900	-1.19026000
Al	0.74772200	-0.19331100	-1.76466800
Al	1.32210100	2.21952800	-0.46249100
Al	-0.16936400	-0.09253400	1.52280000
Al	-0.74160800	-2.53948400	-0.08649900
O	-2.44698600	-2.14470700	0.00934800
Al	-2.26314700	-0.46708200	-0.46967100

O	2.97963400	-1.27409800	1.29988500
Al	1.76825200	-2.18484400	0.40457400
C	-2.81624200	2.85780100	1.33642000
H	-3.21138700	3.64518600	0.67134400
H	-3.73259700	2.42003400	1.74036800
H	-2.25855500	3.37375400	2.11594700
H	-2.28626600	1.53608100	1.30546400
Ga	-1.63537600	2.35748800	-0.37749200

Table 31: Transition state (TS) for the C-H bond activation on Ga^{III}-O^{III} site pair of γ-Al_2O_3 through the polar mechanism.

O	-0.09725000	3.22752200	-0.15852000
O	0.74955800	1.46052800	-1.97454500
O	-2.59070100	1.07416900	-1.22311900
O	3.02656100	1.80872900	-0.23700900
O	2.07172600	-0.93416700	-0.96406000
Al	2.76338100	0.20360100	0.38128200
O	0.16186900	-1.74574500	1.36671300
O	1.05850500	0.88813400	0.90705700
O	-1.77683600	0.41306900	1.18196900
O	0.75014500	-3.40534700	-0.35525400
O	-0.65483700	-0.99342900	-1.19026000
Al	0.74772200	-0.19331100	-1.76466800
Al	1.32210100	2.21952800	-0.46249100
Al	-0.16936400	-0.09253400	1.52280000
Al	-0.74160800	-2.53948400	-0.08649900
O	-2.44698600	-2.14470700	0.00934800
Al	-2.26314700	-0.46708200	-0.46967100
O	2.97963400	-1.27409800	1.29988500
Al	1.76825200	-2.18484400	0.40457400
C	-2.81624200	2.85780100	1.33642000
H	-3.21138700	3.64518600	0.67134400
H	-3.73259700	2.42003400	1.74036800
H	-2.25855500	3.37375400	2.11594700
H	-2.28626600	1.53608100	1.30546400
Ga	-1.63537600	2.35748800	-0.37749200

Table 32: Transition state (TS) for the C-H bond activation on Ga^{III}-O^{II} site pair of γ-Al_2O_3 through the polar mechanism.

O	0.18045700	-1.48436400	0.34994100

O	-0.07362300	-0.30241200	-1.81290100
O	2.72007600	0.37709100	-1.31910800
Al	1.34379700	-0.42848500	-0.59780100
O	-2.90375100	-0.78498000	-1.29239200
O	-1.96780100	1.87701200	-1.88989800
Al	-3.03782600	0.89157000	-0.70563700
O	-0.73075300	2.93409400	0.64792700
O	-1.75976900	0.37741300	0.51706700
O	1.22558800	0.99367000	0.50363600
O	-1.07596800	4.56318300	-1.16871300
O	0.79976800	2.44930200	-1.90296900
Al	-0.41366100	1.33041900	-2.27472400
Al	-1.31418300	-0.97814500	-0.58645400
Al	0.39662900	3.81393800	-0.59347800
O	2.08007800	3.61920400	-0.14723400
Al	2.18385000	1.97029900	-0.73110400
O	-3.59029100	2.44801900	-0.12019600
Al	-2.12573100	3.29282700	-0.58165600
C	-0.05300900	-0.29449400	2.80335700
H	-0.24143700	0.63211000	3.39830000
H	-0.83569400	-0.95583800	3.17499100
H	0.93183300	-0.59000600	3.16504800
Ga	-0.38291300	1.26355500	1.32623900
H	0.06070400	-0.87734700	1.53827700

Table 33: Final state (FS) for the C-H bond activation on Ga^{IV}-O^{II} site pair of γ-Al_2O_3 through the polar mechanism.

O	2.49082300	-2.92407100	-0.37633000
O	1.20483500	-0.74556500	1.01043500
O	-0.38658000	-3.33050400	0.72997500
Al	0.95645500	-2.39015500	0.12764200
O	2.08739900	2.32419000	0.73677000
O	-0.59871800	1.59390500	1.16568000
Al	0.54250200	2.50453300	-0.00543500
O	-1.83555100	0.64558100	-1.22491900
O	0.98091800	1.05057400	-1.19608200
O	-0.22182500	-1.66850600	-1.15704500
O	-3.47354100	1.37149600	0.49927100
O	-1.72483900	-0.90328600	1.18191300
Al	-0.29469800	-0.04028900	1.52489200
Al	-0.30044700	-0.01160000	-1.58130600
Al	-3.02649400	-0.22371900	-0.03872200
O	-3.16940700	-1.86915000	-0.60029100
Al	-1.62236600	-2.36350600	0.01908700
O	-0.87544500	3.32415700	-0.60024600

Al	-1.99096100	2.11354900	-0.03558500
C	4.17942300	-0.19117800	-0.40113700
H	4.01370800	-1.24365400	-0.62563200
H	2.71867400	-3.81205400	-0.64548600
H	4.88992700	-0.11256400	0.42317400
H	4.60804600	0.31376100	-1.26785700
Ga	2.49795700	0.65794900	0.09781100

Table 34: Final state (FS) for the C-H bond activation on Ga^{IV}-O^{III} site pair of γ-Al_2O_3 through the polar mechanism.

O	2.23013600	-1.05821500	-1.25867700
O	1.32184800	-0.95399000	1.11040500
O	-0.07025300	-3.26946800	0.10134400
Al	0.99935900	-1.97387700	-0.45203300
O	2.13373400	1.82358100	-0.03621600
O	-0.40982600	1.35098000	1.09138200
Al	0.51678900	2.31986700	-0.19861300
O	-2.31131100	0.78956500	-0.95893800
O	0.36027000	1.32603700	-1.91577900
O	-0.56552200	-1.36237500	-1.32615000
O	-3.28954800	1.22538800	1.25212700
O	-1.58826300	-1.11173200	1.34096500
Al	-0.13656200	-0.25379600	1.58961100
Al	-0.95623700	0.20715600	-1.77838000
Al	-3.04494100	-0.31022100	0.43648200
O	-3.22107000	-1.88303100	-0.32323400
Al	-1.55688000	-2.37507900	-0.06033000
O	-0.95701600	3.26890300	-0.30856300
Al	-2.01133000	2.06435400	0.39992700
C	4.58825400	-0.09076400	0.97725900
H	5.29035400	0.65231800	0.59606400
H	5.01153800	-1.08113300	0.80621500
H	4.50269100	0.06027400	2.05506800
H	1.22965600	0.90770400	-2.06199700
Ga	2.83349200	0.09745200	0.11016500

Table 35: Final state (FS) for the C-H bond activation on Ga^{III}-O^{III} site pair ofγ-Al_2O_3 through the polar mechanism.

O	-0.87241700	1.40075100	-1.61091900
O	-3.29498300	0.00056700	-0.83037300
Al	-2.25355900	1.33760300	-0.40876100
O	1.59814600	2.83688900	-1.01710300

O	1.64874800	0.00045100	-1.70425100
Al	2.20913000	1.29271600	-0.41808300
O	0.77266100	-1.36754800	0.75660100
O	0.77313000	1.36741100	0.75772500
O	-1.65421100	0.00009400	1.01013800
O	1.59768300	-2.83651300	-1.01867500
O	-0.87263600	-1.39982200	-1.61199500
Al	-0.00402100	0.00057600	-2.03271800
Al	-0.00558000	2.58314800	-0.35274400
Al	-0.00606600	-2.58265400	-0.35431100
O	-1.65966900	-2.83713700	0.22811700
Al	-2.25380400	-1.33689700	-0.40969000
O	3.23787100	-0.00030400	0.17838200
Al	2.20900100	-1.29283200	-0.41880500
C	0.05425900	-0.00297000	3.79400200
H	-0.47400000	-0.88997900	4.14784200
H	1.04385400	-0.00357600	4.25286500
H	-0.47458400	0.88241000	4.15094500
Ga	0.20470300	-0.00035300	1.84434800
H	-2.32427100	-0.00035300	1.70695400

Table 36: Final state (FS) for the C-H bond activation on Ga^{III}-O^{II} site pair of γ-Al_2O_3 through the polar mechanism.

O	-1.65915400	2.83749400	0.22973700
O	-0.00333300	3.29691700	0.13562500
O	-0.00193800	1.66935300	-1.59914800
O	-2.90575600	1.57772600	-1.00883400
Al	-1.36582900	2.11747500	-0.43615700
O	2.90216900	1.58335900	-1.00983900
O	1.44879500	-0.81576300	-1.60531000
Al	2.60658900	-0.04134500	-0.32822800
O	0.00165600	-1.56501000	0.80518800
O	1.38821000	0.84113400	0.79885100
O	-1.38958300	0.83825200	0.79910700
O	0.00309800	-3.27964600	-0.95088600
O	-1.44764400	-0.81857000	-1.60502200
Al	-0.00021000	-0.03060200	-1.96594600
Al	1.36143000	2.12011800	-0.43655700
Al	-1.27516800	-2.24774100	-0.31938600
O	-2.83720300	-1.67129200	0.25572100
Al	-2.60661900	-0.04646900	-0.32762600
O	2.84052700	-1.66569600	0.25510100
Al	1.27951300	-2.24530800	-0.31960400
C	0.00090000	0.11116800	3.75349200
H	-0.88038200	-0.37936200	4.16939500

H	0.88406200	-0.37680100	4.16842500
H	-0.00042000	1.14705700	4.09814100
Ga	0.00022200	0.00187000	1.79587000
H	-0.00371100	3.81836100	0.94222000

γ-Al_2O_3 (single doped)

Table 37: Initial energy state (IS) for the C-H bond activation on Al^{III}-O^{III} site-pair of B^{IV} doped γ-Al_2O_3 via polar pathway.

O	2.21351900	-2.31756300	0.51893500
O	1.52963900	-1.33292600	-1.39245100
O	3.18327800	0.90840800	-0.43770300
Al	2.50908000	-0.61259000	0.07972000
O	0.00056100	-3.02439100	-0.45693700
O	-1.22722700	-0.82267500	-1.42982700
Al	-1.44282200	-2.02394600	0.06306400
O	-1.35864000	1.01898100	0.76194600
O	-0.78243300	-1.60108800	1.63970300
O	1.29253300	0.36190000	1.03399800
O	-2.32728600	1.83222300	-1.34047300
O	0.54331500	1.37564900	-1.56812400
Al	0.28023300	-0.26519400	-1.90311000
Al	-0.29160800	-0.00236600	1.66344900
Al	-0.82780100	2.23851000	-0.51812600
O	0.54381800	3.05975700	0.23685800
Al	1.69125400	1.79911900	-0.14098200
O	-3.06370000	-1.27356600	0.06427100
Al	-2.48714700	0.25920700	-0.55449800
B	1.19078300	-2.43649600	-0.37697700
C	-0.29535100	0.85456000	3.76775000
H	-0.06615800	1.71767500	3.13113300
H	-0.24740800	1.21679700	4.79284000
H	-1.31486500	0.47801600	3.62803800
H	0.46214200	0.05934400	3.72107000

Table 38: Transition state energy (TS) for the C-H bond activation on Al^{III}-O^{III} site-pair of B^{IV} doped γ-Al_2O_3 via polar pathway.

O	1.80315300	-2.66247900	0.1374900o
O	3.33531400	0.48249900	-0.02548800
Al	2.39695100	-0.97687800	0.11142700

O	-0.38185900	-2.76756400	-1.10601200
O	-1.17262500	-0.24608100	-1.64732800
Al	-1.70830200	-1.67443500	-0.50906700
O	-1.21423500	1.07353100	0.88610700
O	-1.14242600	-1.72841100	1.18215300
O	1.24916600	-0.03477400	1.16810100
O	-1.86698700	2.47815600	-1.01826100
O	0.91506500	1.61030300	-1.18509400
Al	0.44352700	0.14268100	-1.88044100
Al	-0.40152500	-0.22868500	1.69633300
Al	-0.40264900	2.45007800	-0.04504900
O	1.00278600	2.86528400	0.93568100
Al	1.97405800	1.53150200	0.37151800
O	-3.18182700	-0.68911000	-0.38678900
Al	-2.32532600	0.82662300	-0.60860700
B	0.87435500	-2.41460800	-0.82928700
H	-1.31861900	-1.50052200	2.47368400
C	-1.01059700	-0.76241600	3.61458200
H	-1.60760500	-1.54311300	4.09766000
H	-0.03501200	-0.81827200	4.10656400
H	-1.51379000	0.17284200	3.87610300

Table 39: Final state energy (FS) for the C-H bond activation on Al^{III}-O^{III} site-pair of B^{IV} doped γ-Al_2O_3 via polar pathway.

O	2.32333500	-2.17738900	0.42727000
O	1.54802900	-1.23570200	-1.47389000
O	3.09488800	1.10736300	-0.53022800
Al	2.52393500	-0.44099100	0.01238200
O	0.16171900	-3.00433400	-0.47532500
O	-1.23882000	-0.87911800	-1.48186300
Al	-1.30866100	-2.05777400	-0.04263400
O	-1.36602500	0.83643700	0.76670700
O	-0.54644200	-1.61626800	1.59028900
O	1.24575700	0.39960200	0.94395200
O	-2.49670300	1.71692200	-1.23317500
O	0.40223300	1.45006800	-1.58980400
Al	0.23638800	-0.19553600	-1.91506800
Al	-0.22746500	0.18330900	1.94550700
Al	-0.98940400	2.17929400	-0.44688100
O	0.34341600	3.07416500	0.27278700
Al	1.55463300	1.89485400	-0.15591200
O	-2.93933700	-1.45744300	0.15556100

Al	-2.52064000	0.13266100	-0.47499500
B	1.32331700	-2.32858900	-0.48676400
C	-0.17224000	0.64418300	3.82287700
H	0.60080900	0.09581100	4.36952200
H	0.03606100	1.70798300	3.96746000
H	0.15176500	-2.22170600	1.86830600
H	-1.12239300	0.43570800	4.32181300

Table 40: Initial state energy (IS) for the C-H bond activation on Al^{IV}-O^{II} site-pair of B^{III} doped γ-Al_2O_3 via polar pathway.

O	2.34865600	-2.13555100	-0.13375100
O	0.79957000	-1.06354100	1.47555600
O	-0.87582200	-3.22996900	0.33696600
Al	0.65584800	-2.42007800	0.15440900
O	2.73106900	1.10860200	0.99418100
O	-0.16323800	1.62439300	1.31524000
Al	1.40059800	1.97984100	0.28935400
O	-1.04883100	0.87899300	-1.27058600
O	1.23790000	0.46091400	-0.86925200
O	-0.26443400	-1.34077000	-1.13149900
O	-2.76732100	2.12111900	-0.00648800
O	-1.97252900	-0.55752200	0.99164300
Al	-0.51688600	-0.00160000	1.68728500
Al	2.29093100	-0.47971400	0.41789700
Al	-2.72113800	0.43783200	-0.45177900
O	-3.16365600	-1.11070700	-1.11425300
Al	-1.87589600	-1.95420800	-0.29951600
O	0.45612900	3.23229200	-0.46885800
Al	-1.06028900	2.43413700	-0.15647400
B	-0.00191900	-0.00093400	-1.22111000
C	4.51962900	0.01478000	-1.61466900
H	4.17457000	-1.00855800	-1.44907200
H	3.74532600	0.58293800	-2.12997400
H	4.76970700	0.50861400	-0.67490000
H	5.41107600	-0.02378300	-2.23897400

Table 41: Transition state energy (TS) for the C-H bond activation on Al^{IV}-O^{II} site-pair of B^{III} doped γ-Al_2O_3 via polar pathway.

O	2.43228000	-1.37460200	-1.33577000
O	1.39213600	-0.59978600	0.80547800
O	-0.04856900	-3.14615500	0.20343100
Al	1.06435900	-1.98190400	-0.45206400

O	2.37949500	2.07536400	-0.11703600
O	-0.26443300	1.77359000	1.10953600
Al	0.73023200	2.48071800	-0.35882900
O	-1.69287600	0.73454400	-1.08244900
O	0.64934000	0.89020700	-1.42226400
O	-0.41441300	-1.22130000	-1.31068700
O	-3.19623600	1.55404300	0.71139400
O	-1.44487900	-0.79685900	1.27113600
Al	-0.01862300	0.12606500	1.46339400
Al	2.36882200	0.36612000	-0.54081700
Al	-2.86002900	-0.07237400	0.20248200
O	-3.12034900	-1.70777800	-0.33212300
Al	-1.47825400	-2.18094700	-0.02054900
O	-0.69459700	3.41660000	-0.71512400
Al	-1.76069000	2.27742500	0.04506900
B	-0.49508000	0.14719300	-1.40641100
H	3.53488900	-0.98358800	-0.91818200
C	4.44918800	-0.04614100	-0.38759200
H	5.16785400	-0.86153600	-0.51569100
H	4.82608100	0.78888600	-0.98218600
H	4.50509900	0.23342700	0.66860900

Table S42: Final state energy (FS) for the C-H bond activation on Al^{IV}-O^{II} site-pair of B^{III} doped γ-Al_2O_3 via polar pathway.

O	3.46585800	-1.70448700	-0.42588400
O	1.55356800	-0.16586800	1.08396200
O	0.91159600	-3.11953000	0.55326900
Al	1.85701700	-1.73739400	0.08635900
O	1.47944500	2.84626900	0.61126000
O	-0.95010200	1.47244500	1.17705500
Al	-0.08471800	2.62625500	-0.02753700
O	-1.46735900	0.13701400	-1.20087900
O	0.67133400	1.13613800	-1.08434400
O	0.43710900	-1.25552500	-1.09941000
O	-3.53895300	0.33112700	0.19820200
O	-1.19755000	-1.29255200	1.15881000
Al	-0.13799000	0.00665700	1.51260500
Al	2.22093000	1.35696000	0.07083100
Al	-2.56523700	-1.04912100	-0.16855600
O	-2.19029700	-2.64802800	-0.71709000
Al	-0.59357700	-2.58892400	-0.05740000
O	-1.63691600	3.00199700	-0.69761800
Al	-2.32315100	1.50783000	-0.16013200
B	-0.09604900	0.00804500	-1.26135700
H	3.96072900	-2.39375900	-0.86353600

C	4.02889800	1.21533300	-0.57844100
H	4.66799800	0.64156900	0.09390500
H	4.06755500	0.70440600	-1.54214500
H	4.45612400	2.21413300	-0.69966900

Table 43: Initial state energy (IS) for the C-H bond activation on Al^{IV}-O^{III} site-pair of B^{III} doped γ-Al_2O_3 via polar pathway.

O	-2.33493100	-2.15709400	0.11505800
O	-0.78398200	-1.07505300	-1.48615400
O	0.90216200	-3.22473700	-0.33161100
Al	-0.63764600	-2.42783800	-0.16073300
O	-2.73885000	1.08121100	-1.02104600
O	0.15315400	1.62183000	-1.32272400
Al	-1.42070700	1.96527100	-0.30770600
O	1.02794300	0.88830500	1.27038200
O	-1.25179500	0.44911600	0.85257700
O	0.26440700	-1.33854400	1.12922300
O	2.74393800	2.14357700	0.01599500
O	1.97973600	-0.54345300	-0.98328900
Al	0.52430700	-0.00137400	-1.69001000
Al	-2.28659400	-0.50228600	-0.44043800
Al	2.70971300	0.46067900	0.46384700
O	3.16143800	-1.08295900	1.13147500
Al	1.88679300	-1.93920900	0.30940400
O	-0.49226600	3.22709400	0.45453100
Al	1.03316600	2.44157600	0.15361800
B	-0.01074900	-0.00093500	1.21468800
C	-4.44897700	0.01311100	1.70402800
H	-4.05211700	-0.99216500	1.54395400
H	-5.39196900	-0.07273100	2.24177200
H	-3.74201000	0.59048300	2.29861400
H	-4.63135500	0.52742100	0.75895400

Table 44: Transition state energy (TS) for the C-H bond activation on Al^{IV}-O^{III} site-pair of B^{III} doped γ-Al_2O_3 via polar pathway.

O	2.89292700	-1.71232700	-0.06781700
O	1.15753800	-0.79194700	1.39039900
O	-0.06232400	-3.29827100	0.30962700
Al	1.26181200	-2.18216800	0.17881600
O	2.36572700	1.64692400	0.86989600

O	-0.47881800	1.54519200	1.29359800
Al	0.89416900	2.26213700	0.23610100
O	-1.31264200	0.64548800	-1.21617700
O	0.98440700	0.96514600	-1.27798800
O	0.08497000	-1.26291500	-1.13356800
O	-3.19569000	1.43781800	0.16489200
O	-1.70366200	-0.97836800	1.06283300
Al	-0.36358900	-0.10846600	1.67506500
Al	2.72089400	0.01372800	0.28762200
Al	-2.76252600	-0.18450400	-0.29847400
O	-2.82332100	-1.77400600	-1.00952300
Al	-1.33120800	-2.27704200	-0.27187500
O	-0.35502400	3.29552500	-0.42605000
Al	-1.62877900	2.16131500	-0.07189500
B	-0.08346600	0.07206900	-1.32715800
H	2.02850800	0.70061800	-1.48071900
C	3.62023400	0.56984400	-1.49529500
H	3.69945600	1.59196300	-1.87473600
H	4.57406500	0.41996100	-0.95883500
H	3.68113800	-0.14302300	-2.31882200

Table 45: Final state energy (FS) for the C-H bond activation on Al^{IV}-O^{III} site-pair of B^{III} doped γ-Al_2O_3 via polar pathway.

O	2.46487200	-0.94443600	-1.24657900
O	1.51949000	-0.79432400	1.06304000
O	0.20114000	-3.19555600	0.04071100
Al	1.25143500	-1.88410200	-0.45911800
O	2.31901500	1.79881800	-0.10828400
O	-0.24831000	1.48902400	1.10005500
Al	0.71313500	2.28284500	-0.31162700
O	-1.78207100	0.61249000	-1.05885700
O	0.44336300	0.95030800	-1.79188800
O	-0.33425800	-1.22083300	-1.29933200
O	-3.16112700	1.27100400	0.87761600
O	-1.37032700	-1.04600900	1.29244100
Al	0.04416700	-0.12433600	1.56553100
Al	2.95690300	0.16148800	0.09659300
Al	-2.80803200	-0.32750400	0.28079600
O	-2.97614800	-1.93695200	-0.36912100
Al	-1.30800000	-2.34966300	-0.08011300
O	-0.72607800	3.23880800	-0.56565700
Al	-1.78399100	2.07529800	0.17760300
B	-0.61413400	0.08725300	-1.48547400

H	1.27365800	0.42964400	-1.93868700
C	4.67264300	-0.04179200	0.98160900
H	4.71470900	0.51469500	1.92237600
H	4.90432900	-1.08524900	1.21209400
H	5.49261300	0.33431700	0.36312700

Table 46: Initial state energy (IS) for the C-H bond activation on Al^{III}-O^{II} site-pair of B^{IV} doped γ-Al_2O_3 via polar pathway.

O	2.12461900	-2.40455800	0.42138500
O	1.42571300	-1.36854500	-1.45679100
O	3.19299200	0.79340800	-0.52448600
Al	2.47618300	-0.70669300	-0.00445900
O	-0.14063600	-3.01239400	-0.50064000
O	-1.30874200	-0.75013300	-1.40289100
Al	-1.52891400	-1.96549800	0.07484000
O	-1.29901000	1.06531900	0.81617300
O	-0.80513100	-1.59192300	1.63671000
O	1.33017500	0.30298700	1.00075800
O	-2.30159000	1.94291100	-1.24483400
O	0.54132700	1.37670500	-1.56802200
Al	0.20443600	-0.24703200	-1.91703800
Al	-0.24689000	-0.01429400	1.66764500
Al	-0.76173900	2.28054400	-0.46868300
O	0.66328000	3.04166700	0.24750100
Al	1.74723200	1.73911700	-0.17257200
O	-3.11708100	-1.15184900	0.13789000
Al	-2.49887500	0.36684200	-0.47407700
B	1.07352200	-2.47153400	-0.44677500
C	0.01757800	0.74687100	3.83944000
H	1.10359000	0.69550200	3.83482500
H	-0.34403000	1.52153700	3.14559300
H	-0.43104900	-0.25531200	3.72754700
H	-0.33753300	1.07712700	4.81370300

Table 47: Transition state energy (TS) for the C-H bond activation on Al^{III}-O^{II} site-pair of B^{IV} doped γ-Al_2O_3 via polar pathway.

O	2.02888400	-2.07795300	0.36284300
O	1.72465900	-1.06408500	-1.65371300
O	3.08393500	1.23205600	0.13870700

Al	2.47164400	-0.35148000	-0.07232100
O	0.14836900	-2.84726200	-1.17427300
O	-1.14558400	-0.44721500	-1.42674300
Al	-1.42013500	-2.11060900	-0.52702900
O	-1.53774100	0.58102000	1.39560900
O	-0.85174100	-2.11761000	1.10814100
O	0.77883000	0.24663700	0.28715000
O	-2.56548800	1.89542400	-0.48678400
O	1.00378100	1.80629500	-1.78699300
Al	0.40475000	0.22674600	-1.66559600
Al	-0.23496000	-0.61074100	1.54926200
Al	-1.27043500	2.15981700	0.61722600
O	0.25247700	2.91518800	0.76196900
Al	1.49325100	2.03734900	-0.10535200
O	-3.08857300	-1.50246500	-0.39979100
Al	-2.54592600	0.14586100	-0.34782500
B	1.23601300	-2.17853600	-0.86294700
H	1.49738200	-1.85928700	1.47663600
C	1.30973200	-1.23316000	2.79693700
H	2.15191700	-0.56547000	2.99202500
H	0.53767400	-0.95828300	3.54600700
H	1.56048400	-2.23369200	3.16148400

Table 48: Final state energy (FS) for the C-H bond activation on Al^{III}-O^{II} site-pair of B^{IV} doped γ-Al_2O_3 via polar pathway.

O	2.32071700	-2.18031400	0.42606500
O	1.54659200	-1.23656300	-1.47453900
O	3.09630300	1.10409500	-0.52939400
Al	2.52319500	-0.44386400	0.01232500
O	0.15812600	-3.00419200	-0.47713600
O	-1.23984500	-0.87648700	-1.48248200
Al	-1.31117800	-2.05599800	-0.04420200
O	-1.36504100	0.83778600	0.76740500
O	-0.54906800	-1.61693600	1.58938800
O	1.24600400	0.39770000	0.94403900
O	-2.49456100	1.72085300	-1.23199800
O	0.40407000	1.45059400	-1.58890800
Al	0.23631500	-0.19456700	-1.91523100
Al	-0.22735200	0.18198900	1.94548100
Al	-0.98657200	2.18062300	-0.44550700
O	0.34727700	3.07387500	0.27442800
Al	1.55727000	1.89360700	-0.15484300
O	-2.94114700	-1.45379700	0.15447900
Al	-2.52051300	0.13610400	-0.47500600
B	1.32050800	-2.32976600	-0.48801600

H	0.14700100	-2.22442400	1.86806800
C	-0.17132100	0.64027000	3.82347100
H	0.04054000	1.70315200	3.96968500
H	-1.12237000	0.43436800	4.32177000
H	0.59964000	0.08856000	4.36972900

Table 49: Initial energy state (IS) for the C-H bond activation on Al^{III}-O^{III} site-pair of Ga^{IV} doped γ-Al_2O_3 via polar pathway.

O	-2.62325800	-1.71748200	0.50296900
O	-1.25335100	-0.89350200	-1.43071300
O	0.21587900	-3.30780200	-0.71957100
Al	-1.07483300	-2.26019200	-0.15446700
O	-2.66300000	1.72479300	-0.69893200
O	0.15611500	1.59110900	-1.42366300
Al	-1.07091100	2.25680900	-0.14581400
O	1.65633900	0.83165200	0.97377700
O	-1.15655300	0.88100100	1.11426300
O	0.22546300	-1.57052600	1.01599500
O	3.02837500	1.61850100	-0.90518300
O	1.59893900	-0.84819100	-1.46415500
Al	0.15316800	-0.04966300	-1.86414000
Al	0.26171000	0.04557100	1.58933000
Al	2.79892700	-0.00253400	-0.26796400
O	3.05369800	-1.62334700	0.36294600
Al	1.50800900	-2.24603000	-0.19026000
O	0.25641900	3.29466300	0.34831200
Al	1.51502700	2.23839400	-0.26783300
Ga	-2.49303900	0.00402600	-0.10193900
C	0.41407800	0.02688100	3.84469300
H	-0.45250000	0.65562000	3.59873400
H	0.43805900	-0.00660800	4.93237600
H	0.30082800	-1.02023500	3.53238100
H	1.36861300	0.46758100	3.53501100

Table 50: Transition state energy (TS) for the C-H bond activation on Al^{III}-O^{III} site-pair of Ga^{IV} doped γ-Al_2O_3 via polar pathway.

O	-2.45725100	-1.79586600	0.74703700

O	-1.32059900	-0.83447100	-1.26887900
O	0.19297500	-3.30249800	-0.93018000
Al	-0.99299800	-2.29777200	-0.11804400
O	-2.59636000	1.71558300	-0.17791100
O	0.10453000	1.62380000	-1.23585300
Al	-0.94541000	2.21725000	0.19034100
O	1.87527500	0.67199100	0.87473200
O	-0.89911000	0.74235800	1.39062400
O	0.44277000	-1.69110600	0.90367800
O	3.01878900	1.61103100	-1.08324000
O	1.51933900	-0.80830400	-1.66406500
Al	0.04831800	0.02103000	-1.79851000
Al	0.63124100	-0.17971200	1.70422900
Al	2.85896900	-0.05675800	-0.54783000
O	3.16913500	-1.72215900	-0.08432600
Al	1.56048300	-2.29427600	-0.48467600
O	0.43964200	3.19129500	0.62859800
Al	1.61141000	2.17265200	-0.20046700
Ga	-2.40201700	-0.05429500	0.21515300
C	0.20222900	0.13954000	3.69257900
H	-0.64069000	0.63529400	2.63131800
H	-0.55929100	0.66992700	4.27656800
H	0.15710300	-0.89073100	4.05734700
H	1.14371700	0.60668600	3.99793000

Table 51: Final state energy (FS) for the C-H bond activation on Al^{III}-O^{III} site-pair of Ga^{IV} doped γ-Al_2O_3 via polar pathway.

O	2.72450000	1.52506100	0.60658900
O	1.39287400	0.87829200	-1.43429300
O	0.00198500	3.33647800	-0.57349600
Al	1.19144300	2.17922900	-0.02436300
O	2.55447200	-1.83955500	-0.50665300
O	-0.15251000	-1.48921400	-1.40474100
Al	0.89120100	-2.32103000	-0.15171000
O	-1.71706700	-0.77624200	0.85099600
O	0.95672600	-1.09437800	1.34872500
O	-0.14203300	1.37994900	0.91711500
O	-3.06749700	-1.41407000	-1.10432900
O	-1.53092900	1.01737800	-1.54451700
Al	-0.10675400	0.15567500	-1.82189200
Al	-0.51201600	-0.04091900	1.90049300
Al	-2.77479400	0.15822800	-0.36165400
O	-2.95274900	1.76259000	0.33335200
Al	-1.36440300	2.30475600	-0.16045900

O	-0.47986900	-3.32858500	0.20013400
Al	-1.65251200	-2.13744200	-0.36834500
Ga	2.56459000	-0.06965600	-0.20936600
C	-0.59674700	-0.00189800	3.83457200
H	1.50949300	-1.40417100	2.07587500
H	-0.74472500	-0.99709600	4.26447700
H	0.30442200	0.41875300	4.29122700
H	-1.43238400	0.61115200	4.18337800

Table 52: Initial state energy (IS) for the C-H bond activation on Al^{IV}-O^{II} site-pair of Ga^{IV} doped γ-Al_2O_3 via polar pathway.

O	2.72450000	1.52506100	0.60658900
O	1.39287400	0.87829200	-1.43429300
O	0.00198500	3.33647800	-0.57349600
Al	1.19144300	2.17922900	-0.02436300
O	2.55447200	-1.83955500	-0.50665300
O	-0.15251000	-1.48921400	-1.40474100
Al	0.89120100	-2.32103000	-0.15171000
O	-1.71706700	-0.77624200	0.85099600
O	0.95672600	-1.09437800	1.34872500
O	-0.14203300	1.37994900	0.91711500
O	-3.06749700	-1.41407000	-1.10432900
O	-1.53092900	1.01737800	-1.54451700
Al	-0.10675400	0.15567500	-1.82189200
Al	-0.51201600	-0.04091900	1.90049300
Al	-2.77479400	0.15822800	-0.36165400
O	-2.95274900	1.76259000	0.33335200
Al	-1.36440300	2.30475600	-0.16045900
O	-0.47986900	-3.32858500	0.20013400
Al	-1.65251200	-2.13744200	-0.36834500
Ga	2.56459000	-0.06965600	-0.20936600
C	-0.59674700	-0.00189800	3.83457200
H	1.50949300	-1.40417100	2.07587500
H	-0.74472500	-0.99709600	4.26447700
H	0.30442200	0.41875300	4.29122700
H	-1.43238400	0.61115200	4.18337800

Table 53: Transition state energy (TS) for the C-H bond activation on Al^{IV}-O^{II} site-pair of Ga^{III} doped γ-Al_2O_3 via polar pathway.

O	-2.40689200	1.99907900	-0.05941900
O	-0.88867700	0.98667300	1.56212800

O	0.74398200	3.23908800	0.75129000
Al	-0.74593600	2.40972000	0.32685500
O	-2.65200600	-1.25734600	1.20568300
O	0.20402100	-1.61965600	1.43188700
Al	-1.32077700	-2.07067000	0.40544600
O	1.41979200	-1.02713400	-1.21796600
O	-1.47809800	-0.65497900	-0.84808200
O	0.30168700	1.68391300	-1.07344900
O	2.90499500	-1.98459100	0.46023500
O	1.89533600	0.62653900	1.21067100
Al	0.45811400	0.00129800	1.86186300
Al	2.81354900	-0.33605000	-0.13955200
O	3.16643800	1.25949800	-0.78207300
Al	1.81781200	2.07410900	-0.00690500
O	-0.24543000	-3.24187400	-0.34162600
Al	1.24658600	-2.40867300	0.06370000
Ga	0.01089900	0.00061900	-1.56854600
Al	-2.34374400	0.33423400	0.51499800
C	-4.90577000	-0.01304000	-0.90817500
H	-4.55373200	1.01979500	-0.86266300
H	-4.19198900	-0.63001000	-1.45576700
H	-5.05227400	-0.42986200	0.08927000
H	-5.85929000	-0.02613400	-1.43436900

Table 54: Final state energy (FS) for the C-H bond activation on Al^{IV}-O^{II} site-pair of Ga^{III} doped γ-Al_2O_3 via polar pathway.

O	-0.54726600	-2.60799800	2.26536100
O	0.04109700	-1.96147100	-0.03304400
O	1.50514900	-4.48971400	0.21125800
Al	0.58596500	-3.33398900	1.15284200
O	-0.84193000	0.72837600	0.60982900
O	1.58186400	0.33713200	-0.82773800
Al	0.81961700	1.19734900	0.67263400
O	3.71991800	-0.40326500	1.06205200
O	0.92941900	-0.11728900	2.05982200
O	2.24766300	-2.78329600	1.80024200
O	4.44624600	0.12976500	-1.21310700
O	2.70068500	-2.20805600	-1.04371100
Al	1.25631900	-1.31171900	-1.04210700
Al	4.32026300	-1.42572200	-0.41628800
O	4.66381400	-3.03770700	0.18038800
Al	2.99319400	-3.55733300	0.23681800
O	2.32301300	2.10137500	0.70875300
Al	3.26293100	0.93005000	-0.19439000

Ga	2.44701900	-1.04383200	2.13321400
Al	-0.69373300	-0.87692600	1.36616800
C	-2.72553700	-1.23421400	1.88298100
H	-1.72917300	-2.15558300	2.15672000
H	-3.38712800	-1.97755800	2.33684200
H	-2.85743600	-0.31766300	2.46497100
H	-3.10787900	-1.05744100	0.87422000

Table 55: Initial state energy (IS) for the C-H bond activation on Al^{IV}-O^{III} site-pair of Ga^{III} doped γ-Al_2O_3 via polar pathway.

O	-2.41367900	1.98944600	-0.05439800
O	-0.89011500	0.98206200	1.56501800
O	0.73386500	3.24036900	0.75281400
Al	-0.75384000	2.40615700	0.32994600
O	-2.64639500	-1.26803100	1.20978700
O	0.21063400	-1.62065700	1.43109200
Al	-1.31384600	-2.07665900	0.40663600
O	1.42129300	-1.02241700	-1.21963900
O	-1.47717700	-0.66030500	-0.84544300
O	0.29446900	1.68535700	-1.07284700
O	2.91164000	-1.97584400	0.45632700
O	1.89436400	0.63143600	1.20907900
Al	0.46024500	0.00078500	1.86186600
Al	2.81416800	-0.32728400	-0.14244800
O	3.16104200	1.26973400	-0.78471000
Al	1.81072300	2.07966600	-0.00759100
O	-0.23540400	-3.24353500	-0.34275800
Al	1.25426300	-2.40527500	0.06094400
Ga	0.00854900	0.00108300	-1.56722700
Al	-2.34457400	0.32482000	0.51927500
C	-4.90009600	-0.01055700	-0.91920400
H	-4.58700000	1.03343300	-0.85585300
H	-4.17002700	-0.58643500	-1.48989100
H	-5.01669600	-0.45459200	0.07069600
H	-5.85981000	-0.05227600	-1.43244400

Table 56: Transition state energy (TS) for the C-H bond activation on Al^{IV}-O^{III} site-pair of Ga^{III} doped γ-Al_2O_3 via polar pathway.

O	-2.58491200	2.16127000	0.27598900
O	-1.01418700	1.02515000	1.71978600

O	0.59131200	3.32634800	0.83093100
Al	-0.90472100	2.46464100	0.53264700
O	-2.52266900	-1.22049700	1.35758700
O	0.24467600	-1.52736100	1.51451600
Al	-1.25951000	-2.07664400	0.54605800
O	1.37241700	-0.95856200	-1.09581100
O	-1.54892300	-0.94175600	-1.02655900
O	0.07897900	1.66007800	-0.89750600
O	2.94740000	-1.83009600	0.55343000
O	1.80898400	0.75232000	1.30887500
Al	0.37866000	0.09925600	1.96391600
Al	2.74562600	-0.19247700	-0.04379000
O	2.99922800	1.39911500	-0.74073300
Al	1.64942500	2.16415500	0.07183900
O	-0.15023800	-3.25774300	-0.14359800
Al	1.30683700	-2.34195100	0.19589300
Ga	-0.07749100	-0.00985900	-1.47702300
Al	-2.68097000	0.45275000	0.77102800
H	-2.58749300	-0.53691600	-1.00457000
C	-4.03990200	-0.00386400	-0.74964700
H	-4.78672200	0.31391100	0.00125000
H	-4.16157700	0.71248000	-1.56216200
H	-4.40856700	-0.98835300	-1.04961600

Table 57: Final state energy (FS) for the C-H bond activation on Al^{IV}-O^{III} site-pair of Ga^{III} doped γ-Al_2O_3 via polar pathway.

O	-3.15147800	0.85684900	-0.44052100
O	-1.60899300	0.42243700	1.50643800
O	-0.93832000	3.22033500	0.69522900
Al	-1.85562300	1.82978800	0.16674800
O	-1.17737800	-1.45264800	-0.51324700
O	0.61498700	-1.50666500	1.71514100
Al	0.01471100	-2.40365400	0.30059000
O	1.50720000	-0.45060000	-0.67147500
O	-0.10564600	-0.68794800	-3.37308900
O	-0.44260100	1.42326100	-0.92075100
O	3.45370400	-0.44000300	0.90785200
O	1.14967500	1.32785800	1.49269300
Al	0.02542500	0.11235800	1.85990100
Al	2.49340300	0.88826700	0.25599800
O	2.22308700	2.44690800	-0.45899400
Al	0.58179200	2.56291100	0.13079600
O	1.52632500	-3.13310000	-0.03440600

Al	2.31932900	-1.63924700	0.44290800
Ga	-0.05241300	-0.18750900	-1.67096600
Al	-2.67201900	-0.62378400	0.35110700
H	-0.73924300	-0.26060200	-3.95291200
C	-3.68689300	-2.07340900	1.15312600
H	-4.50959200	-1.70413000	1.77034600
H	-4.12697400	-2.74105100	0.40734900
H	-3.07377400	-2.70076200	1.81282500

Double atom doped γ-Al_2O_3

Table 58: Lowest energy state (LS) of two sites tetracoordinated boron (B^{IV}) doped γ-Al_2O_3 catalyst surface.

O	2.50063400	-1.88608300	0.00214300
O	1.25130800	-0.78770900	-1.50718800
O	2.72615300	1.57547400	-0.52304400
O	0.17475300	-2.68723700	-0.47699000
O	-1.72959400	-0.61777900	-1.85218500
O	-1.20239000	0.29547700	1.13804500
O	-0.12407900	-2.17606100	1.80642400
O	1.47365900	0.39868400	1.24899500
O	-2.91948200	1.29501400	-0.22595400
O	-0.06636200	1.58782300	-1.06834700
Al	-0.23013600	0.08152300	-1.86812700
Al	0.12669800	-0.49837300	1.82059700
Al	-1.38114900	1.92747900	0.30395000
O	-0.09626300	2.90082400	1.02524600
Al	1.18986400	2.04496800	0.21694900
O	-2.04875400	-2.09969000	0.35241800
Al	-2.37422400	-0.41039700	-0.20524700
Al	2.49071000	-0.10259700	-0.18778400
B	-0.75909600	-2.40582800	0.57593500
B	1.31918200	-1.98291800	-0.65611200

Table 59: Lowest energy state (LS) of two sites tetracoordinated gallium (Ga^{IV}) doped γ-Al_2O_3 catalyst surface.

O	-1.23296600	2.95866100	-0.54114200

O	-0.41237300	1.43204200	1.26664800
O	2.05038700	2.83543200	0.57216700
O	-3.03374500	0.00162800	0.59867900
O	-0.41386400	-1.43026500	1.26617500
O	1.14204300	-1.40999500	-1.20901400
O	-1.33953000	0.00065600	-1.30973600
O	1.14389600	1.40677200	-1.20868400
O	2.04723600	-2.83697600	0.57380000
O	2.03382600	-0.00062100	1.21058700
Al	0.40011700	0.00049100	1.68192300
Al	0.31640800	-0.00101000	-1.67925300
Al	2.62770200	-1.29870500	-0.03366400
O	3.62930100	-0.00218300	-0.65839900
Al	2.63082000	1.29668000	-0.03412600
O	-1.23604100	-2.95845000	-0.53952000
Al	0.39182900	-2.61279300	0.04538500
Ga	-1.98206100	1.38048200	-0.00714300
Ga	-1.98330300	-1.37835800	-0.00842300
Al	0.39473500	2.61230400	0.04358600

Table 60: Initial state energy (IS) for the C-H bond activation on Al^{III}-O^{III} site-pair of two tetracoordinated boron (B^{IV}) doped γ-Al_2O_3 via polar pathway.

O	-2.46757900	1.97713700	-0.00010100
O	-1.20990800	1.03282800	-1.60671200
O	-2.75515700	-1.38987000	-0.95470300
O	-0.10629400	2.75409000	-0.31987300
O	1.76547100	0.83220100	-1.97663900
O	1.14639400	-0.38168200	0.81422200
O	0.18304700	1.93544700	1.87793800
O	-1.50125800	-0.46400300	0.95832200
O	2.90922200	-1.27714100	-0.56310300
O	0.04429800	-1.43652400	-1.49376400
Al	0.24873400	0.17302900	-2.05957700
Al	-0.13339700	0.26109600	1.74051700
Al	1.33753500	-1.91941600	-0.15238100
O	0.02554500	-2.92087400	0.49768700
Al	-1.23315400	-1.95989100	-0.25114800
O	2.10738400	2.03895500	0.42095300
Al	2.38282900	0.43186000	-0.35529200
B	-1.26193800	2.11331900	-0.60732500
C	-0.03765800	-0.74492100	3.73948000

H	-0.05975600	-1.57249000	3.01695200
H	-0.12841900	-1.20574400	4.72127400
H	0.90956500	-0.19610100	3.73944700
H	-0.91846700	-0.08288100	3.68866000
B	0.81431700	2.31097800	0.69283000
Al	-2.48471600	0.22876400	-0.40400600

Table 61: Transition state energy (TS) for the C-H bond activation on Al^{III}-O^{III} site-pair of two tetracoordinated boron (B^{IV}) doped γ-Al_2O_3 via polar pathway.

O	-0.15358800	3.26192500	0.21782700
O	-0.12939100	1.65714700	-1.35426700
O	-2.98415600	1.45224100	-0.86691900
O	1.87425900	1.81687600	-0.00744500
O	1.51210500	-0.93883200	-1.78543900
O	0.15941800	-0.44447700	0.42012500
O	1.40275400	1.09252700	2.18719100
O	-1.68810400	1.16615800	1.20848700
O	0.60415000	-2.86630300	0.15968500
O	-1.46978600	-0.93183000	-1.36750300
Al	0.06483200	-0.08816400	-1.56472300
Al	-0.27038000	0.45688000	1.87935000
Al	-0.90806900	-2.01097300	0.09375300
O	-2.38571500	-1.53077700	0.90189300
Al	-2.55948600	-0.06837300	-0.07560800
O	2.73685600	-0.33824700	0.77806400
Al	1.67935800	-1.47142400	-0.12041000
B	0.66567600	2.35176300	-0.36275000
H	1.04404700	0.16460800	3.02847400
C	0.00126600	-0.61528100	3.60685000
H	-0.27042000	-0.12380000	4.54002100
H	-0.88935700	-1.17926700	3.27105000
H	0.72235800	-1.40893000	3.81754600
Al	-1.58649500	2.26384800	-0.23860100
B	2.11314900	0.84022300	0.98100400

Table 62: Final state energy (FS) for the C-H bond activation on Al^{III}-O^{III} site-pair of two tetracoordinated boron (B^{IV}) doped γ-Al_2O_3 via polar pathway.

O	-2.62373200	1.56339800	0.49698100
O	-1.93859600	0.71620800	-1.47098600
O	-2.57903400	-1.89043100	-0.26613500
O	-0.79093200	2.78916300	-0.66894100

O	0.67592200	1.04195300	-1.32035100
O	1.77018900	-0.27618400	0.83039100
O	0.19554800	1.81812500	1.20353400
O	-0.91156500	-0.62706300	1.00133900
O	2.80868900	-0.73873400	-1.34299100
O	0.00950800	-1.61468500	-1.53713500
Al	-0.45271200	-0.04361900	-1.91619200
Al	0.43294700	0.14133300	1.90652000
Al	1.65125200	-1.67766800	-0.38975800
O	0.70008100	-2.90322100	0.44441700
Al	-0.85341000	-2.21643300	0.03007800
O	1.93183000	2.51717000	-0.26161700
Al	2.32291900	0.76991700	-0.56706700
B	-1.79875000	1.88067400	-0.53701400
H	-0.52707500	2.37176100	1.51921200
C	0.46800500	0.01254000	3.83632500
H	1.30724400	0.56596400	4.26624800
H	-0.44148300	0.40211600	4.30345200
H	0.57114100	-1.02435700	4.16835000
Al	-2.44546200	-0.20859600	0.17687500
B	0.55414100	2.21923400	-0.31682700

Table 63: Lowest energy state (LS) of two sites tetracoordinated boron (B^{III}-B^{IV}) doped γ-Al_2O_3 catalyst surface.

O	-2.34939100	-2.20705800	-0.50042500
O	-1.43165600	-1.11109900	1.24242600
O	-3.02830200	1.13846500	0.17287100
O	-0.13283200	-3.01869500	0.38713200
O	1.34881300	-0.78719500	1.18643700
O	1.15596700	0.76734600	-1.15397000
O	0.32323000	-1.40110900	-1.59785600
O	-1.16636000	0.40597400	-1.24245500
O	2.58769600	1.77978200	0.56171600
O	-0.30406100	1.53304400	1.21628800
Al	-0.10855500	-0.09143800	1.66262300
Al	1.00433600	2.24559600	-0.01415200
O	-0.34811700	3.15130200	-0.65671000
Al	-1.52010000	1.95964000	-0.18019300
O	2.90648300	-1.49463900	-0.54818600
Al	2.52683100	0.11571900	0.01444800
Al	-2.45918000	-0.45109300	-0.23434000
B	-1.27839600	-2.32739200	0.32884800
B	0.12092100	-0.10056300	-1.46431700
Al	1.27171400	-2.07913000	-0.23767800

Table 64: Initial state energy (IS) for the C-H bond activation on Al^{III}-O^{II} site-pair of two tetracoordinated and tricoordinated boron (B^{III}-B^{III}) doped γ-Al_2O_3 via polar pathway.

O	-2.46960400	-1.97461400	0.00182200
O	-1.21049300	-1.03120000	1.60791900
O	-2.75331000	1.39313500	0.95525300
O	-0.10897400	-2.75388600	0.32123600
O	1.76529700	-0.83356300	1.97585500
O	1.14768100	0.38131300	-0.81631800
O	0.18011800	-1.93612100	-1.87691500
O	-1.50054500	0.46508400	-0.95739300
O	2.91063900	1.27453700	0.56238800
O	0.04652900	1.43648500	1.49299100
Al	0.24933300	-0.17288600	2.05982200
Al	-0.13379400	-0.26126800	-1.74045400
Al	1.33979300	1.91854300	0.15117600
O	0.02837000	2.92115300	-0.49814100
Al	-1.23081200	1.96115400	0.25110200
O	2.10500500	-2.04100600	-0.42103800
Al	2.38242800	-0.43378900	0.35421900
B	-1.26396300	-2.11192700	0.60874900
B	0.81153300	-2.31196300	-0.69205500
Al	-2.48457200	-0.22606200	0.40520300
C	-0.04084900	0.74172200	-3.74102000
H	-0.92316500	0.08201700	-3.68824000
H	-0.13125700	1.20177000	-4.72320200
H	-0.05998800	1.57019200	-3.01944500
H	0.90506600	0.19060800	-3.74162900

Table 65: Transition state energy (TS) for the C-H bond activation on Al^{III}-O^{II} site-pair of two tetracoordinated and tricoordinated boron (B^{III}-B^{III}) doped γ-Al_2O_3 via polar pathway.

O	-2.43086100	2.02379000	-0.15588800
O	-1.18638500	0.91085900	-1.65834600
O	-2.62239900	-1.42552000	-0.74256100
O	-0.07202300	2.77728800	-0.60725200
O	1.86163600	0.79910500	-2.05857900
O	0.68392300	0.08446500	0.13597700
O	-0.20162500	2.27071300	1.69268600
O	-1.52745000	-0.35279400	1.20731400
O	2.96054300	-0.92880500	0.01926400

O	0.18103900	-1.68784200	-1.43252300
Al	0.34545200	0.04015000	-1.78532100
Al	-0.08699000	0.51029100	1.70478300
Al	1.40281500	-1.71486000	0.01003000
O	0.21603300	-2.57152500	0.95269100
Al	-1.10939800	-1.89530700	0.01543100
O	1.94887000	2.12382100	0.72408500
Al	2.37545100	0.68752900	-0.40074000
B	-1.25573000	2.07492200	-0.82352900
B	0.55389500	2.52216100	0.60827000
Al	-2.42988400	0.23300000	-0.27646200
H	1.81767100	1.40622600	1.79098100
C	1.63282800	0.43707800	2.86851300
H	1.98056100	1.18589500	3.58359300
H	0.89890900	-0.11571000	3.50287700
H	2.41566100	-0.29805000	2.67988800

Table 66: Final state energy (FS) for the C-H bond activation on Al^{III}-O^{II} site-pair of two tetracoordinated and tricoordinated boron (B^{III}-B^{III}) doped γ-Al_2O_3 via polar pathway.

O	2.55514100	-1.91164900	0.05125400
O	1.38651300	-0.98016900	-1.63855700
O	2.78363600	1.49513700	-0.75448300
O	0.21864400	-2.68017700	-0.42577500
O	-1.58112400	-0.92871600	-2.00683300
O	-1.26151200	0.29245700	0.75113100
O	-0.21674500	-1.92763200	1.80880800
O	1.32245500	0.43454700	0.94625400
O	-2.89464000	1.29026000	-0.77225100
O	-0.01309100	1.44655400	-1.47241000
Al	-0.09709000	-0.15611700	-2.05542500
Al	-0.02652100	-0.13259600	1.99081400
Al	-1.35884000	1.90808500	-0.16847400
O	-0.12162100	2.93224700	0.52127200
Al	1.19409100	1.97864100	-0.12949700
O	-2.06188500	-2.17889900	0.30738100
Al	-2.33708000	-0.36569800	-0.53847800
B	1.41552300	-2.02681100	-0.64742700
B	-0.60165900	-2.31258400	0.61351500
Al	2.52122300	-0.13471500	-0.24123600
H	-2.49507300	-2.26778000	1.16758100
C	-0.12199400	0.55304900	3.79817700
H	0.72462200	0.22205100	4.40662000
H	-0.11025700	1.64673400	3.80684500
H	-1.02799300	0.23719600	4.32297400

Table 67: Initial state energy (IS) for the C-H bond activation on Al^{IV}-O^{II} site-pair of two tetracoordinated and tricoordinated boron (B^{III}-B^{IV}) doped γ-Al_2O_3 via polar pathway.

O	0.49928200	-3.13598200	-0.35642600
O	-0.16116400	-1.78492000	1.32662600
O	-2.77993300	-2.02979200	-0.03583600
O	2.20652100	-1.61705400	0.69478700
O	1.00525900	0.78722800	1.33909400
O	-0.22340600	1.39251700	-1.12291800
O	1.28924900	-0.40287200	-1.42503400
O	-1.05007000	-0.79951900	-1.27001600
O	-0.55281200	3.14684400	0.56539300
O	-1.83479100	0.52722800	1.10020000
Al	-0.37358700	-0.11320200	1.68371400
Al	-1.68234400	2.00834200	-0.12474000
O	-3.07554300	1.29218700	-0.90580900
Al	-2.67727700	-0.31474800	-0.37902100
O	2.52995200	1.81573200	-0.25574900
Al	0.90429800	2.25697600	0.16030100
Al	-1.08611800	-2.34322400	-0.25394300
B	1.05228300	-2.26142600	0.53191700
B	0.05035400	0.06191000	-1.39736300
Al	2.26126000	0.07690700	0.01455100
C	4.61049700	-0.28708600	-0.72291900
H	4.89257300	0.70815200	-1.04902300
H	5.41586000	-1.00902000	-0.84343400
H	4.40562500	-0.27179600	0.35736700
H	3.78840200	-0.66366900	-1.34587000

Table 68: Transition state energy (TS) for the C-H bond activation on Al^{IV}-O^{II} site-pair of two tetracoordinated and tricoordinated boron (B^{III}-B^{IV}) doped γ-Al_2O_3 via polar pathway.

O	0.94780100	4.00568000	0.86206400
O	0.87639600	2.89385500	-1.13605400
O	-1.92183300	2.49991900	-0.25445700
O	3.10580100	3.32394900	-0.24259100
O	2.53890100	0.40975900	-1.38901500
O	0.91184700	-0.80698400	0.49944400
O	2.19149700	1.01752200	1.33396100
O	-0.15952000	1.23132900	0.94594700

O	1.00730700	-2.21849600	-1.55228100
O	-0.31447800	0.40857100	-1.69951400
Al	1.13739300	1.31889900	-1.74739600
Al	-0.30397200	-1.29505200	-0.87354000
O	-1.87629300	-0.90178200	-0.24351000
Al	-1.57347300	0.80224900	-0.31005300
O	3.75576300	-1.14599500	0.14570600
Al	2.26827800	-1.40853600	-0.68517900
Al	-0.34783300	2.97420200	0.29553300
B	1.84385300	3.52856900	-0.06876600
B	1.00099500	0.46915800	1.05138700
Al	3.49069000	0.58225700	0.21580600
H	4.14738000	2.42908800	0.18745300
C	5.15728900	1.74550600	0.44436800
H	5.66527300	2.69980700	0.59087200
H	5.29407700	1.21659900	1.39703500
H	5.69216900	1.23577300	-0.36220700

Table 69: Final state energy (FS) for the C-H bond activation on Al^{IV}-O^{II} site-pair of two tetracoordinated and tricoordinated boron (B^{III}-B^{IV}) doped γ-Al_2O_3 via polar pathway.

O	-2.45739500	-2.52580300	-0.59197500
O	-1.26780900	-1.40460900	1.00490000
O	-3.38260500	0.59207900	0.02176600
O	-0.85993100	-3.76324300	0.79218600
O	1.63747800	-0.28440800	1.12798700
O	0.83054900	1.32629800	-1.03204500
O	0.73772500	-1.03824000	-1.29389400
O	-1.26104400	0.28495600	-1.29235000
O	1.85001400	2.72141800	0.78847500
O	-0.75454700	1.33039300	1.19110000
Al	-0.04021900	-0.22525800	1.36642000
Al	0.23488400	2.63928200	0.18745300
O	-1.29178400	3.20638800	-0.41507600
Al	-2.05519000	1.69155900	-0.12533600
O	3.39908400	0.10762700	-0.67248400
Al	2.36541800	1.20425800	0.12038900
Al	-2.46942600	-0.78386700	-0.45302400
B	-1.51822600	-2.67167500	0.37786300
B	0.14813800	0.15728200	-1.34039800
Al	2.34906900	-1.28241500	-0.41961300
H	-1.07342600	-4.54920000	0.28064300
C	2.80209900	-3.14390500	-0.16108400
H	3.65566100	-3.27064600	0.50898000

H	1.96123500	-3.69438900	0.27074300
H	3.05752200	-3.63949200	-1.10167500

Table 70: Initial state energy (IS) for the C-H bond activation on Al^{III}-O^{III} site-pair of two tetracoordinated gallium (Ga^{IV}) doped γ-Al_2O_3 via polar pathway.

O	1.23609200	2.95449000	0.43278900
O	0.49860500	1.43742300	-1.42847500
O	-1.99476500	2.84070800	-0.82812700
O	3.08793800	-0.00080200	-0.63537100
O	0.49787400	-1.43725000	-1.42895100
O	-1.15380400	-1.39680000	0.97496800
O	1.29515600	-0.00042000	1.18418300
O	-1.15292100	1.39735600	0.97534400
O	-1.99647900	-2.83941600	-0.82870400
O	-1.95776500	0.00073600	-1.47458600
Al	-0.29921300	0.00037600	-1.85478300
Al	-0.36925100	-0.00004100	1.58697100
Al	-2.58474000	-1.29283700	-0.24449200
O	-3.61094700	0.00102400	0.35401400
Al	-2.58400500	1.29446300	-0.24400100
O	1.23429100	-2.95523500	0.43198400
Al	-0.36395100	-2.60216100	-0.23034300
Ga	1.99696400	1.36903700	-0.07217100
C	-0.63036500	-0.00156000	3.82414200
H	-1.65475000	-0.00340700	3.43161000
H	-0.73215300	-0.00122700	4.90786700
H	-0.07451800	-0.91889800	3.58992200
H	-0.07750100	0.91754200	3.58951900
Al	-0.36239600	2.60260900	-0.22964100
Ga	1.99597600	-1.37001900	-0.07249100

Table 71: Transition state energy (TS) for the C-H bond activation on Al^{III}-O^{III} site-pair of two tetracoordinated gallium (Ga^{IV}) doped γ-Al_2O_3 via polar pathway.

O	-2.79828600	-0.14597300	0.86812300
O	-1.33496100	0.04834200	-1.16007900
O	-1.36218700	-2.84919700	-0.77201200
O	-1.17069200	2.93705300	-0.17658300
O	1.18641800	1.38846100	-1.34790700
O	2.17590800	-0.27122100	0.82539800
O	-0.14570900	1.23771100	1.43730000

O	-0.25690200	-1.56233200	1.00534400
O	3.63744200	-0.19190600	-1.14844600
O	1.05423500	-1.45477800	-1.61170300
Al	0.25248300	0.03158900	-1.76701900
Al	0.70950900	-0.33294600	1.72526800
Al	2.61875900	-1.48709600	-0.54021100
O	2.02005300	-3.04405000	0.00363200
Al	0.34112200	-2.69731400	-0.36971000
O	2.39506400	2.61356300	0.47726200
Al	2.74887200	1.07641900	-0.32759200
Ga	-1.83524200	1.29657300	0.30765000
H	0.06280800	1.01527500	2.67583800
C	0.58443200	0.17413300	3.72094900
H	0.19100800	1.00087200	4.32368100
H	0.06212000	-0.70944700	4.10014500
H	1.64490600	0.12698700	3.98651900
Ga	0.60665900	2.59495400	0.12584000
Al	-1.82129900	-1.35213400	0.01610000

Table 72: Final state energy (FS) for the C-H bond activation on Al^{III}-O^{III} site-pair of two tetracoordinated gallium (Ga^{IV}) doped γ-Al_2O_3 via polar pathway.

O	-2.85931600	-0.17369100	0.75161200
O	-1.33410600	0.01026100	-1.24342400
O	-1.29215300	-2.89179900	-0.73814000
O	-1.24769400	2.89908100	-0.21998100
O	1.14515600	1.40681600	-1.41838500
O	2.06779100	-0.12705300	0.79334600
O	-0.20118500	1.26002800	1.48322400
O	-0.25727200	-1.43516700	0.95776200
O	3.65212400	-0.10596000	-1.09300900
O	1.11825400	-1.47729400	-1.60589000
Al	0.28389000	-0.01895900	-1.77819200
Al	0.72979100	-0.33816800	1.91771700
Al	2.63477700	-1.39504600	-0.45649300
O	2.06879800	-2.94208000	0.14336700
Al	0.39595800	-2.65644100	-0.29514400
O	2.30173000	2.73328700	0.38243700
Al	2.71089400	1.15560300	-0.33048800
Ga	-1.92152300	1.24323800	0.13919100
H	-0.43284500	1.76932800	2.27058000
C	0.92995700	-0.45313600	3.84088300
H	1.50592800	0.37969200	4.25568100
H	-0.03020400	-0.47865200	4.36503100
H	1.46036100	-1.36541300	4.12785500

Ga	0.54702800	2.63293600	-0.03428600
Al	-1.80256600	-1.38657900	-0.00846000

Table 73: Lowest energy state (LS) of two sites tetracoordinated gallium (Ga^{III}-Ga^{IV}) doped γ-Al_2O_3 catalyst surface.

O	2.63038000	1.72770900	0.49939900
O	1.22244600	0.90068400	-1.38852900
O	-0.23919500	3.30485600	-0.68955900
O	2.65224200	-1.70682700	-0.72970200
O	-0.17244600	-1.57467300	-1.35379400
O	-1.70562500	-0.87452700	1.07048200
O	1.25060100	-0.91810300	1.16744400
O	-0.21661600	1.64793600	1.09981600
O	-3.03009800	-1.62095200	-0.83744900
O	-1.61712200	0.84302200	-1.37089500
Al	-0.18197100	0.05697300	-1.82250800
Al	-2.82455900	-0.00333400	-0.18213400
O	-3.06083300	1.61884200	0.44875800
Al	-1.53045900	2.26128700	-0.12071200
O	-0.23822000	-3.29932000	0.38250800
Al	-1.51989000	-2.25556300	-0.20595000
Ga	2.51482000	0.00758400	-0.10763100
Al	1.07379900	2.28369000	-0.12680800
Al	1.08827500	-2.27029300	-0.12714700
Ga	-0.23003500	-0.05065100	1.63087400

Table 74: Initial state energy (IS) for the C-H bond activation on Al^{III}-O^{II} site-pair of two tetracoordinated gallium (Ga^{IV}) doped γ-Al_2O_3 via polar pathway.

O	-1.23438600	-2.95518000	0.43251900
O	-0.49796800	-1.43762300	-1.42879200
O	1.99636700	-2.83967400	-0.82837500
O	-3.08781600	-0.00079000	-0.63537300
O	-0.49866300	1.43701900	-1.42861600
O	1.15308600	1.39753900	0.97523100
O	-1.29513700	-0.00017200	1.18430400
O	1.15357400	-1.39678500	0.97499200
O	1.99486900	2.84049700	-0.82859300
O	1.95773300	0.00041400	-1.47460700
Al	0.29918900	-0.00008300	-1.85473000

Al	0.36932400	0.00017800	1.58686800
Al	2.58396800	1.29430700	-0.24420700
O	3.61085000	0.00088600	0.35403500
Al	2.58456200	-1.29301100	-0.24418600
O	-1.23592200	2.95467800	0.43223400
Al	0.36250800	2.60244000	-0.23015300
Ga	-1.99601400	-1.36998800	-0.07212300
Al	0.36380500	-2.60247400	-0.23021500
Ga	-1.99691500	1.36917200	-0.07232300
C	0.63069300	0.00012600	3.82398400
H	0.07343900	0.91672600	3.59007800
H	0.73280400	0.00003000	4.90768400
H	0.07905800	-0.91967700	3.58935900
H	1.65499500	0.00335800	3.43122500

Table 75: Transition state energy (TS) for the C-H bond activation on Al^{III}-O^{II} site-pair of two tetracoordinated gallium (Ga^{IV}) dopedγ-Al_2O_3 via polar pathway.

O	1.09110900	2.69345200	0.71609000
O	0.54769300	1.51402400	-1.46791800
O	-2.01565400	2.88312300	-0.98847800
O	3.14392600	-0.04289100	-0.78310600
O	0.49873600	-1.41065600	-1.41408200
O	-1.09194000	-1.22265100	1.08162900
O	1.33761500	-0.06441000	1.00897000
O	-1.24318900	1.40110800	0.80005800
O	-1.98573000	-2.77530300	-0.63882000
O	-1.94736300	0.02246400	-1.51379900
Al	-0.28209700	0.03254000	-1.83182300
Al	-0.26236100	0.22886200	1.64205200
Al	-2.55220200	-1.20296400	-0.13374300
O	-3.68056300	0.07688300	0.25992500
Al	-2.65745800	1.33892800	-0.38630800
O	1.27322300	-2.97001300	0.41829200
Al	-0.35034500	-2.51053700	-0.08734500
Ga	2.01497700	1.26324200	-0.16066800
Al	-0.44147200	2.57758200	-0.29767800
Ga	2.05532400	-1.42984900	-0.16751900
H	0.75671800	2.17348800	1.82703600
C	0.37606500	1.59201800	3.11772900
H	-0.14940900	0.75112900	3.64362100
H	1.36038100	1.56143600	3.58497600
H	-0.19182800	2.44912200	3.48127800

Table 76: Final state energy (FS) for the C-H bond activation on Al^{III}-O^{II} site-pair of two tetracoordinated gallium (Ga^{IV}) doped γ-Al_2O_3 via polar pathway.

O	-0.75384100	-3.14635300	0.36207000
O	-0.27473700	-1.55793300	-1.40731200
O	2.50070300	-2.49558500	-0.82946400
O	-3.10583700	-0.41462100	-0.66911200
O	-0.74818100	1.31523600	-1.43430600
O	0.88513700	1.46686100	0.91024100
O	-1.23906900	-0.23556400	1.10151800
O	1.31681100	-1.20582700	0.93127200
O	1.53072900	3.09569700	-0.82957700
O	1.95878900	0.25974800	-1.47307800
Al	0.30869100	0.04213800	-1.77277400
Al	0.38709400	0.04658000	1.85259300
Al	2.33758300	1.66675800	-0.20679000
O	3.59420700	0.57954400	0.36619000
Al	2.79054800	-0.85586400	-0.19843100
O	-1.67790900	2.76465800	0.42326200
Al	-0.03368600	2.60163500	-0.20740400
Ga	-1.75639400	-1.51945900	-0.14869200
Al	0.86953800	-2.45046300	-0.26479400
Ga	-2.18632100	1.08570600	-0.03722100
H	-0.88868900	-3.62991900	1.18164000
C	0.50618800	0.00290700	3.78927700
H	1.53415500	0.15202000	4.13209500
H	-0.09800000	0.78702300	4.25437900
H	0.16815600	-0.94724400	4.21469800

Table 77: Initial state energy (IS) for the C-H bond activation on Al^{IV}-O^{II} site-pair of two tetracoordinated gallium (Ga^{III}- Ga^{IV}) doped γ-Al_2O_3 via polar pathway.

O	-0.75341000	-3.04617200	0.50087700
O	0.00795100	-1.60389500	-1.38872000
O	2.57453100	-2.45115400	-0.33995500
O	-2.81496500	-0.51211300	-1.11516200
O	-0.53033000	1.18451800	-1.53625500
O	0.81584600	1.76727600	1.01919800
O	-1.48331600	-0.10740000	0.95304500
O	1.28690400	-1.11209800	1.24115400
O	1.56407400	3.09422600	-0.88830600
O	2.12113800	0.28115700	-1.21896900
Al	0.57562000	-0.06890900	-1.82990300
Al	2.36511200	1.76279000	-0.06782300
O	3.51110100	0.71424000	0.75182000

Al	2.82011600	-0.79203000	0.17653700
O	-1.76892600	2.64120800	-0.01475800
Al	-0.06232600	2.63418800	-0.41389600
Ga	-1.69203200	-1.69257600	-0.29233000
Al	0.85779400	-2.49513900	0.02696400
Al	-2.08758500	0.96882200	-0.46505300
Ga	0.14909300	0.21437900	1.57932100
C	-4.64744200	1.28998700	0.98099500
H	-5.57034800	1.52347500	1.51013000
H	-4.06270600	0.59170500	1.58140000
H	-4.89882400	0.82541200	0.02669700
H	-4.09064900	2.21882700	0.83864200

Table 78: Transition state energy (TS) for the C-H bond activation on Al^{IV}-O^{II} site-pair of two tetracoordinated gallium (Ga^{III}- Ga^{IV}) doped γ-Al_2O_3 via polar pathway.

O	2.57055000	1.86125800	0.55042300
O	1.24537400	0.83636000	-1.31534800
O	-0.21112000	3.32867500	-0.91994400
O	2.65304500	-1.61726400	-0.48186300
O	-0.15711800	-1.67110500	-1.08435000
O	-1.84116000	-0.63704900	1.13303400
O	1.16915600	-0.79060800	1.35046000
O	-0.28424800	1.79415900	0.99183500
O	-3.08601000	-1.54947400	-0.76844500
O	-1.55572000	0.78402200	-1.43946200
Al	-0.12269300	-0.09119000	-1.71137000
Al	-2.87182400	0.11472600	-0.26078500
O	-3.11532300	1.79663300	0.17075700
Al	-1.53051200	2.33047600	-0.34312000
O	-0.49607600	-3.15434700	0.83911600
Al	-1.64434700	-2.15424600	0.02624200
Ga	2.45297300	0.10118800	0.08330800
Al	1.05308600	2.35045000	-0.20752600
Al	0.99858500	-2.36356300	0.29050100
Ga	-0.32874000	0.13722800	1.65420800
H	2.81039500	-2.66914800	0.17505400
C	2.42646800	-3.84897400	0.82395200
H	1.95874000	-4.67937700	0.28908500
H	3.50018100	-4.05818500	0.82567700
H	2.10634400	-3.88915700	1.86851600

Table S79: Final state energy (FS) for the C-H bond activation on Al^{IV}-O^{II} site-pair of two tetracoordinated gallium (Ga^{III}- Ga^{IV}) doped γ-Al_2O_3 via polar pathway.

O	-1.88665500	-2.51879900	0.62148100
O	-0.90802400	-1.13453600	-1.29016900
O	1.14779500	-3.23973600	-0.77268500
O	-3.97732500	-0.26171300	-0.49095200
O	0.01722700	1.66977900	-1.24923600
O	1.67784500	1.06356900	1.07591700
O	-1.37526100	0.62959200	0.92096700
O	0.74861800	-1.61020200	1.04576800
O	2.93604900	2.14118500	-0.75781500
O	1.84841400	-0.47948400	-1.35797700
Al	0.26228600	0.03925500	-1.70367800
Al	2.97935200	0.48919600	-0.19011900
O	3.57592200	-1.06673800	0.32145100
Al	2.16191200	-1.94296100	-0.19708900
O	0.04657600	3.30825700	0.65765100
Al	1.36607800	2.48665100	-0.08781700
Ga	-2.39573000	-0.87743200	0.02546600
Al	-0.33064800	-2.57527700	-0.13582000
Al	-1.24456400	2.32045100	0.00602600
Ga	0.26418000	0.05199700	1.47048500
H	-4.18427800	0.65091000	-0.27681400
C	-2.99862700	2.87663600	-0.60921000
H	-2.96262400	3.91715600	-0.94262300
H	-3.35847500	2.28975000	-1.45928500
H	-3.76167500	2.83634900	0.17478000

Table 80: Initial state energy (IS) for the C-H bond activation on Al^{IV}-O^{III} site-pair of two tetracoordinated gallium (Ga^{III}- Ga^{IV}) doped γ-Al_2O_3 via polar pathway.

O	-0.75326700	-3.04623200	0.50079100
O	0.00812500	-1.60375200	-1.38859700
O	2.57468600	-2.45110500	-0.34004400
O	-2.81488200	-0.51213400	-1.11515600
O	-0.53044600	1.18462700	-1.53608400
O	0.81583000	1.76724000	1.01929900
O	-1.48333700	-0.10747000	0.95315200
O	1.28705300	-1.11210600	1.24111300
O	1.56392100	3.09436000	-0.88813800
O	2.12114400	0.28135600	-1.21910400
Al	0.57554400	-0.06869700	-1.82984200
Al	2.36509500	1.76291200	-0.06780500
O	3.51111900	0.71431400	0.75169100

Al	2.82013300	-0.79193000	0.17628700
O	-1.76904600	2.64120600	-0.01451600
Al	-0.06243700	2.63426200	-0.41360000
Ga	-1.69183000	-1.69256400	-0.29242100
Al	0.85797400	-2.49518400	0.02704900
Al	-2.08770500	0.96885100	-0.46493700
Ga	0.14912300	0.21427100	1.57929900
C	-4.64825000	1.28921900	0.98055900
H	-5.57134100	1.52272200	1.50935800
H	-4.06317200	0.59173100	1.58155500
H	-4.89917100	0.82380700	0.02654800
H	-4.09193300	2.21828800	0.83771400

Table 81: Transition state energy (TS) for the C-H bond activation on Al^{IV}-O^{III} site-pair of two tetracoordinated gallium (Ga^{III}- Ga^{IV}) doped γ-Al_2O_3 via polar pathway.

O	2.67268700	1.64882800	0.43096900
O	1.19283400	0.93561700	-1.44055800
O	-0.19240400	3.34035100	-0.58965900
O	2.47184700	-1.69430500	-0.91224000
O	-0.20951700	-1.55395400	-1.34935800
O	-1.68651900	-0.91185800	1.04543000
O	1.37701400	-0.92310800	1.36764500
O	-0.14741300	1.55882700	1.08154200
O	-3.10774400	-1.51303000	-0.86331100
O	-1.62429000	0.90017400	-1.34176200
Al	-0.21572400	0.07158400	-1.82032600
Al	-2.82089700	0.05546800	-0.14805800
O	-3.00120300	1.65339200	0.55102100
Al	-1.47961400	2.27751300	-0.05563000
O	-0.45768100	-3.44658600	0.13348400
Al	-1.61073700	-2.24282600	-0.31613200
Ga	2.47923300	-0.03308400	-0.24877800
Al	1.11451200	2.26696500	-0.12731100
Al	1.06632600	-2.61002300	-0.25821500
Ga	-0.20720400	-0.12839500	1.63522200
H	1.69081700	-1.98313000	1.50681000
C	2.11869200	-3.48570900	1.32068000
H	1.55341000	-3.95277300	2.12770900
H	2.29779200	-4.30876000	0.60643100
H	3.12639100	-3.23207500	1.65955100

Table 82: Final state energy (FS) for the C-H bond activation on Al^{IV}-O^{III} site-pair of two tetracoordinated gallium (Ga^{III}- Ga^{IV}) doped γ-Al_2O_3 via polar pathway.

O	1.71994100	-2.93997100	0.11977600
O	0.72780800	-1.35456400	-1.65532900
O	3.45915800	-0.14897500	-0.88573100
O	-1.19309700	-1.27325500	0.62740800
O	-1.59919600	0.47808700	-1.50585700
O	-0.51422500	1.63228000	0.88902100
O	-0.05912200	-0.37922900	3.41216500
O	1.49474800	-0.20993800	0.68169500
O	-1.04962400	3.34466100	-0.80545200
O	1.10638900	1.51207500	-1.51417300
Al	0.04891200	0.22677400	-1.84375500
Al	0.48609700	2.76192600	-0.20175700
O	2.11918400	2.71308900	0.42154800
Al	2.45614000	1.14949600	-0.25253600
O	-3.20945000	0.96414100	0.37592500
Al	-1.92242700	1.94400400	-0.23446500
Ga	0.06264300	-2.31321500	-0.13540500
Al	2.34148700	-1.38032600	-0.45667300
Al	-2.67292000	-0.53473800	-0.33910500
Ga	-0.05042500	0.07161200	1.69518700
H	-0.72104200	0.01551000	3.98347400
C	-3.62755500	-2.04888600	-1.09510900
H	-4.08043900	-2.68361700	-0.32859000
H	-4.43556100	-1.73040200	-1.75848000
H	-2.98124100	-2.69845600	-1.69917200

Aluminum 13 atom cluster with single doped oxygen $[Al_{13}O]^-$

singlet state $[Al_{13}O]^-$ cluster

Table 83: Lowest state energy (LS) of aluminum 13 atom with single oxygen dopant $[Al_{13}O]^-$ in singlet state.

Al	2.13723400	1.30021000	0.00358300
Al	-2.32187700	-1.67805900	-0.00517000
Al	-0.20575300	0.00021900	0.00107800
Al	-1.77313600	0.00567300	-2.12418500

Al	0.04057300	2.25554700	1.41930900
Al	0.04109000	2.25881700	-1.41368000
Al	-2.31950700	1.67986200	0.00203600
Al	0.03726000	-2.26095100	1.41074000
Al	0.03842300	-2.25324500	-1.42225400
Al	0.95719700	-0.00469600	2.44061400
Al	2.13494100	-1.30322400	0.00006100
Al	0.96602800	0.00413200	-2.43631300
Al	-1.77904700	-0.00294000	2.12071700
O	3.32568300	-0.00218500	0.00563000

Table 84: Initial state energy (IS) for the C-H bond activation on single oxygen atom doped $(Al_{13})^-$ via polar pathway in singlet state having parallel orientation of oxygen.

Al	-1.57523500	-1.05111400	1.30298500
Al	2.33780900	1.07807800	-1.67890800
Al	0.48244200	0.06500100	0.00020200
Al	2.87318000	-1.05987100	-0.00628500
Al	-0.40566600	1.18872300	2.26129600
Al	0.94626800	-1.30320500	2.25264000
Al	2.34357500	1.06877300	1.67830300
Al	-0.41274400	1.19914500	-2.25314400
Al	0.94107200	-1.29175900	-2.26023200
Al	-1.70504500	1.65364200	0.00679100
Al	-1.57755000	-1.04682800	-1.30282200
Al	0.60677600	-2.63421300	-0.00683600
Al	0.85196600	2.67987100	0.00601800
O	-2.62968100	-1.61021500	0.00018000
C	-5.31578600	0.57666600	-0.00017100
H	-6.31859600	0.14703200	-0.00198900
H	-5.18413300	1.19133300	0.89076500
H	-4.56924700	-0.21867000	-0.00468900
H	-5.18490300	1.20084600	-0.88459500

Table 85: Transition state energy (TS) for the C-H bond activation on single oxygen atom doped $(Al_{13})^-$ via polar pathway in singlet state having parallel orientation of oxygen.

Al	-1.37667200	1.38283600	-1.32537700
Al	2.07626300	-1.49113700	1.59404800
Al	0.47526200	-0.06435700	0.00000200

Al	3.01994000	0.93640400	0.00000300
Al	-0.61729100	-1.04990900	-2.21445000
Al	1.20791000	1.12293100	-2.27342200
Al	2.07632300	-1.49183800	-1.59335700
Al	-0.61724000	-1.04897400	2.21489500
Al	1.20755200	1.12408800	2.27293000
Al	-2.03514600	-1.16325300	0.00030400
Al	-1.37657400	1.38353000	1.32475200
Al	0.71217100	2.58277700	-0.00071100
Al	0.16862400	-2.71026900	0.00050700
O	-2.66456200	1.50031000	-0.00025600
C	-4.23792000	-0.61833700	0.00004700
H	-4.80479500	-0.34426100	0.89433200
H	-4.80463400	-0.34453800	-0.89442700
H	-3.39612400	0.44781100	0.00000400
H	-4.22501300	-1.71825300	0.00024100

Table 86: Final state energy (FS) for the C-H bond activation on single oxygen atom doped $(Al_{13})^-$ via polar pathway in singlet state having parallel orientation of oxygen.

Al	-1.23467300	-1.50685700	1.36539200
Al	1.91942600	1.66500600	-1.53703300
Al	0.42530100	0.07532200	0.00030500
Al	3.11355500	-0.76503100	0.00125700
Al	-0.68613000	0.98626200	2.22238200
Al	1.36574100	-0.99663600	2.25717100
Al	1.91951800	1.66077300	1.53873300
Al	-0.68613900	0.99071300	-2.22001100
Al	1.36719800	-0.99104800	-2.25884600
Al	-2.19858200	1.03230200	0.00187100
Al	-1.23447800	-1.50434700	-1.36965000
Al	0.88132900	-2.53063100	-0.00322200
Al	-0.13564900	2.67796000	0.00267900
O	-2.54166700	-1.94766500	-0.00200500
C	-4.18316400	0.75848800	0.00053000
H	-4.55689100	0.23926700	0.89046200
H	-4.66038600	1.74470000	0.00469400
H	-3.40713600	-1.51941700	-0.00191500
H	-4.55668500	0.24661000	-0.89373300

Table 87: Initial state energy (IS) for the C-H bond activation on single oxygen atom doped $(Al_{13})^-$ via polar pathway in singlet state having opposite orientation of oxygen.

Al	-0.49039000	-1.47101200	-2.14845100
Al	-0.28396400	1.54500400	2.21548600

Al	-0.56583600	0.09645700	-0.00016800
Al	-0.39880700	-1.27065000	2.27603500
Al	-2.77307100	0.03067800	-1.53603700
Al	-2.00627600	-2.13895100	0.13139600
Al	-2.70651200	0.17600100	1.62601600
Al	1.17770400	2.10217100	-0.12690900
Al	1.81470200	-0.08687800	1.30502300
Al	-0.37972400	1.33790000	-2.34746800
Al	1.75930400	-0.20802600	-1.38024700
Al	0.80144400	-2.25488100	0.07775500
Al	-1.58238400	2.58453000	-0.09244000
O	2.43772500	-1.30913200	0.00136800
C	5.37553700	0.47059700	-0.00134800
H	6.43841600	0.24190500	-0.08509900
H	4.79276000	-0.45024000	-0.01148700
H	5.18748300	1.00692600	0.92886200
H	5.06583200	1.10041600	-0.83503800

Table 88: Transition state energy (TS) for the C-H bond activation on single oxygen atom doped $(Al_{13})^-$ via polar pathway in singlet state having opposite orientation of oxygen.

Al	0.61735700	1.04934800	2.21453300
Al	-1.20775700	-1.12306100	-2.27341100
Al	-0.47528700	0.06437100	-0.00000400
Al	0.61755000	1.04928900	-2.21454300
Al	-2.07609600	1.49158800	1.59384300
Al	-0.16815500	2.71024900	0.00017300
Al	-2.07603200	1.49200900	-1.59354100
Al	-0.71255000	-2.58270700	-0.00020300
Al	1.37651100	-1.38361600	-1.32488800
Al	-1.20793700	-1.12349300	2.27307700
Al	1.37632800	-1.38345800	1.32515200
Al	2.03540400	1.16296900	-0.00012000
Al	-3.02003900	-0.93621000	-0.00022500
O	2.66440900	-1.50052100	0.00023000
C	4.23747500	0.61830300	-0.00005100
H	3.39610700	-0.44759700	0.00051900
H	4.22427100	1.71821000	0.00482000
H	4.80644500	0.34118500	0.89199300
H	4.80218900	0.34796600	-0.89680700

Table 89: Final state energy (FS) for the C-H bond activation on single oxygen atom doped $(Al_{13})^-$ via polar pathway in singlet state having opposite orientation of oxygen.

Al	-1.43653700	0.16614700	2.36279700
Al	0.98366600	-0.06025600	-2.38086700
Al	-0.28411300	-0.20700500	0.01340800
Al	-1.42573100	0.96418600	-2.06429000
Al	-1.61045400	-2.23874400	1.05914600
Al	-3.20302700	-0.14113100	-0.09715300
Al	-1.38107700	-1.75974600	-1.76865400
Al	2.55428200	-0.09851600	0.04326200
Al	0.98137900	1.97059600	-0.67079200
Al	0.96256800	-1.71950300	1.80863200
Al	1.04424400	0.96258300	2.02759800
Al	-1.51000400	2.06891400	0.44490500
Al	1.14975800	-2.28707600	-0.87142600
O	-0.11996200	3.37592700	0.02101100
C	4.53409500	0.00253900	0.03178500
H	4.91615400	0.45774300	0.95036200
H	0.24806000	3.84931500	0.77376400
H	4.89108400	0.59978300	-0.81274300
H	4.97541500	-0.99532400	-0.05554100

Triplet state $[Al_{13}O]^-$ cluster

Al	1.32476100	0.73457500	2.29088100
Al	-0.98093800	-0.75218300	-2.25977900
Al	0.18813200	-0.00030000	0.00108700
Al	1.38794500	-1.92202200	-1.39272000
Al	1.42275800	2.35496900	0.01546500
Al	2.84114400	0.00534800	-0.00052700
Al	1.32781200	0.76303700	-2.27935200
Al	-2.48160700	0.00415000	-0.00400800
Al	-0.95408000	-2.39719200	-0.01642200
Al	-0.96017500	1.95531100	1.38179000
Al	-0.98443000	-0.78571200	2.24806200
Al	1.38822300	-1.93810700	1.37060500
Al	-0.95736600	1.97478200	-1.35462400
O	-4.16354400	0.00543300	-0.00074700

Table 90: Initial state energy (IS) for the C-H bond activation on single oxygen atom doped $(Al_{13})^-$ via polar pathway in triplet state having parallel orientation of oxygen.

Al	1.88485100	0.83611500	-1.40481300
Al	-2.48660400	-1.23800900	1.39297800
Al	-0.43178400	0.02604900	0.02792100
Al	-2.86159000	0.01660800	-1.00150500
Al	0.62861800	2.43950900	0.53265700
Al	-0.66034100	1.92870700	-1.85493100
Al	-2.13081500	2.13869500	0.48186300
Al	0.15142500	-1.96553600	1.77083500
Al	-1.15550500	-2.48590200	-0.67611300
Al	1.61258100	0.29169500	1.78759900
Al	1.49151400	-1.80065400	-0.59747600
Al	-0.70698700	-0.64764500	-2.58316700
Al	-1.00489100	0.76321700	2.49892600
O	2.61879600	-0.76392500	-1.43491400
C	5.27644600	0.21661100	0.65980600
H	4.64183200	-0.27327200	-0.07874800
H	4.95832000	1.25369200	0.77125900
H	5.17697800	-0.29151200	1.61948000
H	6.31770500	0.18578300	0.33642200

Table 91: Transition state energy (TS) for the C-H bond activation on single oxygen atom doped $(Al_{13})^-$ via polar pathway in triplet state having parallel orientation of oxygen.

Al	1.65781100	-1.83986100	-0.74169100
Al	-2.21143900	1.78193800	1.04140800
Al	-0.38792800	0.02454100	-0.01930200
Al	-2.79067600	-0.88163900	0.23775400
Al	0.55922500	0.09759100	-2.47510800
Al	-1.02772000	-1.95275700	-1.70932600
Al	-2.15377200	0.60621600	-1.96662700
Al	0.47301300	1.84489200	1.74227900
Al	-1.13390100	-0.32935200	2.55596700
Al	1.82812900	1.31312100	-0.48570800
Al	1.46438600	-0.66792000	1.78187800
Al	-0.60465300	-2.46175400	0.91336400
Al	-0.47613400	2.50638900	-1.00155200
O	2.74402300	-1.19226900	0.61152100
C	4.01621300	0.94087900	-0.34225400
H	4.59473100	0.37440400	-1.07557100
H	3.88841200	1.93820100	-0.79823100

H	3.30265800	-0.07872900	0.12668600
H	4.61230000	1.12070200	0.55509100

Table 92: Final state energy (FS) for the C-H bond activation on single oxygen atom doped $(Al_{13})^-$ via polar pathway in triplet state having parallel orientation of oxygen.

Al	-1.37403500	1.49861200	-1.44081600
Al	2.03312000	-1.46437800	1.50056900
Al	0.31168000	-0.03725700	-0.00015100
Al	2.87878200	0.69213800	-0.00097200
Al	-0.59373800	-1.00775200	-2.28706500
Al	1.24083600	1.06342800	-2.27139500
Al	2.03319300	-1.46421700	-1.50113200
Al	-0.59307300	-1.00703700	2.28784500
Al	1.24280500	1.06304900	2.27093400
Al	-2.05654000	-1.21342100	0.00136200
Al	-1.37201400	1.49880900	1.44097300
Al	0.83779600	2.56229800	-0.00033300
Al	0.13460800	-2.70048000	-0.00018700
O	-2.54615500	2.03002200	0.00113000
C	-4.04603500	-1.23666000	-0.00048500
H	-4.45284200	-0.74753800	-0.89037400
H	-3.43551100	1.65090500	0.00117100
H	-4.41597000	-2.26654300	-0.00006000
H	-4.45468500	-0.74634900	0.88795100

Table 93: Initial state energy (IS) for the C-H bond activation on single oxygen atom doped $(Al_{13})^-$ via polar pathway in triplet state having opposite orientation of oxygen.

Al	0.52460400	0.26836700	-2.59036000
Al	0.47219000	-0.08291900	2.68627900
Al	0.53896600	0.06108600	0.04705000
Al	-1.06093700	1.81876100	1.23628700
Al	2.77732700	0.96851700	-1.00459000
Al	0.25696300	2.48004900	-1.06490000
Al	1.72252000	2.10937000	1.26260500
Al	0.44316300	-2.42809900	1.09345700
Al	-1.77414600	-0.82960800	1.16294700
Al	1.84886800	-1.84093700	-1.36195900
Al	-0.85745600	-1.86688400	-1.19423000
Al	-1.98974300	0.76157900	-1.13962700
Al	2.80252700	-0.97909500	1.09080800
O	-2.40362100	-1.00856700	-0.63882100

C	-5.49531600	0.23281000	0.22077600
H	-4.89175300	-0.58389900	-0.17319400
H	-5.64038600	0.97700500	-0.56251000
H	-6.46278200	-0.14020900	0.55849800
H	-4.96721700	0.69634900	1.05414700

Table 94: Transition state energy (TS) for the C-H bond activation on single oxygen atom doped $(Al_{13})^-$ via polar pathway in triplet state having opposite orientation of oxygen.

Al	-0.87919900	-1.80928100	-1.56445600
Al	1.84263200	1.87926000	1.21804300
Al	0.27429900	0.02674400	-0.02199700
Al	-0.03582600	2.50460100	-0.83775900
Al	1.86526600	-1.47528200	-1.59321100
Al	0.11743900	0.45269600	-2.66601700
Al	2.45961800	1.14457500	-1.31403300
Al	0.51049400	-0.47887400	2.55149800
Al	-0.70389500	1.84788800	1.82275200
Al	0.78717400	-2.58825700	0.62547400
Al	-1.60373600	-1.61546300	1.08423800
Al	-2.29351700	0.80453000	0.12208300
Al	2.71479900	-0.68648600	0.91031900
O	-3.11463200	-0.67667800	0.91546900
C	-4.04238400	0.59085600	-1.17885400
H	-4.66305100	1.45534200	-0.93154900
H	-4.71899000	-0.20944100	-1.50461800
H	-3.44024500	0.81505100	-2.06604800
H	-3.72846400	-0.27914800	-0.12856100

Table 95: Final state (FS) for the C-H bond activation on single oxygen atom doped $(Al_{13})^-$ via polar pathway in triplet state having opposite orientation of oxygen.

Al	-0.86753900	-0.40941300	-2.30424800
Al	1.67252100	0.57533500	2.24575500
Al	0.31242300	0.03885400	0.00640300
Al	-0.29448900	2.29700800	1.22928100
Al	1.75699200	0.36685900	-2.23344000
Al	-0.23206400	2.15777200	-1.49702500
Al	2.20807300	1.99211000	-0.03952500
Al	0.92618600	-2.02611600	1.57612100
Al	-0.94440500	-0.13440200	2.34209100
Al	1.09356500	-2.13998500	-1.38963600
Al	-1.18473700	-2.14782600	-0.05716000

Al	-2.37661600	0.30289200	-0.10560400
Al	2.88421400	-0.75919400	0.14263700
O	-2.95936000	-1.57553000	0.13976600
C	-4.03843800	1.36013700	-0.11234900
H	-4.57162900	1.25991000	0.83845600
H	-4.70562100	1.01652100	-0.90901300
H	-3.83991000	2.42227600	-0.27115900
H	-3.38096500	-1.73590400	0.99421400

Neighboring site-pairs of dopants

Adjacent Al-O site pairs in Gallium doped system

H_2 binding energy

Table 96: H_2 adsorption over site-pair Al^{IV}-O^{II} of pristine γ-Al_2O_3 through polar mechanism.

O	-3.65073200	1.70153600	0.45596800
O	-1.19700700	1.27894100	-0.92968300
O	-3.05121800	-1.13398100	-0.74724300
Al	-2.67433700	0.42991100	-0.07335100
O	1.19361400	3.14241800	-0.69157100
O	1.61724100	0.42540700	-1.17483200
Al	2.02685400	1.81220600	0.01137000
O	1.17608300	-1.10650500	1.20709200
O	0.49046500	1.64877300	1.21241500
O	-1.57434100	-0.46013100	1.17434700
O	2.44424000	-2.33169600	-0.54144000
O	-0.31629800	-1.51161200	-1.20708800
Al	-0.02141900	0.13546000	-1.52078700
Al	-0.38939600	2.80107400	-0.02213400
Al	-0.00268800	0.05986400	1.60524200
Al	0.79481300	-2.50779100	-0.01101600
O	-0.68794500	-3.24715000	0.53340900
Al	-1.71273800	-1.97023600	-0.05244400
O	3.30114600	0.79109200	0.61378000
Al	2.59741500	-0.69091000	0.02481500
H	-4.53917200	1.70102200	0.80260600
H	-1.46335700	3.81772800	0.45409800

Table 97: H_2 adsorption over site-pair Al^{IV}-O^{III} of pristine γ-Al_2O_3 through polar mechanism.

O	-2.97808400	-0.68540500	0.83457700
O	-1.74069200	-0.66830000	-1.33213100
O	-0.81759200	-3.17786300	-0.19640400
Al	-1.76371900	-1.75561500	0.23887800
O	-2.24858000	2.03315800	-0.27082200
O	0.30444600	1.34737800	-1.17198100
Al	-0.62182000	2.43105000	0.02339200
O	1.82461900	0.54933300	1.10296400
O	-0.77773200	1.51983700	1.80559400
O	-0.24643100	-1.31597200	1.27415100
O	3.12743700	0.79792800	-0.96539500
O	1.11636800	-1.27421800	-1.25360400
Al	-0.14896400	-0.21389400	-1.67154300
Al	-3.08478900	0.48269000	-0.52321300
Al	0.32268700	0.18262100	1.78102100
Al	2.56330500	-0.66758500	-0.18342000
O	2.41586700	-2.23002200	0.60123100
Al	0.74507300	-2.48840200	0.13948600
O	0.94002400	3.18643300	0.28934200
Al	1.89195500	1.83203100	-0.28221200
H	-1.72466200	1.30726700	1.86816100
H	-4.38103200	0.59677800	-1.39939600

Table 98: H_2 adsorption over site-pair Al^{III}-O^{III} of pristine γ-Al_2O_3 through polar mechanism.

O	1.46087600	2.94550400	0.50605600
O	0.72279000	1.44878000	-1.30738200
O	-1.82359800	2.72307000	-0.62959900
Al	-0.18717300	2.57893000	-0.02378100
O	3.24810300	0.21361800	-0.56221400
O	0.90748000	-1.34684100	-1.30981700
Al	2.31417800	-1.19746700	-0.14818300
O	-0.65317400	-1.38535100	1.10042600
O	1.62211300	0.11017000	1.30523500
O	-0.83123200	1.29204200	1.10181000
O	-1.45014700	-2.94062400	-0.62461800
O	-1.70174700	-0.11305200	-1.32497400

Al	-0.06364600	-0.00650000	-1.70448500
Al	2.13567600	1.48888400	-0.14501000
Al	-0.13280000	-0.00636800	2.04820300
Al	-2.14371500	-1.43552300	-0.02354600
O	-3.23729000	-0.21331300	0.59782200
Al	-2.31373600	1.14194400	-0.02389600
O	1.83542100	-2.72542800	0.51121900
Al	0.15316000	-2.58088700	-0.01942100
H	0.00997300	0.00220700	3.60420600
H	2.28799900	0.15001800	2.00564000

Table 99: H_2 adsorption over site-pair Al^{III}-O^{II} of pristine γ-Al_2O_3 through polar mechanism.

O	-0.00082400	-3.29032400	0.50311200
O	-0.00043700	-1.69044500	-1.26248000
O	2.90656000	-1.59487300	-0.64889500
Al	1.36060600	-2.12457200	-0.08964800
O	-2.90734100	-1.59343800	-0.64886700
O	-1.44756300	0.79919000	-1.29175100
Al	-2.60876200	0.04342800	-0.00752400
O	0.00040000	1.53637400	1.11071100
O	-1.35582900	-0.81275900	1.11786700
O	1.35536400	-0.81341400	1.11775500
O	0.00081800	3.27073600	-0.63796900
O	1.44790900	0.79847000	-1.29172200
Al	-0.00001900	0.00762500	-1.64653200
Al	-1.36166400	-2.12389500	-0.08957000
Al	0.00002300	0.00283100	1.99198000
Al	1.27861400	2.24016000	-0.01255600
O	2.84138500	1.67011800	0.55863700
Al	2.60878100	0.04212700	-0.00748100
O	-2.84051200	1.67152700	0.55865500
Al	-1.27746900	2.24078200	-0.01255100
H	-0.00103100	-3.78892700	1.32461100
H	0.00016900	-0.09068100	3.55544800

Table 100: H_2 adsorption over site-pair B^{IV}-O^{II} of boron doped γ-Al_2O_3 through polar mechanism.

O	-2.59333600	-1.58201700	-0.49101800

O	-1.11991000	-1.62372000	1.67993300
O	-3.03109300	0.71579500	0.47164800
O	0.43237400	-3.30330100	0.00694900
O	1.59271100	-0.80167700	1.13002900
Al	1.54291900	-1.99937100	-0.34785800
O	1.24846000	1.24525400	-1.13526000
O	0.02201000	-1.22562500	-1.17430900
O	-1.58701800	1.17061000	-1.62161600
O	2.48043800	1.88774800	0.90139500
O	-0.36313200	1.15767700	1.17510800
Al	0.03376200	-0.41873300	1.72471700
Al	-0.99516000	-2.25135500	0.02251600
Al	-0.10922800	0.37555200	-1.72549800
Al	0.89743500	2.35764700	0.34515100
O	-0.55287800	3.29580100	0.01823100
Al	-1.57224600	1.86505800	-0.01961500
O	2.91491000	-1.07578800	-0.92847400
Al	2.49827600	0.37287000	-0.01430700
H	-3.74601700	0.96844800	1.06566600
B	-3.40984200	-0.62260800	-0.17247000
H	-4.59790000	-0.66316200	-0.27062400

Table 101: H_2 adsorption over site-pair B^{IV}-O^{III} of boron doped γ-Al_2O_3 through polar mechanism.

O	3.07836700	1.05794700	0.44647500
O	2.02769400	-0.24927700	-1.70584300
O	1.31282200	2.56184600	-0.31195300
O	2.36866500	-2.28794500	0.21846200
O	-0.32142900	-1.81386800	-1.07594300
Al	0.65443500	-2.33753300	0.46026100
O	-1.86581000	-0.15527200	1.10019600
O	0.91255000	-0.53738000	1.09409600
O	-0.36203300	2.07244000	1.74424000
O	-2.98662100	-0.82436200	-0.97153400
O	-0.69291800	0.89283400	-1.30838100
Al	0.37459000	-0.38927200	-1.74482300
Al	2.49196200	-0.52561000	-0.01340400
Al	-0.36717700	0.32447700	1.72867400
Al	-2.38331400	0.74094700	-0.48957800
O	-2.13551300	2.45991000	-0.14282000
Al	-0.37174200	2.36021600	-0.26533300
O	-0.91868100	-2.78490800	1.10322700
Al	-1.83008400	-1.72972200	0.01748700

H	-1.21386200	2.47358700	1.97492800
B	2.62191300	2.28236100	0.07742800
H	3.37484300	3.21331500	0.10344500

Table 102: H_2 adsorption over site-pair B^{III}-O^{III} of boron doped γ-Al_2O_3 through polar mechanism.

O	1.65524000	-2.82553600	-0.63023600
O	0.82386800	-1.40958500	1.22925700
O	-1.63889400	-2.84268000	0.40873800
Al	0.00069900	-2.54638100	-0.10617900
O	3.27192100	0.00001200	0.42575600
O	0.82385700	1.40958800	1.22925400
Al	2.22784500	1.33652200	0.04276200
O	-0.69128200	1.17433300	-1.12240700
O	1.45045000	0.00000700	-1.27731100
O	-0.69127300	-1.17433400	-1.12240500
O	-1.63891600	2.84266600	0.40874300
O	-1.71550400	-0.00000700	1.26862700
Al	-0.05868800	-0.00000200	1.60769900
Al	2.22785600	-1.33650800	0.04276800
Al	-2.24323300	1.26880400	-0.06594900
O	-3.28764100	-0.00001300	-0.65134700
Al	-2.24322400	-1.26882000	-0.06594500
O	1.65521900	2.82555100	-0.63023300
Al	0.00068100	2.54638200	-0.10617300
H	1.93693900	0.00000700	-2.11193900
B	-0.16639000	0.00000100	-1.75324500
H	-0.09652600	0.00000000	-2.95010500

Table 103: H_2 adsorption over site-pair B^{III}-O^{II} of boron doped γ-Al_2O_3 through polar mechanism.

O	0.00000600	-3.28155100	-0.61558400
O	0.00000300	-1.70649600	1.20972100
O	-2.91393700	-1.60592900	0.44311300
Al	-1.33174600	-2.10979100	-0.01029600
O	2.91394300	-1.60591800	0.44311300
O	1.46665600	0.80751900	1.24087700
Al	2.58992200	0.05466300	-0.09246400
O	-0.00000300	1.33520400	-1.09507900
O	1.20512400	-0.72000600	-1.12139200

O	-1.20512100	-0.72001100	-1.12139200
O	-0.00000600	3.28315100	0.41710300
O	-1.46666000	0.80751300	1.24087700
Al	0.00000000	0.01353300	1.54005000
Al	1.33175400	-2.10978600	-0.01029500
Al	-1.28219200	2.21131400	-0.09243400
O	-2.85010900	1.67416200	-0.65143900
Al	-2.58992200	0.05465300	-0.09246400
O	2.85010300	1.67417300	-0.65143900
Al	1.28218400	2.21131900	-0.09243400
H	0.00000800	-3.71929500	-1.47176500
B	0.00000000	-0.00556100	-1.69708000
H	0.00000000	-0.02416000	-2.89630000

Table 104: H_2 adsorption over site-pair Ga^{IV}-O^{II} of gallium doped γ-Al_2O_3 through polar mechanism.

O	-2.48359900	-2.05249100	0.66604400
O	-1.20531100	-0.91450800	-1.23813000
O	0.39298100	-3.36317100	-0.60261200
Al	-0.94726200	-2.40563400	-0.03415800
O	-2.38986100	3.04053100	-0.47584600
O	0.26153900	1.66028800	-1.17395100
Al	-0.88667100	2.48638400	0.07509900
O	1.62311200	0.76051100	1.20781600
O	-1.29744900	0.87677500	0.96968000
O	0.25698500	-1.62107500	1.16486800
O	3.19010600	1.57604000	-0.54183500
O	1.63772900	-0.80126900	-1.20077800
Al	0.18776900	0.00520800	-1.60003800
Al	0.11424500	0.03453500	1.52269200
Al	2.87750700	-0.04740500	0.01626000
O	3.14998400	-1.67917600	0.56302900
Al	1.61629400	-2.27466100	-0.01150800
O	0.51896000	3.30037100	0.71395900
Al	1.68223400	2.22021100	0.03869100
Ga	-2.68013400	-0.35022500	0.02523200
H	-3.90765500	0.47983900	-0.41077100
H	-2.62311400	3.87224100	-0.88087800

Table 105: H_2 adsorption over site-pair Ga^{IV}-O^{III} of gallium doped γ-Al_2O_3 through polar mechanism.

O	-2.49860700	1.10608600	-1.04002300
O	-1.41089600	0.95603000	1.24735300
O	-0.07900800	3.27663400	0.15547300
Al	-1.19627200	1.99406200	-0.32389400
O	-2.30150500	-1.79825500	0.13257000
O	0.30608400	-1.35370500	1.11236600
Al	-0.70208400	-2.31948000	-0.11526100
O	2.06140200	-0.79415800	-1.05867700
O	-0.64835400	-1.34270200	-1.85318100
O	0.29685700	1.36207400	-1.30203300
O	3.19222100	-1.23501400	1.07802100
O	1.50771500	1.10718200	1.28353500
Al	0.07467400	0.25199400	1.62855800
Al	0.65761000	-0.20500300	-1.78670600
Al	2.89622800	0.30105400	0.28111700
O	3.02291700	1.87195900	-0.49202300
Al	1.38463900	2.37166200	-0.11111900
O	0.75583000	-3.27683800	-0.31458900
Al	1.85785800	-2.07169300	0.31542200
Ga	-2.98134300	-0.07499000	0.34479200
H	-4.32303100	0.05663800	1.13617400
H	-1.53710400	-0.96001900	-1.96056900

Table 106: H_2 adsorption over site-pair Ga^{III}-O^{III} of gallium doped γ-Al_2O_3 through polar mechanism.

O	3.23592200	0.08311300	0.34526400
O	1.65912300	0.04414900	-1.54576000
O	1.53214800	2.87751600	-0.85747900
Al	2.18044400	1.35004300	-0.25773900
O	1.67733300	-2.79240900	-0.86465500
O	-0.82443200	-1.41861800	-1.46938800
Al	0.06399400	-2.58359400	-0.21050400
O	-1.65746200	-0.04454200	1.15348900
O	0.80474700	-1.35135700	0.91059500
O	0.73211500	1.38564900	0.90969300
O	-3.28541700	-0.08370100	-0.70039100
O	-0.89734700	1.38054000	-1.47091600
Al	0.00963500	0.00325200	-1.88650400
Al	2.24695100	-1.23583400	-0.25967500

Al	-2.28478200	1.28236200	-0.27884300
O	-1.73220200	2.79416600	0.36563100
Al	-0.06908700	2.58399900	-0.20572900
O	-1.58603200	-2.88096400	0.36021100
Al	-2.21521300	-1.39635000	-0.27815300
H	-2.33439900	-0.06118300	1.84331000
H	0.06958400	0.00046000	3.53095200
Ga	0.18973000	0.00199900	1.98188000

Table 107: H_2 adsorption over site-pair Ga^{III}-O^{II} of gallium doped γ-Al_2O_3 through polar mechanism.

O	-2.84217700	-1.66392400	0.37860100
O	-1.44880000	-0.79256600	-1.46954700
O	-0.00578900	-3.26533600	-0.84296500
Al	-1.28225700	-2.23883900	-0.20126800
O	-2.90034500	1.60012200	-0.84497400
O	0.00297800	1.69133900	-1.43272400
Al	-1.36003000	2.13001600	-0.26572800
O	1.39011300	0.82953700	0.95405400
O	-1.38703800	0.83426900	0.95392600
O	-0.00289000	-1.57262500	0.93374800
O	2.90597600	1.58996300	-0.84502500
O	1.44605600	-0.79758800	-1.46954100
Al	-0.00001800	-0.00362000	-1.82193900
Al	-2.60813700	-0.03332900	-0.18543300
Al	2.60799500	-0.04248100	-0.18573500
O	2.83603700	-1.67381700	0.37875300
Al	1.27421100	-2.24333500	-0.20125600
O	0.00588100	3.29700000	0.32249500
Al	1.36751700	2.12522500	-0.26574400
H	0.00019800	0.06658800	3.48771300
Ga	0.00008200	-0.01613500	1.93202000
H	0.00657600	3.80528300	1.13759500

Doped system H_2 binding energy

Table 108: H_2 adsorption over site-pair Al^{III}-O^{III} of double boron (B^{IV}) doped γ-Al_2O_3 through polar mechanism.

O	-2.62527900	1.58249700	0.52206200
O	-1.83940800	0.72551400	-1.40346900
O	-2.56287100	-1.87322400	-0.22867600
O	-0.72077500	2.79125200	-0.54226000
O	0.76210000	1.02706400	-1.09770800
O	1.73390700	-0.28586700	1.10711800
O	0.15603800	1.82473300	1.38995400
O	-0.95736100	-0.61608200	1.12151100
O	2.88310800	-0.75993800	-1.00829600
O	0.09335300	-1.62116900	-1.35827100
Al	-0.33764900	-0.04782700	-1.76314600
Al	0.33687500	0.14755300	2.09291400
Al	1.66945800	-1.68969600	-0.11897700
O	0.66463500	-2.90514900	0.66311600
Al	-0.85894400	-2.21244800	0.15952000
O	1.97193000	2.50445900	0.00885500
Al	2.36965100	0.75343000	-0.26233900
B	-1.74182000	1.89079800	-0.46425300
Al	-2.44481400	-0.19131700	0.21599800
B	0.59803500	2.21414700	-0.12005600
H	0.26347600	0.05165900	3.65016000
H	-0.56907200	2.39485400	1.66827200

Table 109: H_2 adsorption over site-pair Al^{III}-O^{II} of boron (B^{IV}) doped γ-Al_2O_3 through polar mechanism.

O	2.28442900	-2.22788400	0.37994100
O	1.50115900	-1.12160400	-1.42658600
O	3.10226600	1.11029200	-0.31928100
Al	2.51259300	-0.46760900	0.10313200
O	0.09685600	-2.94287100	-0.55544600
O	-1.27765400	-0.71688300	-1.35593700
Al	-1.35148100	-2.01392700	-0.02585200
O	-1.34821700	0.81420500	1.03119700
O	-0.55810000	-1.71849700	1.62840000
O	1.25973000	0.31553100	1.11809700
O	-2.48519200	1.86754900	-0.87933000
O	0.40087400	1.58350200	-1.30323700

Al	0.20240400	-0.02651400	-1.75921100
Al	-0.19972200	0.03656100	2.11607200
Al	-0.96063700	2.24267700	-0.08151100
O	0.40004300	3.05305200	0.68249000
Al	1.58331700	1.89364400	0.13845900
O	-2.96601300	-1.40174900	0.25079100
Al	-2.52859500	0.22880200	-0.25060700
B	1.27010000	-2.28757300	-0.52862800
H	0.12920500	-2.35900300	1.84971700
H	-0.11356600	0.26248800	3.65835000

Table 110: H_2 adsorption over site-pair Al^{IV}-O^{II} of double boron (B^{III}) doped γ-Al_2O_3 through polar mechanism.

O	3.63909300	1.49120300	-0.59630900
O	1.30258200	1.19100400	0.99114700
O	2.97336100	-1.33494800	0.52430000
Al	2.62666600	0.28235600	-0.00586900
O	-0.90461000	3.22605700	0.46226500
O	-1.60814500	0.55178900	1.15861000
Al	-1.85376200	1.92664800	-0.10097100
O	-1.05597800	-0.84855700	-1.17349200
O	-0.27346100	1.38294800	-1.16510700
O	1.27070400	-0.45638100	-1.13151900
O	-2.60993700	-2.13798200	0.31065500
O	0.20233700	-1.55865000	1.19695300
Al	0.01092700	0.11778600	1.49014300
Al	0.66647800	2.67783200	-0.06985000
Al	-0.94914800	-2.42052800	-0.07716100
O	0.45011700	-3.28672500	-0.61592300
Al	1.53181300	-2.07386500	-0.02499700
O	-3.21554500	1.04848400	-0.71008900
Al	-2.61371800	-0.46255000	-0.12021400
B	-0.00723300	0.03798300	-1.29087100
H	4.43629100	1.44947700	-1.11802800
H	1.78539100	3.59484800	-0.62358600

Table 111: H_2 adsorption over site-pair Al^{IV}-O^{III} of double boron (B^{III}) doped γ-Al_2O_3 through polar mechanism.

O	-2.74493900	-1.01513600	0.95530200
O	-1.59577800	-0.82537500	-1.25464000
O	-0.32134100	-3.20582100	-0.12906100
Al	-1.44208700	-1.92264900	0.28018100

O	-2.55445500	1.74033600	-0.15937600
O	0.11692500	1.49306100	-1.13315800
Al	-0.98373400	2.26172300	0.18548900
O	1.46951000	0.63923500	1.15280000
O	-0.81772700	0.92868200	1.68484200
O	0.04565400	-1.22563200	1.25980200
O	3.00237000	1.33619100	-0.64975400
O	1.30712000	-1.01690600	-1.22910600
Al	-0.09573700	-0.12432700	-1.62685700
Al	-3.12518200	0.09041600	-0.41737200
Al	2.63336000	-0.27206300	-0.09094900
O	2.77676500	-1.87982300	0.56800200
Al	1.15141500	-2.32786100	0.12901900
O	0.40563300	3.24531000	0.57317300
Al	1.55119900	2.10717500	-0.07337900
B	0.28002900	0.08738300	1.47238400
H	-1.64596800	0.39297100	1.76491400
H	-4.43210900	-0.10426100	-1.25715200

Table 112: H_2 adsorption over site-pair Al^{III}-O^{III} of double gallium (Ga^{IV}) doped γ-Al_2O_3 through polar mechanism.

O	-2.86061500	-0.17475500	0.74907700
O	-1.33362800	0.01004100	-1.24313900
O	-1.29185200	-2.89209100	-0.73838500
O	-1.24626600	2.89683300	-0.21613900
O	1.14546200	1.40643500	-1.41812700
O	2.06818000	-0.12685400	0.79316500
O	-0.19963500	1.25811500	1.49054300
O	-0.25774800	-1.43541800	0.95783800
O	3.65194800	-0.10649900	-1.09358300
O	1.11820300	-1.47720500	-1.60564400
Al	0.28409400	-0.01909800	-1.77795000
Al	0.72823200	-0.33629600	1.90972500
Al	2.63632600	-1.39671600	-0.45842800
O	2.06877300	-2.94233300	0.14148500
Al	0.39626300	-2.65861400	-0.29707200
O	2.30289700	2.73362600	0.38018200
Al	2.71319500	1.15643600	-0.33193800
Ga	-1.92384300	1.24251600	0.13833900
H	-0.43294200	1.76942400	2.27589500
Ga	0.54877000	2.63452700	-0.03602000
Al	-1.80444700	-1.38802600	-0.00974900
H	0.88613500	-0.42187300	3.46394100

Table 113: H_2 adsorption over site-pair Al^{III}-O^{II} of double gallium (Ga^{IV}) doped γ-Al_2O_3 through polar mechanism.

O	-3.64358200	1.76507400	0.28268600
O	-1.16792100	1.29084400	-1.03918300
O	-3.07003500	-1.08739400	-0.90613800
Al	-2.68342400	0.46907800	-0.21758300
O	1.26303500	3.10621300	-0.87133000
O	1.62197300	0.38303300	-1.30292100
Al	2.07641700	1.77392700	-0.14034000
O	1.19773700	-1.17459400	1.08793200
O	0.56143400	1.70652300	1.08347000
O	-1.65009900	-0.46077800	1.05493600
O	2.39632000	-2.38663700	-0.69770200
O	-0.34678400	-1.51067300	-1.32519600
Al	-0.02121000	0.12716700	-1.64616000
Al	0.74904000	-2.53701500	-0.14388400
O	-0.75156600	-3.24460000	0.40027000
Al	-1.75929100	-1.95247200	-0.18581200
O	3.32638200	0.72099100	0.46231300
Al	2.59251700	-0.75280400	-0.11666500
Ga	-0.00641500	0.06914700	1.53069400
Al	-0.32194200	2.82141800	-0.17859000
H	-4.53503700	1.78322400	0.62115900
H	-1.37864700	3.86831500	0.27168500

Table 114: H_2 adsorption over site-pair Al^{IV}-O^{II} of double gallium (Ga^{III}) doped γ-Al_2O_3 through polar mechanism.

O	-2.44099900	-2.02497600	0.52108100
O	-1.15460300	-1.03419500	-1.27662000
O	0.65760400	-3.29957100	-0.60857900
Al	-0.69486600	-2.36318300	-0.08147000
O	-2.82387500	1.53354000	-0.61178000
O	-0.01386800	1.62380400	-1.27483400
Al	-1.27204300	2.17597400	0.01948900
O	1.47052500	0.93065700	1.10001000
O	-1.23802300	0.69053800	1.16518500
O	0.34661300	-1.53409000	1.10626200
O	2.86055900	1.92566200	-0.67683300
O	1.71238500	-0.70073300	-1.29189800
Al	0.20859000	-0.01190800	-1.63148200
Al	0.23193700	0.03587800	1.99395500
Al	2.78204000	0.29543000	-0.02769700

O	3.24177300	-1.29527200	0.56402700
Al	1.78984000	-2.07119600	0.00516900
O	-0.07105300	3.32390300	0.52964700
Al	1.28561100	2.36441000	-0.03967600
Ga	-2.38839100	-0.13813600	-0.06354000
H	-2.82793400	-2.32496400	1.34835700
H	0.18737000	-0.03724700	3.55832400

Table 115: H_2 adsorption over site-pair Al^{IV}-O^{III} of double gallium (Ga^{III}) doped γ-Al_2O_3 through polar mechanism.

O	-2.76760400	-1.45969500	0.66258300
O	-1.35503600	-0.87509300	-1.34508900
O	-0.04010100	-3.34312800	-0.37373600
Al	-1.22563800	-2.15217800	0.10119200
O	-2.46896200	1.87927000	-0.43684200
O	0.24330700	1.45682500	-1.23870300
Al	-0.80905500	2.33498200	-0.02452400
O	1.74063600	0.75795800	1.05750600
O	-0.92859700	1.17368900	1.50773200
O	0.08879800	-1.33952700	1.05881400
O	3.14789700	1.33203300	-0.87820800
O	1.57792400	-1.07157000	-1.33625500
Al	0.17867200	-0.18512200	-1.65844300
Al	0.47773300	0.06300700	2.06126500
Al	2.80132600	-0.22080500	-0.12006700
O	2.91310900	-1.81853000	0.60346800
Al	1.33374600	-2.33100500	0.05798900
O	0.57480400	3.32800900	0.32352200
Al	1.73440400	2.10099100	-0.18779900
Ga	-2.55421500	0.11084300	-0.18233400
H	-1.51742200	1.48080400	2.20579600
H	0.50320700	-0.00719700	3.62324500

Al_2O_3_new

Al	0.01170800	1.31303100	1.41152200
Al	-2.50794200	0.06720100	0.00003000
Al	4.34483500	2.79817600	0.00002800
Al	0.01203800	1.31291300	-1.41128300
Al	-3.55889000	3.29876100	0.00006800
O	-3.40164800	-1.38273800	-0.00020300
O	-1.25173700	0.00942100	-1.39700500
O	-1.25195200	0.00948300	1.39713400

O	0.02803900	2.29562200	0.00001000
O	-3.15803000	1.64542100	0.00000100
Al	-0.01193900	-1.31331700	-1.41142700
Al	-4.34600100	-2.79761700	-0.00013900
Al	2.50780700	-0.06732000	-0.00011700
Al	3.56091900	-3.29820000	0.00044300
Al	-0.01208700	-1.31330300	1.41140600
O	3.40083000	1.38305300	-0.00024000
O	1.25159300	-0.00975100	1.39684700
O	3.15854400	-1.64523900	-0.00004500
O	1.25180600	-0.00988300	-1.39734400
O	-0.02817300	-2.29591900	-0.00002300

List of Publications

1.“Nitrogen reduction to ammonia. A short review on bio-inspired approach” Published in “Journal of emerging technologies and innovative research” volume 6, Issue 1. ISSN:2349-5162, Impact Factor 7.95

2. “Assessing the effect of dopants on the C-H activation activity of gamma Alumina using First Principle calculation” published in “ChemPhysChem” 14394235-14397641, Impact Factor 3.5

List of Conferences

1. RAFAS 2023
2. Expert e talk organized by Department of Civil Engineering K.D.K. College of Engineering Nagpur
3. Webinar Organized by Department of Civil Engineering and Engineering Council of India, Adithya Institute of Technology